# Proton Decay Matrix Elements from Lattice QCD


*Paul Cooney*

A thesis submitted in fulfilment of the requirements for the degree of

Doctor of Philosophy

to the

University of Edinburgh

2009

# Abstract

We present results for the matrix elements relevant for proton decay in Grand Unified Theories (GUTs), using two methods. In the *indirect* method, we rely on an effective field theory description of proton decay, where we need to estimate two low energy constants. We then relate these low energy constants to the proton decay matrix elements using leading order chiral perturbation theory. In the *direct* method, we calculate the required matrix elements directly; this is computationally more expensive, but the calculation has no systematic error from the use of chiral perturbation theory.

The calculations are performed with 2+1 flavors of domain wall fermions on lattices of size $16^3 \times 32$ and $24^3 \times 64$ with a fifth dimension of length 16. We work at fixed inverse lattice spacing, $a^{-1} = 1.73(3)$ GeV, leading to physical volumes of $(1.8 \text{ fm})^3$ and $(2.7 \text{ fm})^3$ for the $16^3 \times 32$ and $24^3 \times 64$ lattices respectively.

In the first four chapters we present the background theory. We start with a brief review of the standard model and the motivation for GUTs. We show that GUTs must lead to proton decay, and that the proton lifetime is an experimentally testable prediction which can be used to constrain GUT parameters, or rule out classes of GUT which predict a minimum lifetime shorter than the experimental minimum bound. We then review continuum and lattice QCD, including outlines of the lattice methods used to calculate the proton decay matrix elements.

In the last three chapters we present the results and analysis. We calculate the nucleon and pion two–point correlation functions, and determine their ground state masses and amplitudes. These quantities will then be used to calculate the matrix elements using the *indirect* and *direct* methods outlined above. The matrix elements can then be combined with experimental bounds on the proton lifetime to bound parameters of individual GUTs.

# Declaration

I do hereby declare that this thesis was composed by myself and that the work described within is my own, except where explicitly stated otherwise.

The results for nucleon masses and amplitudes from Chapter 5 and the results for the indirect calculation and the non–perturbative renormalization, both from Chapter 6, also appear in the following papers:

- Proton lifetime bounds from chirally symmetric lattice QCD,
  Phys. Rev. D **78** (2008) 054505 [arXiv:0806.1031 [hep-lat]].
  Ref. [1]

- Proton lifetime bounds from chirally symmetric lattice QCD,
  PoS (Lattice 2008) 283.
  Ref. [2].

In both cases, I was one of the lead authors. I carried out all or part of the analysis presented and I contributed significantly to writing the text.

*Paul Cooney*
September 2009

# Contents

# List of Figures

# List of Tables

# Chapter 1

# Introduction

## 1.1 The Standard Model

The Standard Model [3, 4] describes fundamental particles and their interactions via the strong, weak and electromagnetic forces. It is the subject of many review articles, lecture courses and text books and the following arguments were based on those found in Refs. [5, 6, 7, 8, 9].

The Standard Model describes 6 flavours of quarks arranged into three generations each with one up type quark and one down type quark. Also present are 6 leptons, again arranged into three generations (see Table 1.1).

$$\text{quarks} \quad \begin{pmatrix} u \\ d \end{pmatrix} \quad \begin{pmatrix} c \\ s \end{pmatrix} \quad \begin{pmatrix} t \\ b \end{pmatrix} \quad = \begin{pmatrix} u^i \\ d^i \end{pmatrix}$$

$$\text{leptons} \quad \begin{pmatrix} e \\ \nu_e \end{pmatrix} \quad \begin{pmatrix} \mu \\ \nu_\mu \end{pmatrix} \quad \begin{pmatrix} \tau \\ \nu_\tau \end{pmatrix} \quad = \begin{pmatrix} e^i \\ \nu^i \end{pmatrix}$$

Table 1.1: The quark and lepton content of the Standard Model. The far right column introduces notation involving a generation index i, which runs from 1 to 3.

As well as these matter fields, the Standard Model describes the interactions of these fields. The Standard Model is a gauge theory, a theory which is invariant under local group transformations. For the case of the Standard Model, the gauge group is $SU(3) \times SU(2) \times U(1)$. $SU(3)$ is the group of the strong interactions, mediated by 8 gluons. Together $SU(2) \times U(1)$ form the gauge group for the electroweak interactions which are mediated by $3 + 1$ electroweak gauge bosons. The forces and their associated gauge bosons are summarised in Table 1.2.

| Force | Gauge group | Gauge bosons | Symbol |
|---|---|---|---|
| Strong | $SU(3)$ | 8 gluons | $A^a_\mu$ |
| Electroweak | $SU(2) \times U(1)$ | 3+1 electroweak gauge bosons | $W^i_\mu$, $B_\mu$ |

Table 1.2: The forces, gauge group and gauge bosons of the Standard Model.

### 1.1.1 The Standard Model Lagrangian

The particles and their interactions are described by the Standard Model Lagrangian, which is composed of:

$$\mathcal{L}_{\rm SM} = \mathcal{L}_{\rm Dirac} + \mathcal{L}_{\rm Gauge} + \mathcal{L}_{\rm Yukawa} + \mathcal{L}_{\rm Higgs}. \tag{1.1}$$

$\mathcal{L}_{\rm Dirac}$ contains kinetic terms for all of the matter fields. In order to write this down we define the left and right handed fields,

$$\begin{aligned} u^i_{R/L} &= P_{R/L} u^i \qquad & d^i_{R/L} &= P_{R/L} d^i \\ e^i_{R/L} &= P_{R/L} e^i \qquad & \nu^i_L &= P_L \nu^i \end{aligned} \tag{1.2}$$

where $P_{R/L} = \frac{1}{2}(1 \pm \gamma_5)$ is a two–index spin tensor and all spin indices have been suppressed. Note that there are no right handed neutrinos. We then arrange these such that the left handed fields are arranged in weak doublets,

$$q^i_L = \begin{pmatrix} u^i_L \\ d^i_L \end{pmatrix}, \quad l^i_L = \begin{pmatrix} e^i_L \\ \nu^i_L \end{pmatrix}, \tag{1.3}$$

and the right handed fields are arranged in weak singlets, $u^i_R, d^i_R$, $e^i_R$. We can now write down an expression for $\mathcal{L}_{\rm Dirac}$,

$$\begin{aligned} \mathcal{L}_{\rm Dirac} \;=\; & \sum_i \bar{q}^i_L \gamma^\mu D_\mu q^i_L + \bar{u}^i_R \gamma^\mu D_\mu u^i_R + \bar{d}^i_R \gamma^\mu D_\mu d^i_R \\ & + \bar{l}^i_L \gamma^\mu D_\mu l^i_L + \bar{e}^i_R \gamma^\mu D_\mu e^i_R \end{aligned} \tag{1.4}$$

where the the sum over $i$ is a sum over generations and $D_\mu$ is covariant derivative with space–time index $\mu$. The covariant derivative acts differently upon the different quark and lepton

fields,

$$\begin{aligned}
D_\mu u_L &= \left[\partial_\mu + igT^i W^i_\mu + ig'Y(u_L)B_\mu + ig_s T^a_s A^a_\mu\right] u_L \\
D_\mu d_L &= \left[\partial_\mu + igT^i W^i_\mu + ig'Y(d_L)B_\mu + ig_s T^a_s A^a_\mu\right] d_L \\
D_\mu u_R &= \left[\partial_\mu + ig'Y(u_R)B_\mu + ig_s T^a_s A^a_\mu\right] u_R \\
D_\mu d_R &= \left[\partial_\mu + ig'Y(u_R)B_\mu + ig_s T^a_s A^a_\mu\right] d_R \\
D_\mu e_L &= \left[\partial_\mu + igT^a W^a_\mu + ig'Y(e_L)B_\mu\right] e_L \\
D_\mu \nu_L &= \left[\partial_\mu + igT^a W^a_\mu + ig'Y(\nu_L)B_\mu\right] \nu_L \\
D_\mu e_R &= \left[\partial_\mu + ig'Y(e_R)B_\mu\right] e_R. \qquad (1.5)
\end{aligned}$$

The terms of the form $igT^iW^i_\mu$ contain a sum over the generators of $SU(2)$, $T^i$ with $i = 1\ldots3$, and the associated $SU(2)$ gauge bosons $W^i$. The terms of the form $ig'Y(u_L)B_\mu$ contain the $U(1)$ gauge boson $B_\mu$ and the factor $Y$, which is the hypercharge of the field being acted upon by the derivative, $Y(q^i_L) = \frac{1}{6}$, $Y(u^i_R) = \frac{2}{3}$, $Y(d^i_R) = -\frac{1}{3}$, $Y(l_L) = -\frac{1}{2}$ and $Y(e_R) = -1$. Together, these give the $SU(2) \times U(1)$ electroweak interactions with the matter fields. The terms of the form $ig_sT^a_sA^a_\mu$ contain a sum over the generators, $T^a_s$ $a = 1\ldots8$, and associated gauge bosons, $A^a_\mu$, of the group $SU(3)$ for the strong interactions.

The gauge term, $\mathcal{L}_{\text{Gauge}}$ contains the kinetic and self interaction terms for the gauge bosons,

$$\mathcal{L}_{\text{Gauge}} = -\frac{1}{4}F^{a\mu\nu}F^a_{\mu\nu} - \frac{1}{4}W^{i\mu\nu}W^i_{\mu\nu} - \frac{1}{4}B^{\mu\nu}B_{\mu\nu}, \qquad (1.6)$$

where the field strength tensors are,

$$\begin{aligned}
F^a_{\mu\nu} &= \partial_\mu A^a_\nu - \partial_\nu A^a_\mu + g_s f^{abc} A^{b\mu} A^{c\nu} \\
W^i_{\mu\nu} &= \partial_\mu W^i_\nu - \partial_\nu W^i_\mu - g\epsilon^{ijk} W^{j\mu} W^{k\nu} \\
B_{\mu\nu} &= \partial_\mu B_\nu - \partial_\nu B_\mu, \qquad (1.7)
\end{aligned}$$

with $f^{abc}$ the structure constants of the Lie algebra of $SU(3)$ and $\epsilon^{ijk}$ (the totally antisymmetric tensor) the structure constants of the Lie algebra of $SU(2)$.

The kinetic, gauge interaction and potential terms for a scalar field, known as the Higgs field, are contained within $\mathcal{L}_{\text{Higgs}}$,

$$\mathcal{L}_{\text{Higgs}} = (D_\mu\varphi)^\dagger D_\mu\varphi - V(\varphi), \qquad (1.8)$$

where $\varphi$ is the complex Higgs scalar which is a doublet under $SU(2)$,

$$\varphi = \begin{pmatrix} \varphi^+ \\ \varphi^0 \end{pmatrix}, \qquad (1.9)$$

$D_\mu$ is the covariant derivative,

$$D_\mu = \partial_\mu + igT^a W_\mu^a + ig'Y(q)B_\mu, \tag{1.10}$$

and the potential term $V(\varphi)$ is,

$$V(\varphi) = \mu^2\varphi^\dagger\varphi + \lambda(\varphi^\dagger\varphi)^2. \tag{1.11}$$

Finally, the Yukawa term, $\mathcal{L}_{\text{Yukawa}}$ is,

$$-\mathcal{L}_{\text{Yukawa}} = \sum_{i,j} \Gamma^u_{ij}\bar{q}^i_L\bar{\varphi}u^j_R + \Gamma^d_{ij}\bar{q}^i_L\varphi d^j_R + \Gamma^e_{ij}\bar{l}^i_L\varphi e^j_R, \tag{1.12}$$

where again the sum over $i, j$ are sums over generations and $\Gamma^a_{ij}$ are the Yukawa couplings between the flavours $i, j$ of fields of type $a = u, d, e$.

### 1.1.2 The Higgs mechanism

Under the constraint that the Standard Model Lagrangian must be invariant under local gauge transformations, explicit mass terms for the fermions and gauge bosons are forbidden. It is for this reason that we have added the $\mathcal{L}_{\text{Yukawa}}$ and $\mathcal{L}_{\text{Higgs}}$ terms to the Standard Model Lagrangian, to give masses to the fermions and gauge bosons in a gauge invariant way. This is known as the Higgs mechanism [4] which we now summarise.

First we introduce a complex vector,

$$v = \langle 0|\varphi|0\rangle, \tag{1.13}$$

which has components equal to the vacuum expectation values (VEVs) of the components of the Higgs doublet. We can write the Higgs doublet as,

$$\varphi = \begin{pmatrix} \varphi^+ \\ \varphi^0 \end{pmatrix} = \begin{pmatrix} \varphi_1 - i\varphi_2 \\ \varphi_3 - i\varphi_4 \end{pmatrix}, \tag{1.14}$$

and then choose the axis in this four–dimensional space such that $\langle 0|\varphi_i|0\rangle = 0$, for $i = 1, 2, 4$ and $\langle 0|\varphi_3|0\rangle = v$ giving,

$$\varphi = \frac{1}{\sqrt{2}}\begin{pmatrix} 0 \\ v \end{pmatrix}. \tag{1.15}$$

The Higgs potential from Eq. 1.11 may therefore be rewritten as a function of $v$,

$$V(\varphi) \to V(v) = \frac{1}{2}\mu^2 v^2 + \frac{1}{4}\lambda v^4. \tag{1.16}$$

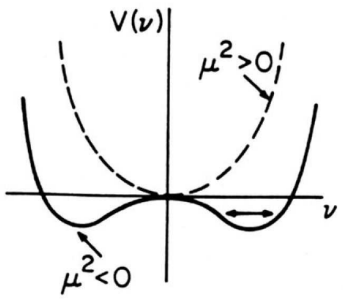


Figure 1.1: The Higgs potential $V(v) = \frac{1}{2}\mu^2 v^2 + \frac{1}{4}\lambda v^4$ for the cases $\mu^2 > 0$ (dotted line) and $\mu^2 < 0$ (solid line). Figure taken from [9].

For the case $\mu^2 > 0$, $\lambda > 0$ the minimum of the potential is at $v = 0$ and the ground state leaves the $SU(2) \times U(1)$ electroweak gauge symmetry intact. However, for $\mu^2 < 0$, $\lambda > 0$ the minimum is instead at,

$$v = \sqrt{\frac{-\mu^2}{\lambda}}. \tag{1.17}$$

Now the VEV is no longer at $v = 0$, and the new VEV spontaneously breaks the $SU(2) \times U(1)$ electroweak gauge symmetry, see Figure 1.1. So through Goldstone's theorem [10], we expect the appearance of massless Goldstone bosons for every broken generator in the broken symmetry group. In this case, we have three broken generators from the $SU(2) \times U(1)$ symmetry, so we expect three massless Goldstone bosons.

To see why this is not the case, we now consider fluctuations around the VEV,

$$\varphi = \frac{1}{\sqrt{2}} \begin{pmatrix} 0 \\ v + H \end{pmatrix}, \tag{1.18}$$

where $H$ represents the as yet undiscovered, massive spin 0 gauge boson called the Higgs boson.

Inserting 1.18 into the scalar kinetic term from $\mathcal{L}_{\text{Higgs}}$ gives,

$$\begin{aligned} (D_\mu \varphi)^\dagger D_\mu \varphi &= \frac{1}{2}(0, v) \left[ i\frac{g}{2} T^a W_\mu^a + \frac{g'}{2} B_\mu \right]^2 \begin{pmatrix} 0 \\ v \end{pmatrix} + H \text{ terms} \\ &= M_W^2 W^{+\mu} W_\mu^- + \frac{M_Z^2}{2} Z^\mu Z_\mu + H \text{ terms}, \end{aligned} \tag{1.19}$$

where the kinetic and gauge interaction terms of the Higgs field H have been omitted. $W^\pm, Z$

are now physical massive fields given by,

$$\begin{aligned} W^{\pm} &= \frac{1}{\sqrt{2}}\left(W^1 \mp iW^2\right) \\ Z &= -\sin\theta_W\, B + \cos\theta_W\, W^3, \end{aligned} \tag{1.20}$$

with masses given by,

$$\begin{aligned} M_W &= \frac{gv}{2} \\ M_Z &= \sqrt{g^2+g'^2}\frac{v}{2} = \frac{M_W}{\cos\theta_W}. \end{aligned} \tag{1.21}$$

The photon field,

$$A = \cos\theta_W\, B + \sin\theta_W\, W^3, \tag{1.22}$$

remains massless.

The angle $\theta_W$ is known as the Weinberg angle, and is defined as

$$\tan\theta_W \equiv \frac{g'}{g}. \tag{1.23}$$

As our theory is a gauge theory, the Higgs mechanism [4] which we have just outlined means that the massless goldstone bosons are "eaten" by the gauge bosons, giving them a mass. In the case of electroweak symmetry breaking, the three broken generators give masses to three of the four electroweak gauge bosons.

### 1.1.3 CP violation

The mass eigenstates (the physical quarks) of the Standard Model Lagrangian are not the same as the eigenstates of the electroweak interactions. The weak force acts on the left handed doublets,

$$\begin{pmatrix} u \\ \tilde{d} \end{pmatrix}, \begin{pmatrix} s \\ \tilde{c} \end{pmatrix}, \begin{pmatrix} t \\ \tilde{b} \end{pmatrix}, \tag{1.24}$$

where,

$$\begin{pmatrix} \tilde{d} \\ \tilde{c} \\ \tilde{b} \end{pmatrix} = V_{\mathrm{CKM}} \begin{pmatrix} d \\ c \\ b \end{pmatrix}, \tag{1.25}$$

and $V_{\mathrm{CKM}}$ is a $3 \times 3$ unitary matrix known as the CKM matrix [11, 12],

$$V_{\mathrm{CKM}} = \begin{pmatrix} V_{ud} & V_{us} & V_{ub} \\ V_{cd} & V_{cs} & V_{cb} \\ V_{td} & V_{ts} & V_{tb} \end{pmatrix}. \tag{1.26}$$

The CKM matrix can be parametrised by 3 mixing angles and a complex phase responsible for CP violation in the Standard Model. A CP transformation combines a charge conjugation (particles and anti–particles are interchanged) with a parity transformation where $\vec{x} \rightarrow -\vec{x}$. Weak interactions are not symmetric under C or P transformations, as W bosons for example couple only to left handed particles and right handed anti–particles. CP symmetry violation was first observed in neutral kaon decays [13]; it has since been observed in B decays [14, 15].

As we already mentioned, the CP violation is related to the complex phase in the CKM matrix. If all the elements of the CKM matrix were real, then the quark weak eigenstates would be real superpositions of the quark mass eigenstates. As the mass eigenstates are a CP eigenstate, so the superposition would also be a CP eigenstate, and there would be no CP violation. Introducing a complex component to the CKM matrix means the superposition of mass eigenstates is no longer a CP eigenstate, and hence CP violation can occur.

In total the Standard Model without neutrino masses has 19 free parameters, 6 quark masses, 3 lepton masses, 4 CKM–mixing matrix parameters, 3 gauge coupling constants, $g_s$, $g$ and $g'$, the QCD vacuum angle $\theta_{\mathrm{QCD}}$ and two parameters from the Higgs potential, the Higgs self coupling and the Higgs quadratic coupling. For the Standard Model with neutrino masses, there are also an additional 9 parameters, 3 neutrino masses and 6 MNS–mixing matrix parameters. The MNS–mixing matrix is analogous to the CKM matrix, but mixes the neutrinos, rather than quarks. Using these as inputs, the Standard Model can then be used to make predictions for other quantities. The success of the model can then be gauged by how accurately these predictions agree with experiment.

### 1.1.4 Successes of the Standard Model

One example of an accurate prediction from the Standard Model is the prediction for the anomalous magnetic moment of the muon. The spin ($\vec{s}$) and magnetic dipole moment ($\vec{\mu}$) are aligned as,

$$\vec{\mu} = g \left( \frac{e}{2m_\mu} \right) \vec{s}, \tag{1.27}$$

where $e$ is the electric charge of the muon, and $m_\mu$ the mass. The factor $g$ is known as the gyromagnetic ratio; and in the classic Dirac theory, the gyromagnetic ratio is exactly 2. In the Standard Model, quantum corrections lead to a small deviation from $g = 2$, parametrised by the anomalous magnetic moment, $a_\mu = \frac{1}{2}(g_\mu - 2)$.

Many experiments have been undertaken to measure the muon's anomalous magnetic moment. The latest results from experiments at Brookhaven National Laboratory [16], give $a_\mu = 11659208.0(5.4)(3.3) \times 10^{-10}$, where the first error is statistical and the second is systematic. This is calculated by studying the precession of the spin axis of muons, as they circle around a storage ring in a constant magnetic field. For comparison, the latest standard model prediction is $a_\mu = 116591788(2)(46)(35) \times 10^{-11}$ [17], where now the errors are from the different contributions to the magnetic moment. The first error is from the electroweak contributions, while the second and third are from lowest order and higher order hadronic contributions respectively. This gives an agreement between experiment and theory up to 6 significant figures. The difference between experimental measurements and theoretical predictions is therefore,

$$\Delta a_\mu = a_\mu^{\text{exp}} - a_\mu^{\text{th}} = 292(63)(58) \times 10^{-11}, \tag{1.28}$$

a discrepancy of only $3.4\sigma$ at this high degree of accuracy.

A second prediction from the Standard Model are the accurate fits to numerous data sources giving the values of the CKM matrix elements. In the Standard Model, the unitarity of the CKM matrix elements gives us several consistency checks,

$$\sum_i V_{ij} V_{ik}^* = \delta_{jk}, \quad \sum_j V_{ij} V_{kj}^* = \delta_{ik}. \tag{1.29}$$

Where the $\delta$ does not vanish, we get relations such as, $|V_{ud}|^2 + |V_{us}|^2 + |V_{ub}|^2 = 1$. Using $V_{ud} = 0.97418(27)$ and $V_{us} = 0.2255(19)$ [17]; and ignoring $V_{ub} \simeq 1 \times 10^{-5}$ as it is negligible in comparison, gives:

$$|V_{ud}|^2 + |V_{us}|^2 + |V_{ub}|^2 = 0.9999(10). \tag{1.30}$$

This is in extremely good agreement with unitarity.

Where the $\delta$ vanishes, the equations can be represented by triangles in the complex plane. The most commonly used unitarity triangle is:

$$V_{ud} V_{ub}^* + V_{cd} V_{cb}^* + V_{td} V_{tb}^* = 0, \tag{1.31}$$

where each term corresponds to one side of the triangle. If we divide through by the best known term ($V_{cd} V_{cb}^*$), we get a triangle with two vertices fixed at exactly (0,0) and (1,0) and the third vertex at some co-ordinates ($\bar{\rho}$, $\bar{\eta}$). Figure 1.2 shows many experimental constraints upon the lengths of the sides of the triangle, and upon the internal angles of the triangle [17].

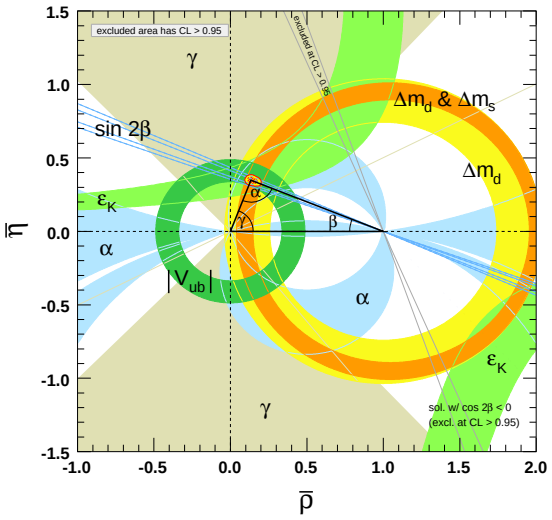


Figure 1.2: Constraints on the $\bar{\rho}, \bar{\eta}$ plane. The shaded areas have 95% CL. Figure taken from [17]

## 1.2 Baryon number

An important conserved quantum number of the Standard Model Lagrangian is baryon number. Quarks have baryon number $+\frac{1}{3}$, antiquarks have baryon number $-\frac{1}{3}$ and the remaining particles of the Standard Model (leptons and gauge bosons) have baryon number 0. Therefore, baryons (which consist of three quarks) have baryon number +1 and mesons (a quark and an antiquark) have baryon number 0. Proton decay, by the reaction $p \to \pi^0, e^+$ for example, is therefore ruled out in the Standard Model as it violates baryon number conservation.

To see why baryon number is conserved in the Standard Model, we take a closer look at the symmetries of the Standard Model Lagrangian from Eq. 1.1. For $N_f$ flavours of massless quarks, Eq. 1.4 has a $U(N_f)_L \times U(N_f)_R$ flavour symmetry,

$$f_L^i \to U_L^{ij} f_L^j, \quad f_R^i \to U_R^{ij} f_R^j, \tag{1.32}$$

where $f_{L/R}$ is a quark field with flavour given by the indices $i, j$ which now run from $1 \ldots N_f$.

If we now add a mass term for the quarks,

$$\mathcal{L} = m_{u^i} \bar{u}_R^i u_L^i + m_{u^i} \bar{u}_L^i u_R^i + m_{d^i} \bar{d}_R^i d_L^i + m_{d^i} \bar{d}_L^i d_R^i, \tag{1.33}$$

then this breaks the $U(N_f) \times U(N_f)_R$ symmetry, leaving a global $U(1)$ vector symmetry,

$$f_L^i \to \mathrm{e}^{i\phi/3} f_L^i, \quad f_R^i \to \mathrm{e}^{i\phi/3} f_R^i, \tag{1.34}$$

where the factor of 1/3 is purely for convention, so that the baryon number of the proton will be +1. There is a conserved Noether current given by,

$$j^\mu = \sum_i \frac{1}{3}\left(\bar{u}^i\gamma^\mu u^i + \bar{d}^i\gamma^\mu d^i\right), \tag{1.35}$$

and a conserved charge given by,

$$\begin{aligned} Q = \int d^4x j^0 &= \sum_i \frac{1}{3}\int d^4x \left(\bar{u}^i\gamma^0 u^i + \bar{d}^i\gamma^0 d^i\right) \\ &= \sum_i \frac{1}{3}\int d^4x \left(u^{\dagger,i}u^i + d^{\dagger,i}d^i\right) \\ &= \frac{1}{3}\sum_i \left(N_u^i + N_d^i\right), \end{aligned} \tag{1.36}$$

where $N_u^i$ and $N_d^i$ are the number of up type quarks and down type quarks respectively. Combined with the factor of $\frac{1}{3}$, this means the conserved charge is baryon number. This conserved charge is a consequence of a symmetry of the matter content of the standard model. As we shall see in Section 1.3, if we change the representation of the matter content, then this symmetry will no longer exist.

## 1.3 Grand Unification

Although the Standard Model has been very successful, it leaves many unanswered questions. Why are the electroweak and strong interactions different? Why does the Standard Model have so many arbitrary parameters? Why are there three generations of quarks and leptons? Grand Unified Theories (GUTs) attempt to address these concerns.

A GUT attempts to embed the strong and electroweak interactions within a single theory. The interactions in the model are described by a single gauge group with a single unified coupling constant at the GUT scale. At lower energies this is then spontaneously broken to the $SU(3) \times SU(2) \times U(1)$ structure that we observe in nature. The three different couplings we observe are a consequence of the theory, and not an experimental input.

The Standard Model couplings $g, g', g_s$ are running couplings, they change with energy. The left hand plot of Figure 1.3 shows the running of the three couplings and how close they come to meeting at a point $\approx 10^{15}$GeV. If we add new physics beyond the Standard Model at a scale of $\sim$1 TeV, then this changes the running of the couplings through virtual loop corrections involving the new heavier particles. For example, the right hand plot of Figure 1.3 shows the running of the three couplings in the Minimal Supersymmetric Standard Model (MSSM) [18, 19, 20, 21]. In this case, the coupling constants come even closer to unification at a slightly

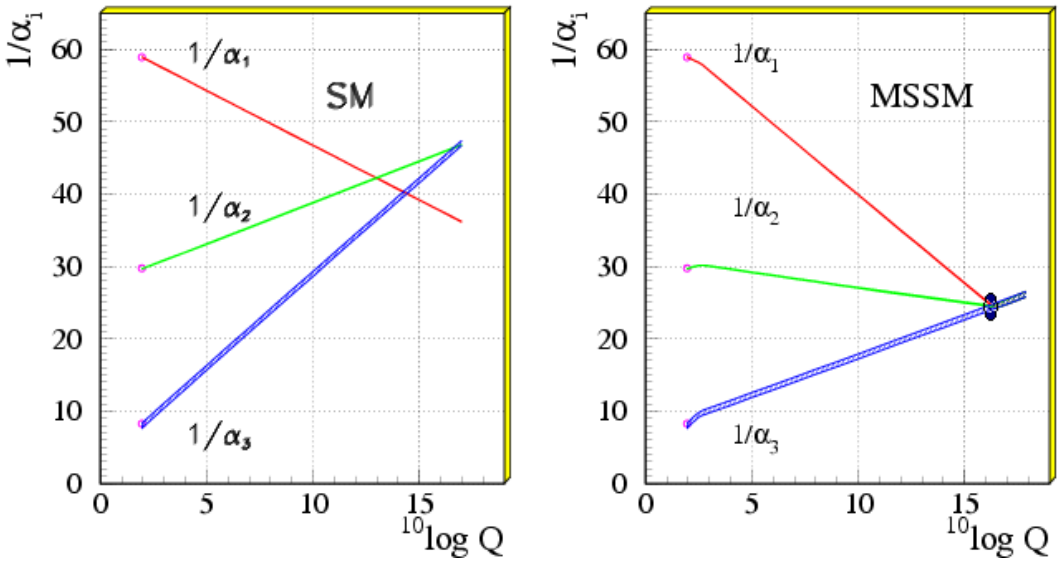


Figure 1.3: The approximate gauge coupling unification in the Standard Model (left) and the MSSM (right). Instead of the standard model couplings $g, g', g_s$, both plots show $\alpha_{1,2,3}$, where $\alpha_1 = \frac{g^2 \sin^2\theta_W}{4\pi}$, $\alpha_2 = \frac{g^2 \cos^2\theta_W}{4\pi}$ and $\alpha_3 = \frac{g_s^2}{4\pi}$. $\sin^2\theta_W$ is related to the couplings $g$ and $g'$ by $\sin^2\theta_W = \frac{g'^2}{g^2+g'^2}$ Figure taken from [17]

higher scale $\approx 10^{16}$GeV.

Although there are many different classes of GUTs, they all share many of the same features. One such feature is baryon number violation. As we saw in Section 1.2, baryon number conservation is a consequence of the symmetry of the matter content of the standard model Lagrangian. In grand unified theories, the matter content is arranged differently, in multiplets containing quarks and leptons. In the Standard Model, our weak multiplets contained only quarks or only leptons, so these were unable to mix. In GUTs, this is no longer the case. The violation of baryon number leads to a prediction common to all GUTs. Unlike in the Standard Model where the proton is stable, in GUTs, protons can decay.

## 1.4 Proton Decay

Experiments have searched for proton decay and although this has not yet been directly observed, this lack of observation constrains the proton lifetime. The proton lifetime predicted by a particular GUT is therefore a test of the validity of that GUT.

By integrating out the heavy degrees of freedom from the GUT, we can write down an effective Lagrangian expressed in terms of only the usual Standard Model fields. Generically,

this will be of the form [22],

$$\mathcal{L}^{\Delta B} = \sum_{d=1,2} \sum_{i=1}^{4} C_d^{(i)} Q_d^{(i)} + \sum_{d=1,2} \sum_{i=1}^{6} \tilde{C}_d^{(i)} \tilde{Q}_d^{(i)}, \tag{1.37}$$

where $d$ denotes the generation of the lepton produced in the decay, $i$ is a label for the baryon number violating operators and the coefficients of these operators $C_d^{(i)}$ and $\tilde{C}_d^{(i)}$ are known as Wilson coefficients. The first sum contains four operators, $Q^{(i)}$, for decays to nonstrange final states. The second sum contains 6 operators, $\tilde{Q}^{(i)}$, for decays to strange final states. These operators were identified on symmetry grounds in [23, 24, 25], and will be discussed in more detail in Section 2.4.

For a particular GUT, the decay width $\Gamma$ for a proton $N$ decaying to a pseudoscalar meson $M$ and a lepton $l$ is,

$$\Gamma(N \to M + l) = \frac{1}{16\pi} \frac{1}{m_N} \left[ 1 - \left( \frac{m_M}{m_N} \right)^2 \right] \left| \sum_i C^i \langle M, l | \mathcal{O}^i | N \rangle \right|^2, \tag{1.38}$$

where $m_N$ is the proton mass, $m_M$ is the pseudoscalar meson mass and $\langle M, l | \mathcal{O}^i | N \rangle$ are QCD matrix elements between the Proton and Meson states. Depending on the process, different operators $\mathcal{O}^i$ (and corresponding Wilson coefficients) will contribute to the sum. These matrix elements, and the exact relation to the form factors we are interested in will be discussed in detail in Chapters 2 and 6.

Note that the sum in Eq. 1.38 is decomposed into Wilson coefficients which will vary depending on which GUT we are dealing with, and matrix elements which are the same for all GUTs. The aim in this thesis will be to calculate these matrix elements, to allow the proton decay width, and hence the lifetime $\tau = 1/\Gamma$ to be determined.

### 1.4.1 The minimal $SU(5)$ GUT

The minimal $SU(5)$ GUT was proposed by H. Georgi and S. L. Glashow, in 1974 [26]. In this GUT, the quarks and leptons sit in two irreducible representations, a 10 ($Q$, $u^c$, $e^c$) and a $\bar{5}$ ($d^c$, $L$), where the superscript c represents charge conjugation.

In the gauge sector, $SU(5)$ has 24 generators corresponding to 24 gauge bosons, compared with 12 from the Standard Model. The extra 12 gauge bosons are usually split into two sets of 6 denoted as $X$ and $Y$. As these new gauge bosons carry colour and flavour, they may mediate Baryon and Lepton number violating interactions, such as the interaction shown in Figure 1.4(a).

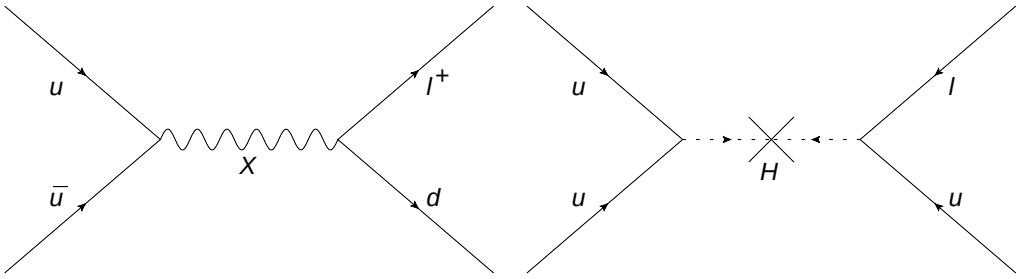


(a) X boson (b) Colour triplet Higgs boson

Figure 1.4: Baryon number violating interactions

### 1.4.2 Other GUTs

The Pati–Salam model [27] adds a fourth quark colour and identifies this with the leptons.

In Supersymmetric (SUSY) GUTs [28], proton decay can also be mediated by additional Higgs bosons contained in an enlarged Higgs sector (see Figure 1.4(b)), the simplest Supersymmetric GUT is the Supersymmetric $SU(5)$ GUT.

GUTs based upon larger Groups, such as $SO(10)$ [29, 30, 31] are also possible, but these will still contain the same proton decay interactions as in Figures 1.4(a) and 1.4(b). Different GUTs will predict different lifetimes due to the differences in the Wilson Coefficients from the effective Low–Energy Lagrangian.

## 1.5 Experimental evidence for GUTs

Experiments such as Super-Kamiokande have been searching for proton decay. Though proton decay has not yet been observed, the lack of observation can be used to set stringent limits on the proton partial lifetimes [32, 33], see Table 1.3.

| Decay Mode | Partial Lifetime Bound (years) |
|---|---|
| $p \to e^+\pi^0$ | $> 8.2 \times 10^{33}$ |
| $p \to \mu^+\pi^0$ | $> 6.6 \times 10^{33}$ |
| $p \to \bar{\nu}K^+$ | $> 2.3 \times 10^{33}$ |
| $n \to \bar{\nu}K^0$ | $> 1.3 \times 10^{32}$ |
| $p \to \mu^+K^0$ | $> 1.3 \times 10^{33}$ |
| $p \to e^+K^0$ | $> 1.0 \times 10^{33}$ |

Table 1.3: The minimum bound on the partial lifetimes for proton decay via various decay modes. Lifetimes were taken from Ref. [32] for decay modes $p \to e^+\pi^0$ and $p \to \mu^+\pi^0$, and from Ref. [33] for decay modes $p \to \bar{\nu}K^+$, $n \to \bar{\nu}K^0$, $p \to \mu^+K^0$, $p \to e^+K^0$. All bounds are at a 90% confidence level.

Together, the experimental lifetimes and measurements of the QCD form factors from Eq. 1.38 can be used to constrain GUT parameters, or even entirely rule out a particular GUT. The minimal $SU(5)$ and minimal SUSY $SU(5)$ GUTs have both already been ruled out [34, 35] because of the experimental bounds on the proton lifetime.

## 1.6 Summary

The conservation of baryon number in the Standard Model is a consequence of the $U(1)$ global symmetry of the matter content of the Standard Model Lagrangian. In GUTs, this accidental symmetry no longer exists to protect baryon number, leading to proton decay mediated by massive gauge bosons at the GUT scale. Although heavily suppressed, this proton decay should still be observed in current experiments such as that at Super–Kamiokande. The current non-observation of proton decay places strong constraints on the proton lifetime, which can potentially be used to rule out certain classes of GUT.

# Chapter 2

# Quantum Chromodynamics

In this thesis, I shall concentrate on the theory of strong interactions, quantum chromodynamics (QCD), as this is what will be important for calculating the proton decay matrix elements. In this chapter, I shall first discuss the QCD Lagrangian in Section 2.1 and then discuss some of its important symmetries in Section 2.2. I then move on to discuss Chiral Perturbation Theory ($\chi$PT) in Section 2.3. How to incorporate proton decay from GUTs into QCD is discussed in Sections 2.4. Finally in Section 2.5, we briefly discuss the need for renormalisation of scale dependent quantities, such as the proton decay matrix elements.

## 2.1 The QCD Lagrangian

The QCD Lagrangian is:

$$L_{QCD} = -\frac{1}{4}\mathrm{Tr}\left[F^a_{\mu\nu}F^{a\mu\nu} + \bar{\psi}^i_{\alpha f}(i\not{D}^{ij}_{\alpha\beta ff'} - m^{ij}_{\alpha\beta ff'})\psi^j_{\alpha f'}\right], \tag{2.1}$$

where the indices $a, b, c$ represent colour in the adjoint representation, while the indices $i, j, k$ will represent colour in the fundamental representation. The indices $f, f'$ represent flavour, $\alpha$, $\beta$ are spinor indices and $\mu$, $\nu$ are space-time indices and the trace is over all indices. (this follows the conventions in Ref. [5]).

The first term in the Lagrangian contains $F^{a\mu\nu}$, the field strength tensor, which is constructed from the gauge fields $A^{a\mu}$,

$$F^{a\mu\nu} = \partial^\mu A^{a\nu} - \partial^\nu A^{a\mu} + g f^{abc} A^{b\mu} A^{c\nu}, \tag{2.2}$$

where $g$ is the strong coupling constant and $f^{abc}$ are the structure constants of the Lie algebra for $SU(N_c)$ where $N_c$ is the number of colours. The field strength tensor can also be formed from the commutator,

$$F^{a\mu\nu}T^a = [D^\mu, D^\nu], \tag{2.3}$$

where $T^a$ are the generators of the group $SU(N_c)$ and $D^\mu$ is the covariant derivative,

$$D^\mu = \partial^\mu + igA^{a\mu}T^a. \tag{2.4}$$

$F^a_{\mu\nu}F^{a\mu\nu}$ contains the kinetic term and self interactions of the gauge fields $A^{a\mu}$, which for QCD are the gluons. Both $F^{a\mu\nu}$ and $A^{a\mu}$ belong to the Lie algebra of the group $SU(N_c)$.

The second term in the Lagrangian is the fermionic term. Here the $\psi$ and $\bar{\psi}$ represent quark and antiquark fields. In 4 dimensions they are 4 component spinors, $\psi_\alpha$, $\alpha = 1 \ldots 4$. They are also charged under colour, $\psi^a_\alpha$, $a = 1 \ldots N_c$. If there are several flavours, then we have $\psi^i_{\alpha f}$, with $f = 1 \ldots N_f$, where $N_f$ is the number of flavours. The matrix $m$ is the quark mass matrix, it is diagonal in flavour, spinor and colour indices. Finally the slashed notation ($\not{D}$) means,

$$\not{D} = \gamma_\mu D^\mu, \tag{2.5}$$

where $\gamma_\mu$ are the Dirac $\gamma$ matrices, defined by the anticommutation relations,

$$\{\gamma_\mu, \gamma_\nu\} = 2g_{\mu\nu}, \tag{2.6}$$

and where $g_{\mu\nu}$ is the metric in Minkowski space.

## 2.2 Symmetries

We have already seen that baryon number is conserved in the Standard Model and hence in QCD. But the QCD Lagrangian is also invariant under a number of other important symmetries.

### 2.2.1 Gauge symmetry

The QCD Lagrangian is invariant under a local gauge transformation,

$$\psi(x) \rightarrow \psi'(x) = G(x)\psi(x), \tag{2.7}$$

$$\bar{\psi}(x) \rightarrow \bar{\psi}'(x) = \bar{\psi}(x)G^{-1}(x), \tag{2.8}$$

$$A^{a\mu}T^a \rightarrow A'^{a\mu}T^a = G(x)A^{a\mu}T^aG^{-1}(x) + \left(\frac{i}{g}\partial^\mu G(x)\right)G^{-1}(x), \tag{2.9}$$

$$F^{a\mu\nu}T^a \rightarrow F'^{a\mu\nu}T^a = G(x)F^{a\mu\nu}T^aG^{-1}(x), \tag{2.10}$$

where $G(x) = \mathrm{e}^{i\omega^a(x)T^a}$ is an element of the gauge group ($G(x) \in SU(N_c)$) and the quark fields $\psi(x)$ and $\bar{\psi}(x)$ have had all indices suppressed. Note that if the QCD Lagrangian contained just a derivative, rather than a covariant derivative, the action would not be invariant under this local gauge transformation.

### 2.2.2 Chiral Symmetry

In the limit of massless quarks, the QCD Lagrangian is also invariant under independent $U(N_f)$ rotations of the left and right handed fields.

$$\begin{aligned} \psi_L &\rightarrow \mathrm{e}^{(i\omega_L^a \lambda^a)}\, \psi_L, \\ \psi_R &\rightarrow \mathrm{e}^{(i\omega_R^a \lambda^a)}\, \psi_R, \end{aligned} \tag{2.11}$$

where $\lambda^a$ are the generators of $U(N_f)$, acting upon flavour space.

This $U(N_f) \times U(N_f)$ symmetry can be decomposed into $SU(N_f)_L \times SU(N_f)_R \times U(1)_V \times U(1)_A$. As we saw in Section 1.2 the $U(1)_V$ symmetry is associated with baryon number conservation and is not broken even when the quarks are given a mass. The $SU(N_f)_L \times SU(N_f)_R$ is known as chiral symmetry and is spontaneously broken by the quark condensate,

$$\langle \bar{\psi}\psi \rangle = \langle \bar{\psi}_R \psi_L + \bar{\psi}_L \psi_R \rangle, \tag{2.12}$$

to an $SU(N_f)_V$ symmetry,

$$\begin{aligned} \psi_L &\rightarrow \mathrm{e}^{(i\omega^a \lambda^a)}\, \psi_L, \\ \psi_R &\rightarrow \mathrm{e}^{(i\omega^a \lambda^a)}\, \psi_R. \end{aligned} \tag{2.13}$$

This symmetry is then explicitly broken by the quark masses. The $u$, $d$ and to some extent $s$ quarks are all much lighter than the typical scale of hadrons $\sim$ 1GeV and so they can be thought of as approximately massless. The QCD Lagrangian therefore exhibits an approximate $SU(2)$ or $SU(3)$ chiral symmetry.

For two flavours of massless quarks, $u$ and $d$, the $SU(2) \times SU(2)$ symmetry is therefore broken to an $SU(2)_V$ symmetry, this is known as isospin. Goldstone's theorem [10] states that whenever a symmetry is spontaneously broken, one massless scalar particle appears in the theory for each broken generator of the spontaneously broken symmetry group. These are known as Goldstone bosons and for the case of $SU(2) \times SU(2)$, these are the pions, $\pi^{\pm}, \pi^0$. As the $u$ and $d$ quarks are only approximately massless, the $SU(2) \times SU(2)$ symmetry is not exact, and so the pions do have a small mass. They are therefore known as pseudo Goldstone bosons.

For three flavours of massless quarks, $u$, $d$ and $s$, the $SU(3) \times SU(3)$ symmetry is therefore broken to an $SU(3)_V$ symmetry, spontaneously breaking 8 generators and leading to 8 pseudo Goldstone bosons. In this case, as well as the pions, we have the kaons ($K^{\pm}$, $K^0$, $\bar{K^0}$) and the $\eta$. The $s$ quark has a higher mass than the $u$ and $d$ quarks, so this approximate symmetry holds less well. The masses of the $K^{\pm}$, $K^0$, $\bar{K^0}$ and the $\eta$ are therefore higher than the masses of the pions.

### 2.2.3 Classification of Hadrons

The bound states of QCD are the hadrons. These consist of several valence quarks, bound together to form a colourless particle. There are therefore two different types of hadron; mesons consist of one quark and one antiquark, while baryons consist of 3 quarks, one of each colour. Different mesons and baryons can be classified according to their valence quark flavour content.

For three flavours of quarks, there are nine possible meson flavour combinations of a quark and an antiquark. These can be decomposed into a meson octet and a singlet,

$$3 \otimes \bar{3} = 8 \oplus 1. \tag{2.14}$$

These are irreducible representations of $SU(3)$. The octet (see Figure 2.1) contains the eight pseudo–goldstone bosons discussed in the previous section, while the singlet contains the $\eta\prime$.

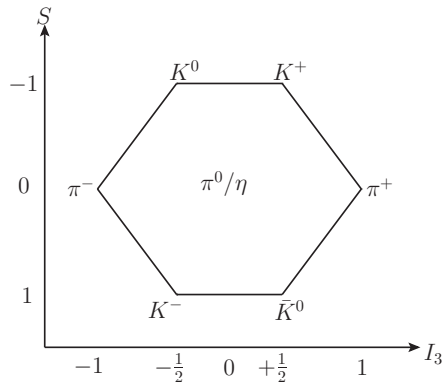


Figure 2.1: Showing the pseudo–scalar meson octet, arranged according to strangeness $S$ and isospin $I_3$.

Baryons can also be classified in the same way, where this time the 27 flavour combinations of a three quark state can be decomposed into irreducible representations of $SU(3)$ as follows,

$$3 \otimes 3 \otimes 3 = 10 \oplus 8 \oplus 8 \oplus 1. \tag{2.15}$$

Of the four multiplets, the decuplet contains the states which are completely symmetric in quark flavour, while the singlet contains the completely flavour antisymmetric state. The two octets contain the states which are antisymmetric under interchange of two of the three quarks flavours. The first octet, which contains the proton and neutron, is shown in Figure 2.2.

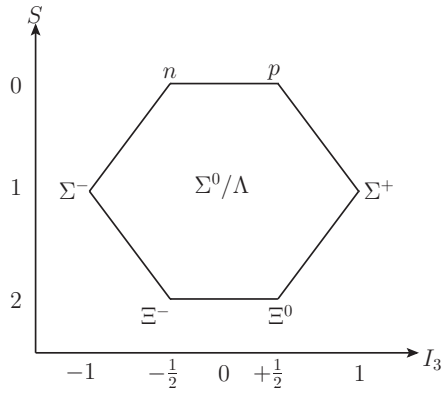


Figure 2.2: Showing the classification of baryons into an octet. The second octet, the decuplet and the singlet which are also part of the baryon decomposition are not shown. The octet shown is arranged according to strangeness $S$ and isospin $I_3$.

## 2.3 Chiral Perturbation Theory

As we have seen, the QCD Lagrangian exhibits an approximate chiral symmetry for the lightest three flavours. Due to quark confinement, the states in the spectrum of QCD are the baryons and mesons, rather than individual quarks. At low energies we can therefore write an effective field theory with only light mesons, baryons and their interactions. This effective theory is known as Chiral Perturbation Theory ($\chi$PT). The following arguments are based on those appearing in Ref. [22]

In order to develop $\chi$PT, we define a matrix $\phi$ containing the meson octet of pseudo Goldstone bosons,

$$\phi = \begin{pmatrix} \pi^0 + \frac{1}{\sqrt{3}}\eta & \sqrt{2}\pi^+ & \sqrt{2}K^+ \\ \sqrt{2}\pi^- & -\pi^0 + \frac{1}{\sqrt{3}}\eta & \sqrt{2}K^0 \\ \sqrt{2}K^- & \sqrt{2}\bar{K}^0 & -\sqrt{\frac{2}{3}}\eta \end{pmatrix}. \tag{2.16}$$

We can then form the $SU(3)$ matrix $\Sigma$,

$$\Sigma = \mathrm{e}^{\frac{2i\phi}{f}}, \tag{2.17}$$

which transforms under an $SU(3)_L \times SU(3)_R$ transformation as,

$$\Sigma \to L\Sigma R^\dagger, \tag{2.18}$$

where $L$ is an element of $SU(3)_L$ and $R$ an element of $SU(3)_R$.

Baryons can also be included in the effective theory, by again collecting together the lightest

baryon octet into the matrix,

$$B = \begin{pmatrix} \frac{1}{\sqrt{2}}\Sigma^0 + \frac{1}{\sqrt{6}}\Lambda^0 & \Sigma^+ & p \\ \Sigma^- & -\frac{1}{\sqrt{2}}\Sigma^0 + \frac{1}{\sqrt{6}}\Lambda^0 & n \\ \Xi^- & \Xi^0 & -\sqrt{\frac{2}{3}}\Lambda^0 \end{pmatrix}. \tag{2.19}$$

These baryon fields transform under an $SU(3)_L \times SU(3)_R$ transformation as,

$$B \to UBU^\dagger, \tag{2.20}$$

with $U$ defined from the transformations of the matrix $\xi$,

$$\xi = \mathrm{e}^{\frac{i\phi}{f}} \to L\xi U^\dagger = U\xi R^\dagger. \tag{2.21}$$

We form a general $SU(3)_L \times SU(3)_R$ invariant Lagrangian, by writing all possible terms for interactions involving strong interactions of baryons and mesons,

$$\begin{aligned} \mathcal{L}_0 =& \frac{f^2}{8}\mathrm{Tr}(\partial_\mu\Sigma)(\partial_\mu\Sigma^\dagger) + \mathrm{Tr}\bar{B}(\gamma_\mu\partial_\mu + M_B)B \\ &+ \frac{1}{2}\mathrm{Tr}\bar{B}\gamma_\mu\left[\xi\partial_\mu\xi^\dagger + \xi^\dagger\partial_\mu\xi\right]B + \frac{1}{2}\mathrm{Tr}\bar{B}\gamma_\mu B\left[(\partial_\mu\xi)\,\xi^\dagger + \left(\partial_\mu\xi^\dagger\right)\xi\right] \\ &- \frac{1}{2}(D-F)\mathrm{Tr}\bar{B}\gamma_\mu\gamma_5 B\left[(\partial_\mu\xi)\,\xi^\dagger - \left(\partial_\mu\xi^\dagger\right)\xi\right] \\ &+ \frac{1}{2}(D+F)\mathrm{Tr}\bar{B}\gamma_\mu\gamma_5\left[\xi\partial_\mu\xi^\dagger - \xi^\dagger\partial_\mu\xi\right]B, \end{aligned} \tag{2.22}$$

where the $i,j$th element of the matrix $\bar{B}$ is given by

$$\bar{B}_{ij} = \gamma_0 B^\dagger_{ij}. \tag{2.23}$$

The first term in this Lagrangian, when expanded to lowest order, gives a kinetic term for the mesons. Similarly the second term in the Lagrangian is a kinetic term for the baryons. The remaining terms give interactions between the mesons and baryons.

The low energy constants, $f, D, F$ encode the information on non–perturbative strong dynamics, and need to be extracted from phenomenological analyses. In particular, following the notation in Ref. [22], $f$ is the pion decay constant in the chiral limit, 130(5) MeV [17]. The combination $F+D$ yields the nucleon axial charge, $g_A = 1.2695(29)$ [17], while the combination $F-D$ is related to the ratio of the zero–momentum form factors for semileptonic hyperon decay, $g_1/f_1$ [36]. Together these give, $F = 0.47(1)$ and $D = 0.80(1)$.

So far we have assumed the quarks are exactly massless. We can add in chiral symmetry

breaking terms to the effective theory by introducing a diagonal quark mass matrix:

$$M = \begin{pmatrix} m_u & & \\ & m_d & \\ & & m_s \end{pmatrix}, \tag{2.24}$$

and then adding the following symmetry breaking terms:

$$\begin{aligned}\mathcal{L}_1 = &- v^3 \mathrm{Tr}\left(\Sigma^\dagger M + M\Sigma\right) - a_1 \mathrm{Tr}\bar{B}\left(\xi^\dagger M \xi^\dagger + \xi M \xi\right) B - a_2 \mathrm{Tr}\bar{B}B\left(\xi^\dagger M \xi^\dagger + \xi M \xi\right) \\ &- b_1 \mathrm{Tr}\bar{B}\gamma_5\left(\xi^\dagger M \xi^\dagger - \xi M \xi\right) B - b_2 \mathrm{Tr}\bar{B}\gamma_5 B\left(\xi^\dagger M \xi^\dagger - \xi M \xi\right).\end{aligned} \tag{2.25}$$

The low energy parameters $a_1$ and $a_2$ are symmetry–breaking parameters which are not required in this work. The parameters $b_1$,$b_2$ are not precisely determined, and where they are required, we will set them to 0. This will therefore introduce an extra source of systematic error.

## 2.4 Proton decay in QCD

As we have already seen, a GUT will have baryon number violating terms which are not naturally present in the QCD Lagrangian. By integrating out the heavy particles from the GUT Lagrangian, we are left with a low–energy effective Lagrangian describing nucleon decay written only in terms of the QCD fundamental fields.

The baryon number violating terms added to the QCD Lagrangian can be written generically as in Eq. 1.37,

$$\mathcal{L}^{\Delta B} = \sum_{d=1,2}\sum_{i=1}^{4} C_d^{(i)} Q_d^{(i)} + \sum_{d=1,2}\sum_{i=1}^{6} \tilde{C}_d^{(i)} \tilde{Q}_d^{(i)}. \tag{2.26}$$

Refs. [23, 24, 25] identified the operators, $Q_i$ and $\tilde{Q}_i$ on symmetry grounds. These operators must contain at least 3 quark fields in order to be a colour singlet, and must contain at least four fermion fields in order to be a Lorentz scalar. The lowest dimension operators which contribute to proton decay are therefore dimension 6, and contain 3 quark fields and a lepton field. Although higher dimension operators with more fields / derivatives are possible, these are suppressed by additional powers of the GUT–scale mass, and hence are ignored.

There are only four different types of dimension 6 operators for proton decay,

$$\begin{aligned}\mathcal{O}^{(1)}_{abcd} &= (D_a^i, U_b^j)_R (q_c^{k\alpha}, l_d^\beta)_L \epsilon^{ijk}\epsilon^{\alpha\beta}, \\ \mathcal{O}^{(2)}_{abcd} &= (q_a^{i\alpha}, q_b^{j\beta})_L (U_c^k, l^d)_R \epsilon^{ijk}\epsilon^{\alpha\beta}, \\ \tilde{\mathcal{O}}^{(4)}_{abcd} &= (q_a^{i\alpha}, q_b^{j\beta})_L (q_c^{k\gamma}, l_d^\delta)_L \epsilon^{ijk}\epsilon^{\alpha\beta}\epsilon^{\gamma\delta}, \\ \mathcal{O}^{(5)}_{abcd} &= (D_a^i, U_b^j)_R (U_c^k, l^d)_R \epsilon^{ijk},\end{aligned} \tag{2.27}$$

where $l$ is a generic lepton field, $q$ is a left handed quark field, $U$ and $D$ are up and down type right handed fields respectively, $a, b, c, d$ are generation indices, labelling $u, c, t$ or $e, \mu, \tau$ etc, $i, j, k, l$ label colour and $\alpha, \beta, \gamma, \delta$ are $SU(2)$ indices. The inner product $(x, y)$ denotes $(x^T C P_{R/L} y)$. $C$ is the charge conjugation matrix, and $P_{R/L} = \frac{1}{2}(1 \pm \gamma_5)$ are the right and left handed projection matrices. The operators $Q^i, \tilde{Q}^i$ from Eq. 1.37 are just linear combinations of the four operators in Eq. 2.27.

There are four linearly independent operators, $Q^i$, which contribute to nucleon decay to nonstrange final states,

$$\begin{aligned} Q^{(1)} &= \mathcal{O}^{(1)}_{1111}, \\ Q^{(2)} &= -\frac{1}{2}\mathcal{O}^{(2)}_{1111}, \\ Q^{(3)} &= \tilde{\mathcal{O}}^{(4)}_{1111}, \\ Q^{(4)} &= \mathcal{O}^{(5)}_{1111}. \end{aligned} \tag{2.28}$$

For nucleon decay to strange final states there are 6 linearly independent operators, $\tilde{Q}^i$, which are given by,

$$\begin{aligned} \tilde{Q}^{(1)} &= \mathcal{O}^{(1)}_{2111}, \\ \tilde{Q}^{(2)} &= \mathcal{O}^{(1)}_{1121}, \\ \tilde{Q}^{(3)} &= \mathcal{O}^{(2)}_{2111}, \\ \tilde{Q}^{(4)} &= 2\tilde{\mathcal{O}}^{(4)}_{2111} + \tilde{\mathcal{O}}^{(4)}_{1211}, \\ \tilde{Q}^{(5)} &= \tilde{\mathcal{O}}^{(4)}_{2111} - \tilde{\mathcal{O}}^{(4)}_{1211}, \\ \tilde{Q}^{(6)} &= \mathcal{O}^{(5)}_{2111}. \end{aligned} \tag{2.29}$$

In order to calculate the decay width for proton decay, we need to evaluate the amplitude, $\langle M, l|\mathcal{O}|N\rangle$, Where $\mathcal{O}$ is one of the baryon violating operators from Eqs. 2.28 and 2.29. We can factor out the leptonic part of the matrix element to give,

$$\langle M, l|\mathcal{O}|N\rangle = \langle M|\mathcal{O}|N\rangle_{\mathrm{QCD}} \bar{u}(q, s),$$

where $\bar{u}(q, s)$ is a Dirac spinor for the outgoing antilepton of momentum $q$, spin $s$ and mass $m_l$. $\langle M|\mathcal{O}|N\rangle_{\mathrm{QCD}}$ is a pure QCD matrix element between nucleon and meson states. This is a three

quark operator, whose structure is given by that in Eqs. 2.27, but without the antilepton field,

$$\begin{aligned}
\mathcal{O}^{RL}_{fgh} &= (\psi_f\psi_g)_R(\psi_h)_L = \epsilon^{ijk}(\psi^{i,T}_f C P_R \psi^j_g) P_L \psi^k_h, \\
\mathcal{O}^{LR}_{fgh} &= (\psi_f\psi_g)_L(\psi_h)_R = \epsilon^{ijk}(\psi^{i,T}_f C P_L \psi^j_g) P_R \psi^k_h, \\
\mathcal{O}^{LL}_{fgh} &= (\psi_f\psi_g)_L(\psi_h)_L = \epsilon^{ijk}(\psi^{i,T}_f C P_L \psi^j_g) P_L \psi^k_h, \\
\mathcal{O}^{RR}_{fgh} &= (\psi_f\psi_g)_R(\psi_h)_R = \epsilon^{ijk}(\psi^{i,T}_f C P_R \psi^j_g) P_R \psi^k_h. \qquad (2.30)
\end{aligned}$$

We use the notation $\mathcal{O}^{\Gamma\Gamma'}_{fgh}$ to represent the possible spin ($\Gamma, \Gamma' = R, L$) and flavour ($f, g, h = u, d, s$) of the possible baryon number violating operators.

It is important to note that the operators in Eq. 2.30 contain only Standard Model quark fields. Therefore, in order to calculate the matrix elements in Eq. 1.38, we do not need to add an explicit, GUT dependent, baryon number violating sector to the QCD Lagrangian. All of the GUT–scale physics is contained within the Wilson coefficients.

A parity transformation gives the following relation between matrix elements of opposite chirality,

$$\begin{aligned}
\langle M(\vec{p})|\mathcal{O}^{RL}|N(\vec{k},s)\rangle &= -\langle M(\vec{p})|\mathcal{O}^{LR}|N(\vec{k},s)\rangle, \qquad (2.31) \\
\langle M(\vec{p})|\mathcal{O}^{LL}|N(\vec{k},s)\rangle &= -\langle M(\vec{p})|\mathcal{O}^{RR}|N(\vec{k},s)\rangle, \qquad (2.32)
\end{aligned}$$

such that only two of the four operators are independent. Without loss of generality, we can therefore consider only the operators $\mathcal{O}^{RL}$ and $\mathcal{O}^{LL}$. We shall occasionally use the notation $\mathcal{O}^{R/L\,L}$ to refer to either of these two operators.

Now we assume the up and down quarks are degenerate in mass, i.e. isospin symmetry. This is a good approximation for the range of accuracy expected from our calculations. By exchanging up and down quarks we get the relations:

$$\begin{aligned}
\langle \pi^0|\mathcal{O}^{R/L\,L}_{udu}|p\rangle &= \langle \pi^0|\mathcal{O}^{R/L\,L}_{dud}|n\rangle, \qquad (2.33) \\
\langle \pi^+|\mathcal{O}^{R/L\,L}_{udd}|p\rangle &= -\langle \pi^-|\mathcal{O}^{R/L\,L}_{duu}|n\rangle, \qquad (2.34) \\
\langle K^0|\mathcal{O}^{R/L\,L}_{usu}|p\rangle &= -\langle K^+|\mathcal{O}^{R/L\,L}_{dsd}|n\rangle, \qquad (2.35) \\
\langle K^+|\mathcal{O}^{R/L\,L}_{usd}|p\rangle &= -\langle K^0|\mathcal{O}^{R/L\,L}_{dsu}|n\rangle, \qquad (2.36) \\
\langle K^+|\mathcal{O}^{R/L\,L}_{uds}|p\rangle &= -\langle K^0|\mathcal{O}^{R/L\,L}_{dus}|n\rangle, \qquad (2.37) \\
\langle K^+|\mathcal{O}^{R/L\,L}_{dsu}|p\rangle &= -\langle K^0|\mathcal{O}^{R/L\,L}_{usd}|n\rangle, \qquad (2.38) \\
\langle \eta^0|\mathcal{O}^{R/L\,L}_{udu}|p\rangle &= -\langle \eta^0|\mathcal{O}^{R/L\,L}_{dud}|n\rangle. \qquad (2.39)
\end{aligned}$$

In the isospin limit, there is a further relation between matrix elements involving $\pi^+/\pi^-$ and

$\pi^0$,

$$\langle \pi^+ | \mathcal{O}^{R/L\,L}_{udd} | p \rangle = \sqrt{2} \langle \pi^0 | \mathcal{O}^{R/L\,L}_{udu} | p \rangle \tag{2.40}$$

$$-\langle \pi^- | \mathcal{O}^{R/L\,L}_{duu} | n \rangle = \sqrt{2} \langle \pi^0 | \mathcal{O}^{R/L\,L}_{dud} | n \rangle \tag{2.41}$$

Such that the 12 matrix elements on the left hand side of Eqs. 2.33 and 2.35-2.39 can be used to reconstruct any of 28 possible nucleon decay matrix elements.

### 2.4.1 Proton decay form factors

We wish to write down an expression for the QCD matrix elements in terms of form factors. Under the requirement of Lorentz and parity invariance, the proton decay QCD matrix elements are parametrised by two form factors which encode the non–perturbative dynamics:

$$\langle M(\vec{p}) | \mathcal{O}^A | N(\vec{k}, s) \rangle = P_L \left[ W_0^A(N \to M; q^2) - i\not{q} W_q^A(N \to M; q^2) \right] u(k, s), \tag{2.42}$$

where $M(\vec{p})$ is a meson with momentum $\vec{p}$, $N(\vec{k}, s)$ is a nucleon with momentum $\vec{k}$ and spin $s$ and $q = k - p$ is the four–momentum transferred to the outgoing antilepton. $\mathcal{O}^A$ is a baryon number violating operator as given in Eq. 2.30 and $A$ is a collective label for the operators spin and flavour structure. Under multiplication with the leptonic structure from Eq. 2.30 this gives,

$$\langle M, l | \mathcal{O} | N \rangle = \left( P_L \left[ W_0^A(N \to M; q^2) - i\not{q} W_q^A(N \to M; q^2) \right] u(k, s) \right) \bar{u}(q, s'). \tag{2.43}$$

To calculate the decay width of the proton (see Eq. 1.38) we need to square the amplitude from Eq. 2.30. Substituting in the form factor representation of the QCD matrix element and using the notation, $W_0^A(N \to M; q^2) \equiv W_0$ and $W_q^A(N \to M; q^2) \equiv W_q$ for simplicity gives,

$$\begin{aligned}
|\langle M, l | \mathcal{O} | N \rangle|^2 &= \sum_{s,s'} \mathrm{Tr} \left( P_L \left[ W_0 - i\not{q} W_q \right] u(k, s) \right) \bar{u}(q, s') u(q, s') \left( \bar{u}(k, s) \left[ W_0 + i\not{q} W_q \right] P_L \right) \\
&= \mathrm{Tr} \left( \not{k}\not{q} \right) \left( W_0^2 + q^2 W_q^2 \right) \\
&= k.q (W_0^2 + q^2 W_q^2) \\
&= \frac{m_N^2}{2} \left( 1 - \left( \frac{m_M}{m_N} \right)^2 \right) \left( W_0^2 + q^2 W_q^2 \right),
\end{aligned} \tag{2.44}$$

where we have also used the approximation $m_l \ll m_M, m_N$. We see that the term in Eq. 2.44 involving $W_q^A(N \to M; q^2)$ is multiplied by $q^2 = m_l^2$, which is negligible and can be ignored. The decay rate therefore depends only on $W_0^A(N \to M; q^2)$. For this reason, $W_0^A(N \to M; q^2)$ is known as the relevant form factor, and $W_q^A(N \to M; q^2)$ is known as the irrelevant form factor. If we substitute this expression for the matrix element into the equation for the proton

partial decay width (Eq. 1.38), then we get,

$$\Gamma(N \to M + l) = \frac{m_N}{32\pi}\left(1 - \left(\frac{m_M}{m_N}\right)^2\right)^2 \left|\sum_i C^i W_0^i(N \to M + l)\right|^2 . \tag{2.45}$$

When we do our QCD calculation however, we calculate the QCD matrix element from Eq. 2.42, which contains contributions from both the relevant and irrelevant form factors. In this case, there is no reason to assume that the $W_q^A(N \to M; q^2)$ term is negligible, and therefore we must disentangle the irrelevant form factor, in order to find $W_0^A(N \to M; q^2)$ and calculate the proton partial decay width. We will come back to this point in Chapter 6, when we calculate the proton decay QCD matrix elements.

### 2.4.2 Proton decay and $\chi$PT

If we add a baryon number violating sector to the chiral Lagrangian, then we can form expressions relating the baryon number violating matrix elements to the two new low energy constants in the chiral Lagrangian. Measuring just these two low energy constants can then be used to reconstruct all of the proton decay matrix elements.

The operators from Eqs. 2.28 and 2.29 can be written in terms of the chiral perturbation theory matrices $B$, $\xi$ and $\xi^\dagger$ as follows [37],

$$\begin{aligned}
Q^{(1)} &= \alpha\left(\bar{e}_L^c \mathrm{Tr}\mathcal{F}\xi B_L \xi - \bar{\nu}_L^c \mathrm{Tr}\mathcal{F}'\xi B_L \xi\right), \\
Q^{(2)} &= \alpha \bar{e}_R^c \mathrm{Tr}\mathcal{F}\xi^\dagger B_R \xi^\dagger, \\
Q^{(3)} &= \beta\left(\bar{e}_L^c \mathrm{Tr}\mathcal{F}\xi B_L \xi^\dagger - \bar{\nu}_L^c \mathrm{Tr}\mathcal{F}'\xi B_L \xi^\dagger\right), \\
Q^{(4)} &= \beta \bar{e}_R^c \mathrm{Tr}\mathcal{F}\xi^\dagger B_R \xi, \\
\tilde{Q}^{(1)} &= \alpha\left(\bar{e}_L^c \mathrm{Tr}\tilde{\mathcal{F}}\xi B_L \xi - \bar{\nu}_L^c \mathrm{Tr}\tilde{\mathcal{F}}'\xi B_L \xi\right), \\
\tilde{Q}^{(2)} &= \alpha \bar{e}_R^c \mathrm{Tr}\tilde{\mathcal{F}}\xi^\dagger B_R \xi^\dagger, \\
\tilde{Q}^{(3)} &= \beta\left(\bar{e}_L^c \mathrm{Tr}\tilde{\mathcal{F}}\xi B_L \xi^\dagger - \bar{\nu}_L^c \mathrm{Tr}\tilde{\mathcal{F}}'\xi B_L \xi^\dagger\right), \\
\tilde{Q}^{(4)} &= \beta \bar{e}_R^c \mathrm{Tr}\tilde{\mathcal{F}}\xi^\dagger B_R \xi, \\
\tilde{Q}^{(5)} &= \alpha \bar{\nu}_L^c \mathrm{Tr}\tilde{\mathcal{F}}''\xi B_L \xi, \\
\tilde{Q}^{(6)} &= \beta \bar{\nu}_L^c \mathrm{Tr}\tilde{\mathcal{F}}''\xi B_L \xi^\dagger,
\end{aligned} \tag{2.46}$$

where the matrices $\mathcal{F}, \mathcal{F}', \tilde{\mathcal{F}}, \tilde{\mathcal{F}}'$, and $\tilde{\mathcal{F}}''$ are projectors in flavour space:

$$\mathcal{F} = \begin{pmatrix} 0 & 0 & 0 \\ 0 & 0 & 0 \\ 1 & 0 & 0 \end{pmatrix}, \quad \mathcal{F}' = \begin{pmatrix} 0 & 0 & 0 \\ 0 & 0 & 0 \\ 0 & 1 & 0 \end{pmatrix}, \quad \tilde{\mathcal{F}} = - \begin{pmatrix} 0 & 0 & 0 \\ 1 & 0 & 0 \\ 0 & 0 & 0 \end{pmatrix},$$
$$\tilde{\mathcal{F}}' = - \begin{pmatrix} 0 & 0 & 0 \\ 0 & 1 & 0 \\ 0 & 0 & 0 \end{pmatrix}, \quad \tilde{\mathcal{F}}'' = \begin{pmatrix} 0 & 0 & 0 \\ 0 & 0 & 0 \\ 0 & 0 & 1 \end{pmatrix}. \tag{2.47}$$

and $\alpha$ and $\beta$ are the two new low–energy constants.

Using these expressions for the baryon number violating operators, we can add baryon number violating terms to the chiral Lagrangian [22],

$$\begin{aligned}
\mathcal{L}^{\Delta B} =& \alpha \sum_{d=1}^{2} \Big\{ C_d^{(1)} \left[ e_{dL} \mathrm{Tr} \mathcal{F} \xi B_L \xi - \nu_{dL} \mathrm{Tr} \mathcal{F}' \xi B_L \xi \right] \\
& + C_d^{(2)} e_{dR} \mathrm{Tr} \mathcal{F} \xi^\dagger B_R \xi^\dagger + \tilde{C}_d^{(1)} \left[ e_{dL} \mathrm{Tr} \tilde{\mathcal{F}} \xi B_L \xi - \nu_{dL} \mathrm{Tr} \tilde{\mathcal{F}}' \xi B_L \xi \right] \\
& + \tilde{C}_d^{(2)} e_{dR} \mathrm{Tr} \tilde{\mathcal{F}} \xi^\dagger B_R \xi^\dagger + \tilde{C}_d^{(5)} \nu_{dL} \mathrm{Tr} \tilde{\mathcal{F}}'' \xi B_L \xi \Big\} + \\
& \beta \sum_{d=1}^{2} \Big\{ C_d^{(3)} \left[ e_{dL} \mathrm{Tr} \mathcal{F} \xi B_L \xi^\dagger - \nu_{dL} \mathrm{Tr} \mathcal{F}' \xi B_L \xi^\dagger \right] \\
& + C_d^{(4)} e_{dR} \mathrm{Tr} \mathcal{F} \xi^\dagger B_R \xi + \tilde{C}_d^{(3)} \left[ e_{dL} \mathrm{Tr} \tilde{\mathcal{F}} \xi B_L \xi^\dagger - \nu_{dL} \mathrm{Tr} \tilde{\mathcal{F}}' \xi B_L \xi^\dagger \right] \\
& + \tilde{C}_d^{(4)} e_{dR} \mathrm{Tr} \tilde{\mathcal{F}} \xi^\dagger B_R \xi + \tilde{C}_d^{(6)} \nu_{dL} \mathrm{Tr} \tilde{\mathcal{F}}'' \xi B_L \xi^\dagger \Big\} + \text{h.c.}
\end{aligned} \tag{2.48}$$

We can then find expressions for matrix elements $\langle M(p), l(q) | \mathcal{O} | N(k,s) \rangle$, in terms of the parameters from the chiral Lagrangian $\alpha, \beta, f, D, F...$ and the kinematic variables $p, k, q, m_N, m_M, m_l....$ To do this, we expand all exponentials in the Lagrangian, and collect together the leading order terms with the correct fields for the process we are interested in, i.e. one nucleon field, one meson field and one lepton field.

Consider the matrix elements, $\langle \pi^+(\vec{p}) | \mathcal{O}_{udu}^{RL} | p(\vec{k}, s) \rangle$ and $\langle \pi^+(\vec{p}) | \mathcal{O}_{udu}^{LL} | p(\vec{k}, s) \rangle$. There are two diagrams which contribute to this, see Figure 2.3.

The first of these diagrams consisting of a single baryon number violating vertex comes from expanding the terms in Eq. 2.48, while the second diagram contains a baryon number conserving vertex where a proton radiates a pion, this comes from expanding the terms in Eq.

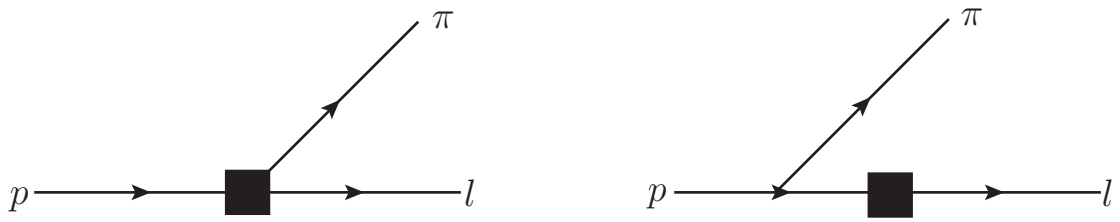


Figure 2.3: The chiral perturbation theory diagrams contributing to proton decay to a pion and a lepton.

2.22. To leading order, the two diagrams yield,

$$\begin{aligned}
\langle \pi^0 | \, \mathcal{O}^{RL}_{udu} \, | p(\mathbf{k},s) \rangle &= \alpha P_L u(\vec{k},s) \left[ \frac{1}{\sqrt{2}f} - \frac{D+F}{\sqrt{2}f} \frac{-q^2+m_N^2}{-q^2-m_N^2} - \frac{4b_1}{\sqrt{2}f} \frac{m_u m_N}{-q^2-m_N^2} \right] \\
&- \alpha P_L i\not{q} u(\vec{k},s) \left[ \frac{D+F}{\sqrt{2}f} \frac{2m_N}{-q^2-m_N^2} + \frac{4b_1}{\sqrt{2}f} \frac{m_u}{-q^2-m_N^2} \right], \qquad (2.49) \\
\langle \pi^0 | \, \mathcal{O}^{LL} \, | p(\mathbf{k},s) \rangle &= \beta P_L u(\vec{k},s) \left[ \frac{1}{\sqrt{2}f} - \frac{D+F}{\sqrt{2}f} \frac{-q^2+m_N^2}{-q^2-m_N^2} - \frac{4b_1}{\sqrt{2}f} \frac{m_u m_N}{-q^2-m_N^2} \right] \\
&- \beta P_L i\not{q} u(\vec{k},s) \left[ \frac{D+F}{\sqrt{2}f} \frac{2m_N}{-q^2-m_N^2} + \frac{4b_1}{\sqrt{2}f} \frac{m_u}{-q^2-m_N^2} \right]. \qquad (2.50)
\end{aligned}$$

In the limit where $q^2 \ll m_N^2$ and $b_1 m_u \ll m_N$, these expressions simplify to:

$$\begin{aligned}
\langle \pi^0 | \, \mathcal{O}^{RL} \, | p(\mathbf{k},s) \rangle &\simeq \alpha P_L u(\mathbf{k},s) \left[ \frac{1}{\sqrt{2}f} + \frac{D+F}{\sqrt{2}f} \right] + O(m_l^2/m_N^2), \qquad (2.51) \\
\langle \pi^0 | \, \mathcal{O}^{LL} \, | p(\mathbf{k},s) \rangle &\simeq \beta P_L u(\mathbf{k},s) \left[ \frac{1}{\sqrt{2}f} + \frac{D+F}{\sqrt{2}f} \right] + O(m_l^2/m_N^2), \qquad (2.52)
\end{aligned}$$

So the matrix element can be written in terms of the low energy constants $\alpha$ and $\beta$ along with some known QCD–scale constants $f, D, F$ as given in Section 2.3. Table 2.1 gives similar relations for all of the different proton decay matrix elements which we are interested in.

| Matrix Element | $\chi$PT prediction |
|---|---|
| $\langle\pi^0\|\mathcal{O}^{RL}_{udu}\|p\rangle$ | $\frac{\alpha}{\sqrt{2}f}(1+D+F)$ |
| $\langle\pi^0\|\mathcal{O}^{LL}_{udu}\|p\rangle$ | $\frac{\beta}{\sqrt{2}f}(1+D+F)$ |
| $\langle K^0\|\mathcal{O}^{RL}_{usu}\|p\rangle$ | $-\frac{\alpha}{f}(1+(D-F)\frac{m_N}{m_B})$ |
| $\langle K^0\|\mathcal{O}^{LL}_{usu}\|p\rangle$ | $\frac{\beta}{f}(1-(D-F)\frac{m_N}{m_B})$ |
| $\langle K^+\|\mathcal{O}^{RL}_{usd}\|p\rangle$ | $\frac{\alpha}{f}\frac{2D}{3}\frac{m_N}{m_B}$ |
| $\langle K^+\|\mathcal{O}^{LL}_{usd}\|p\rangle$ | $\frac{\beta}{f}\frac{2D}{3}\frac{m_N}{m_B}$ |
| $\langle K^+\|\mathcal{O}^{RL}_{uds}\|p\rangle$ | $\frac{\alpha}{f}\left(1+\left(\frac{D}{3}+F\right)\frac{m_N}{m_B}\right)$ |
| $\langle K^+\|\mathcal{O}^{LL}_{uds}\|p\rangle$ | $\frac{\beta}{f}\left(1+\left(\frac{D}{3}+F\right)\frac{m_N}{m_B}\right)$ |
| $\langle K^+\|\mathcal{O}^{RL}_{dsu}\|p\rangle$ | $\frac{\alpha}{f}\left(1+\left(\frac{D}{3}-F\right)\frac{m_N}{m_B}\right)$ |
| $\langle K^+\|\mathcal{O}^{LL}_{dsu}\|p\rangle$ | $-\frac{\beta}{f}\left(1-\left(\frac{D}{3}-F\right)\frac{m_N}{m_B}\right)$ |
| $\langle\eta^0\|\mathcal{O}^{RL}_{udu}\|p\rangle$ | $-\frac{\alpha}{\sqrt{6}f}(1+D-3F)$ |
| $\langle\eta^0\|\mathcal{O}^{LL}_{udu}\|p\rangle$ | $\frac{\beta}{\sqrt{6}f}(3-D+3F)$ |

Table 2.1: The $\chi$PT predictions for various proton decay matrix elements. $f, D, F$ are QCD–scale constants with values given earlier in Section 2.3. $m_N$ is the nucleon mass, $m_B$ is an average baryon mass $m_B \cong m_\Sigma \cong m_\Lambda$. All of these $\chi$PT predictions are leading order, and computed in the limit $m_{u,d} \ll m_s \ll m_{N,B}$, $q^2 \ll m^2_{N,B}$ and $b_i m_u \ll m_N$.

## 2.5 Renormalisation of Operators in the Continuum

As we saw in Section 1.3, the strong coupling constant is a running coupling, and changes with the energy scale being considered. Similarly, the masses and fields from our QCD Lagrangian are also running quantities. Any physical quantity that we measure should be scale invariant, for example the mass of the proton. The baryon number violating operators we wish to measure however, are not physical quantities, and so will have a scale dependence. Once we have measured these quantities, we will therefore need to convert to a standard renormalisation scheme at a specified scale, such that the results will be readily comparable with other results which may have been calculated in a different way.

The baryon number violating operators, $\mathcal{O}^{\Gamma\Gamma'}_{ijk}$, which we will have to renormalize are composite operators and may require a renormalisation beyond the simple renormalisation of their component fields. This is because unlike the quark fields, which all have unique quantum numbers, there may be a class of composite operators which all have the same quantum numbers, and so will mix under renormalisation. In order to renormalize the operator, we must therefore consider the renormalisation matrix $Z^{AB}$, which renormalizes an operator $\mathcal{O}^B$ as,

$$\mathcal{O}^A_{\text{ren}} = Z^{AB}\mathcal{O}^B, \tag{2.53}$$

where $A, B$ represent composite indices for the spin and flavour structure of the operator $\mathcal{O}$. The sum over $B$ is therefore the sum over all operators which have the same quantum numbers, and hence mix under renormalisation.

# Chapter 3

# Lattice QCD

At energies much greater than the energy scale of hadrons, the strong coupling constant is small enough that we can use perturbative methods to evaluate observables. This is known as asymptotic freedom [38, 39]. At the hadronic energy scale, this is no longer the case and we must use a non–perturbative approach. The subject of lattice QCD was started by KG Wilson in 1974 [40] and was introduced as a way of analysing QCD in the non–perturbative regime. It involves discretising space-time into a lattice of points in a finite box (see a 2–dimensional example in Figure 3.1). The main advantage to this is that it introduces a natural ultraviolet regularisation to the theory. A second advantage is that with a finite number of discrete space–time points this reduces the number of degrees of freedom to a finite number, allowing numerical simulations to be undertaken

To perform the discretisation, we replace continuum of space-time with a discrete lattice of points. This four–dimensional grid has axes given by the unit vectors $\hat{\mu}$ and the spacing between neighbouring lattice sites is $a\hat{\mu}$. $a$ is therefore known as the lattice spacing and the inverse lattice spacing, $a^{-1}$, acts as a cut–off in momentum space which regulates the theory. Continuum results are obtained by taking the limit $a \to 0$, after having properly normalised the theory. Results obtained at finite lattice spacing should therefore be extrapolated to $a = 0$. The total volume of the lattice is $V = a^3 L_x^3 \times a L_t$, where we allow different sizes for the spatial ($L_x$) and temporal ($L_t$) axes. The fact that this volume is not infinite introduces a second source of systematic error into our calculation, this is the finite volume error.

The continuum space-time variables, $x_\mu$ are now discrete points on the lattice, $\hat{x}_\mu$. Quark fields, $\psi(x)$, are replaced by $\hat{\psi}(\hat{x})$, which are now functions of the discrete space-time variable and can be thought of as being situated at sites on the lattice. Derivatives $\partial_\mu$ are replaced with symmetric finite difference operators $\hat{\partial}_\mu \hat{\psi}(\hat{x}) = \frac{1}{2a}\left(\hat{\psi}(\hat{x}+\hat{\mu}) - \hat{\psi}(\hat{x}-\hat{\mu})\right)$. Finally the fields and masses are rescaled by powers of the lattice spacing, such that each of them is dimensionless.

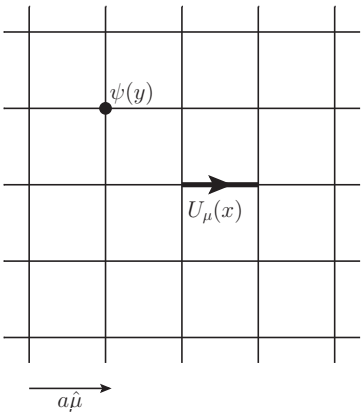


Figure 3.1: Representation of a 2–dimensional lattice with lattice spacing $a$, Quark fields $\psi$ are situated on lattice sites, while link variables $U$ are situated on the links between sites

The full list of lattice variables and fields is:

$$\begin{aligned} a\hat{x}_\mu &= x_\mu, \\ a^{-\frac{3}{2}}\hat{\psi}(\hat{x}) &= \psi(x), \\ a^{-\frac{3}{2}}\hat{\bar{\psi}}(\hat{x}) &= \bar{\psi}(x), \\ a^{-\frac{3}{2}}\hat{\partial}_\mu\hat{\psi}(\hat{x}) &= \partial_\mu\psi(x), \\ a\hat{A}_\mu(\hat{x}) &= A_\mu(x), \\ a^{-1}\hat{m} &= m. \end{aligned} \tag{3.1}$$

From now on we ignore the hat notation, and all variables will be considered to be their rescaled lattice equivalents.

In order to introduce gauge fields on the lattice we define the link matrices,

$$U(x, x+\hat{\mu}) \equiv U_\mu(x) = \mathrm{e}^{igaA_\mu(x)}, \tag{3.2}$$

$$U_\mu^\dagger(x) = \mathrm{e}^{-igaA_\mu(x)}. \tag{3.3}$$

These are the parallel transporters of the matter fields along the links between lattice points. For this reason we associate the link matrices with the links between sites on our lattice (see Figure 3.1). Rather than writing the QCD Lagrangian in terms of the gauge fields $A_\mu(x)$, we shall instead write expressions in terms of these link matrices.

In this chapter, we will first discuss the calculation of observables in the path integral formulation (Section 3.1), and then move on to discuss some of the problems associated with the discretisation of Lattice QCD, starting with the discretisation of the gauge action (Section 3.2) and then moving onto the discretisation of the fermionic action (Sections 3.3-3.6).

## 3.1 Observables

In the path integral formalism, the expectation value of an observable $\mathcal{O}$ in Minkowski space is,

$$\langle \mathcal{O} \rangle = \frac{\int [D\bar{\psi}][D\psi][DU] \mathcal{O} \, \mathrm{e}^{iS^M[\psi,\bar{\psi},U]}}{\int [D\bar{\psi}][D\psi][DU] \, \mathrm{e}^{iS^M[\psi,\bar{\psi},U]}}. \tag{3.4}$$

Due to the oscillating nature of the exponential, a numerical evaluation of this is difficult.

We perform a Wick rotation to Euclidean space, defined as

$$x_4^E = ix_0^M, \quad x_i^E = x_i^M, \tag{3.5}$$

where the superscript $E$ represents Euclidean space, and $M$ represents Minkowski space. We also need to use Euclidean gamma matrices,

$$\gamma_4^E = \gamma_0^M, \quad \gamma_j^E = -i\gamma_j^M, \tag{3.6}$$

which obey Euclidean commutation relations

$$\{\gamma_\mu^E, \gamma_\nu^E\} = 2\delta_{\mu\nu}. \tag{3.7}$$

Substituting these into the action from Eq. 2.1 gives,

$$S^E = -iS^M, \tag{3.8}$$

and the expectation value of an observable in Euclidean space can therefore be written as,

$$\langle \mathcal{O} \rangle = \frac{\int [D\bar{\psi}][D\psi][DA] \mathcal{O} \, \mathrm{e}^{-S^E[\psi,\bar{\psi},A]}}{\int [D\bar{\psi}][D\psi][DA] \, \mathrm{e}^{-S^E[\psi,\bar{\psi},A]}}, \tag{3.9}$$

where the decaying exponential in the integrand can now be thought of as a statistical weight, allowing the possibility of numerical methods to be used to calculate the integral. From now on, unless explicitly stated, we shall work in Euclidean space and drop the $E$ superscripts.

## 3.2 The discrete gauge action

The simplest object we can form on the lattice, which is constructed purely from the gauge fields (link matrices) and preserves all of the symmetries of the QCD Lagrangian, is the plaquette $U_{\mu\nu}$. This is defined as a path ordered product of link matrices forming a one by one loop in

the $\mu$ and $\nu$ directions (see Figure 3.2),

$$U_{\mu\nu}(x) = U_\mu(x)U_\nu(x+\hat{\mu})U_\mu^\dagger(x+\hat{\nu})U_\nu^\dagger(x+\hat{\nu}). \tag{3.10}$$

Under a local gauge transformation, $G(x)$, $U_\mu(x)$ transforms as,

$$U_\mu(x) \to G(x)U_\mu(x)G^{-1}(x+\hat{\mu}), \tag{3.11}$$

so the plaquette is gauge invariant.

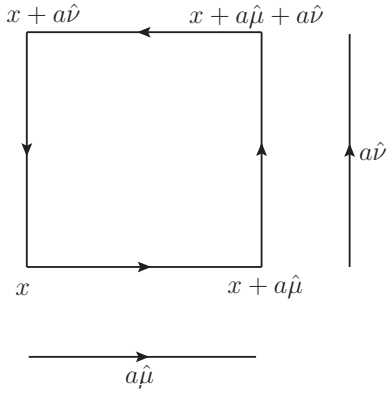


Figure 3.2: Graphical representation of a plaquette $U_{\mu\nu}(x)$.

The simplest gauge action we can write is that proposed by Wilson, where we sum over all possible plaquettes:

$$S^G = -\frac{\beta}{6}\sum_P \mathrm{Re}\,\mathrm{Tr}\,(U_P)\,, \tag{3.12}$$

where $\beta = 6/g_0^2$ and $U_P \equiv U_{\mu\nu}(x)$ labels a plaquette.

In order to see that this is equivalent to the continuum gauge action (see Eq. 2.1) we write the plaquette in terms of the gauge field $A_\mu$,

$$\begin{aligned} U_{\mu\nu} &= U_\mu(x)U_\nu(x+\hat{\mu})U_\mu^\dagger(x+\hat{\nu})U_\nu^\dagger(x) \\ &= \mathrm{e}^{iag_0A_\mu(x)}\mathrm{e}^{iag_0A_\nu(x+\hat{\mu})}\mathrm{e}^{-iag_0A_\mu(x+\hat{\nu})}\mathrm{e}^{-iag_0A_\nu(x)}. \end{aligned} \tag{3.13}$$

Then we make repeated use of the Baker–Campbell–Hausdorff formula to combine the four exponentials into a single exponential,

$$\mathrm{e}^A\mathrm{e}^B\mathrm{e}^C\mathrm{e}^D = \mathrm{e}^{A+B+C+D+\frac{1}{2}([A,B]+[C,D]+[A,C]+[A,D]+[B,C]+[B,D])+\ldots}, \tag{3.14}$$

and expand $A_\mu(x+\hat{\nu}) = A_\mu(x) + a\partial_\nu A_\mu(x) + ...$ to show that,

$$\begin{aligned} U_{\mu\nu} &= \exp\left(ig_0 a^2 \partial_\mu A_\nu + \partial_\nu A_\mu + i^2 a^2 g_0^2 [A_\mu, A_\nu] + \mathcal{O}(a^4)\right) \\ &\equiv \exp\left(ig_0 a^2 F_{\mu\nu} + \mathcal{O}(a^4)\right). \end{aligned} \tag{3.15}$$

If we expand this exponential, and substitute this into Eq. 3.12 then we get

$$\begin{aligned} S^G &= -\frac{\beta}{6}\sum_P \mathrm{Re}\,\mathrm{Tr}\,(U_P) \\ &= -\frac{a^4}{4}\mathrm{Tr}\left(F_{\mu\nu}F_{\mu\nu} + \mathcal{O}(a^2)\right), \end{aligned} \tag{3.16}$$

and so we see that this gauge action is equivalent to the gauge action in the continuum with $F_{\mu\nu}$ the lattice field strength tensor. It is also important to note that the discritisation errors are of order $a^2$.

There are other gauge invariant loops we can form from link variables, for example there are three different six link objects, see Figure 3.3. These six link loops are usually referred to as Rectangles, Chairs and 3D type loops. We can write an improved gauge action with a generic combination of these six and four link gauge invariant loops as [41],

$$S^G = -\frac{\beta}{6}\left[c_0\sum_P \mathrm{Tr}\,(U_P) + c_1\sum_R \mathrm{Tr}\,(U_R) + c_2\sum_{R'} \mathrm{Tr}\left(U'_R\right) + c_3\sum_{R''} \mathrm{Tr}\left(U''_R\right)\right]. \tag{3.17}$$

where the restriction that this must equal the continuum gauge action gives the renormalisation condition [42],

$$c_0 + 8c_1 + 8c_2 + c_3 = 1. \tag{3.18}$$

There is therefore a family of improved gauge actions which all give the same continuum limit. One example of an improved action is given in Ref. [43], which expands the action given in 3.17 in a similar way to the expansion of the plaquette action above. It then sets the $c_i$'s such that the errors of order $a^2$ are also cancelled. This gives $c_1 = -\frac{1}{12}$, $c_2 = 0$ and $c_3 = 0$ with $c_0$ then fixed by the renormalisation condition.

In this thesis, we will use the Iwasaki gauge action [42, 44, 45], which uses a renormalisation group analysis to set the constants $c_i$ such that the action is close to the normalised trajectory. On the normalised trajectory, the scaling of observables with the coupling constant $g$ is minimised. Choosing the observable to be the plaquette, it is shown that on the normalised trajectory the constants $c_2$ and $c_3$ are small. Therefore, as they would have a large impact on the time taken to compute the gauge action, they are set to zero. $c_1$ is found to be $-0.3375$ and $c_0$ is then fixed by the renormalisation condition.

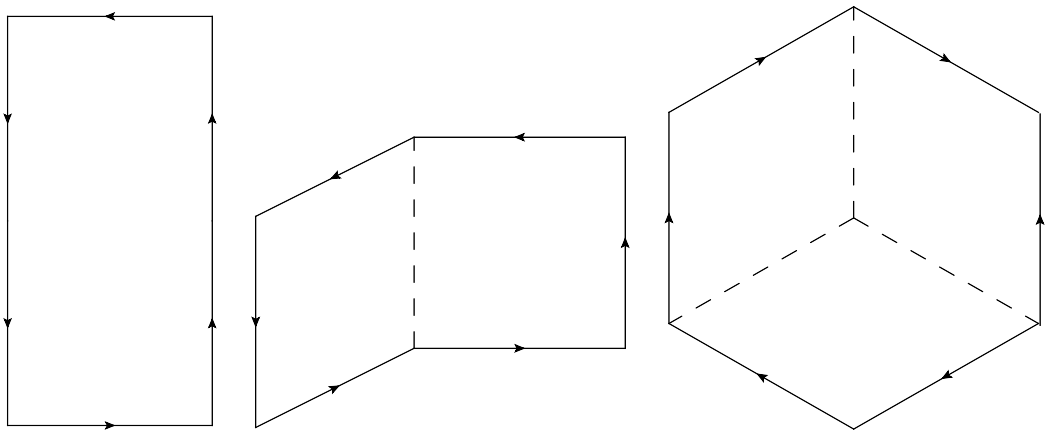

(a) Rectangle (b) Chair (c) 3D loop

Figure 3.3: Graphical representations of the three different types of 6 link gauge invariant loops.

## 3.3 Naive fermion discretisation

The discretisation of the fermionic action introduces many problems. As an example, let us consider the simplest lattice fermionic action,

$$S_F = \sum_{xy} \bar{\psi}(x)(D_{\text{latt}}(x,y) + m\delta_{xy})\psi(y), \tag{3.19}$$

where $\psi$ and $\bar{\psi}$ label quark fields with spin, colour and flavour indices suppressed, $x$ and $y$ label discretised four–dimensional space–time coordinates and $D_{\text{latt}}$ is given by,

$$D_{\text{latt}}(x,y) = \frac{1}{2}\gamma^{\mu}\left(U_{\mu}(x)\delta_{x,y+\hat{\mu}} - U^{\dagger}_{\mu}(x-\hat{\mu})\delta_{x,y-\hat{\mu}}\right), \tag{3.20}$$

and the presence of the link matrices, $U_{\mu}(x)$, ensures that the fermionic action is gauge invariant.

A major problem with this naive fermion action is called the fermion doubling problem. If we consider the fermion propagator,

$$\begin{aligned}\left\langle \psi(x)\bar{\psi}(y)\right\rangle &= (D_{\text{latt}}(xy) + m\delta_{xy})^{-1} \\ &= \lim_{a\to 0}\int_{-\pi/a}^{\pi/a}\frac{d^4p}{(2\pi)^4}\left(-i\frac{\left[\sum_{\mu}\gamma_{\mu}\tilde{\tilde{p_{\mu}}} + m\right]_{\alpha\beta}}{\sum_{\mu}\tilde{\tilde{p_{\mu}^2}} + m^2}\,\mathrm{e}^{ip(x-y)}\right) + \mathcal{O}(a^2),\end{aligned} \tag{3.21}$$

where

$$\tilde{\tilde{p_{\mu}}} = \frac{1}{a}\sin(p_{\mu}a), \tag{3.22}$$

then in the limit where $a \to 0$ this is the same as in the continuum with the replacement

$p_\mu \to \tilde{\tilde{p_\mu}}$. This is fine for small values of $p_\mu$ where $p_\mu \approx \tilde{\tilde{p_\mu}}$, but towards the edge of the Brillouin zone, there are additional poles in the integral which do not appear in the continuum. In four dimensions there are $2^4 = 16$ poles to this equation rather than 1 in the continuum. One way to interpret these additional poles is as extra fermions, so our integral has given us 16 fermions rather than 1.

## 3.4 Wilson Fermions

In order to counter the doubling problem, we must alter the action. One possible modified action is the Wilson action [40],

$$S_F^W = \sum_{xy} \bar{\psi}(x)(D^W_{\text{latt}}(x,y) + m\delta_{xy})\psi(y), \tag{3.23}$$

$$D^W_{\text{latt}}(x,y) = D_{\text{latt}}(x,y) - a\frac{r}{2}\Box, \tag{3.24}$$

where,

$$\begin{aligned} \Box\psi(x) &= a^2\partial_\mu\partial^\mu\psi(x) \\ &= \frac{1}{2}\left(U_\mu(x)\psi(x+\hat{\mu}) - 2\psi(x) + U^\dagger_\mu(x-\hat{\mu})\psi(x-\hat{\mu})\right), \end{aligned} \tag{3.25}$$

is the four–dimensional laplacian operator on a lattice. The extra term in the action is known as the Wilson term and $r$ is the Wilson parameter. As this term varies linearly with $a$, it disappears in the continuum limit and so does not affect physical results.

The net effect of this modification to the action is to change Eq. (3.21) to the following:

$$\left\langle \bar{\psi}(x)\psi(y)\right\rangle = \lim_{a\to 0}\int_{-\pi/a}^{\pi/a}\frac{d^4p}{(2\pi)^4}\left(-i\frac{\left[\sum_\mu \gamma_\mu \tilde{\tilde{p_\mu}} + m(p)\right]}{\sum_\mu \tilde{\tilde{p_\mu}}^2 + m(p)^2}e^{ip(x-y)}\right), \tag{3.26}$$

where $m(p) = m + \frac{2r}{a}\sum_\mu \sin^2(p_\mu a/2)$. As $a \to 0$, $m(p) \to m$ for any fixed value of $p_\mu$. Near the edges of the Brillouin zone, however, the sine tends to 1 and $m(p)$ is $\mathcal{O}(a^{-1})$. Therefore the mass of the additional fermions becomes large as $a \to 0$. The action therefore tends to 0 thus suppressing the additional fermions and eliminating the doubling problem.

### 3.4.1 Chiral symmetry breaking with Wilson fermions

In the limit of massless quarks, our continuum QCD Lagrangian from Eq. 2.1 is invariant under vector and axial vector flavour transformations. We will now show that the additional Wilson term in our Lagrangian is responsible for breaking this chiral symmetry. Consider a vector

flavour transformation,

$$\begin{aligned} \delta_V^a \psi(x) &= i\alpha_V^a \frac{1}{2}\lambda^a \psi(x), \\ \delta_V^a \bar{\psi}(x) &= -i\bar{\psi}(x)\alpha_V^a \frac{1}{2}\lambda^a, \end{aligned} \tag{3.27}$$

where $\alpha_V^a$ is the infinitesimal parameter of the transformation, and $\lambda^a$ are the generators of $SU(N_f)$.

Without the Wilson term ($r = 0$) and with equal bare quark masses, the lagrangian is invariant under this vector flavour transformation and there is a conserved vector current,

$$V_\mu^a(x) = \frac{1}{2}\left[\bar{\psi}(x+\mu)\frac{\lambda^a}{2}\gamma_\mu U_\mu(x)\psi(x) + h.c.\right]. \tag{3.28}$$

When we add the Wilson term, although the Lagrangian itself is still invariant, the conserved vector current from Eq. 3.28 is not. We can instead form a new current,

$$\tilde{V}_\mu^a(x) = V_\mu^a(x) - \frac{r}{2}\left[\bar{\psi}(x)U_\mu(x)\psi(x+\mu) - \bar{\psi}(x+\mu)U_\mu^\dagger(x)\psi(x)\right], \tag{3.29}$$

which is exactly conserved for equal bare quark masses, under the vector flavour transformation, even for $r \neq 0$.

Now we consider an axial flavour transformation,

$$\begin{aligned} \delta_A^a \psi(x) &= i\alpha_A^a \frac{1}{2}\lambda^a \gamma_5 \psi(x), \\ \delta_A^a \bar{\psi}(x) &= i\bar{\psi}(x)\alpha_A^a \frac{1}{2}\lambda^a \gamma_5. \end{aligned} \tag{3.30}$$

Again, without the Wilson term and with zero bare quark masses, the lagrangian is invariant under this transformation and we can define a conserved axial current,

$$A_\mu^a(x) = \frac{1}{2}\left[\bar{\psi}(x+\mu)\frac{\lambda^a}{2}\gamma_\mu\gamma_5 U_\mu(x)\psi(x) + h.c.\right]. \tag{3.31}$$

When we add the Wilson term however, the lagrangian is not invariant under this axial transformation. We can therefore not define a conserved axial current in analogy to the new vector current introduced in Eq. 3.29. The cost of the Wilson term is therefore the non–conservation of the axial vector current, meaning chiral symmetry is explicitly broken for Wilson fermions.

To see how much the chiral symmetry is broken, we follow the arguments from Ref. [46]

and consider the functional integral from Eq. 3.4,

$$\langle \mathcal{O} \rangle = \frac{\int [D\bar{\psi}][D\psi][DU] \mathcal{O} \, \mathrm{e}^{-S[\psi,\bar{\psi},U]}}{\int [D\bar{\psi}][D\psi][DU] \, \mathrm{e}^{-S[\psi,\bar{\psi},U]}}. \tag{3.32}$$

Substituting the axial flavour transformations from Eqs. 3.30 into Eq. 3.32 we get,

$$\langle \frac{\delta \mathcal{O}}{\delta \alpha_A^a} \rangle - \langle \mathcal{O} \frac{\delta S}{\delta \alpha_A^a} \rangle = 0, \tag{3.33}$$

where,

$$i\langle \mathcal{O} \frac{\delta S}{\delta \alpha_A^a} \rangle = \nabla_x^\mu \langle \mathcal{O} A_\mu^a(x) \rangle - \langle \mathcal{O} \left[ \bar{\psi}(x) \{ \frac{\lambda^a}{2}, m \} \gamma_5 \psi(x) + X^a(x) \right] \rangle, \tag{3.34}$$

and the notation $\nabla_x^\mu f(x)$ is shorthand for

$$\nabla_x^\mu f(x) = \frac{1}{a} \left( f(x) - f(x - \hat{\mu}) \right). \tag{3.35}$$

The functional derivative of $\mathcal{O}$ is defined such that,

$$\delta \mathcal{O} = \int dx \frac{\delta \mathcal{O}}{\delta \alpha_A^a} \alpha_A^a, \tag{3.36}$$

and $X^a(x)$ is the chiral variation of the Wilson term,

$$\begin{aligned} X^a(x) \;\; = \;\; & -\frac{r}{2a} \sum_\mu \Big[ \bar{\psi}(x) \frac{\lambda^a}{2} \gamma_5 U_\mu(x) \psi(x + \hat{\mu}) + \\ & + \bar{\psi}(x + \hat{\mu}) \frac{\lambda^a}{2} \gamma_5 U_\mu^\dagger(x) \psi(x) + (x \to x - \hat{\mu}) - 4 \bar{\psi}(x) \frac{\lambda^a}{2} \gamma_5 \psi(x) \Big]. \end{aligned} \tag{3.37}$$

Using Eq. 3.33, we can now obtain the partial conservation of the axial current,

$$\langle \alpha | \nabla_\mu A_\mu^a | \beta \rangle = \langle \alpha | \left[ \bar{\psi}(x) \{ \frac{\lambda^a}{2}, m \} \gamma_5 \psi(x) + X^a(x) \right] | \beta \rangle. \tag{3.38}$$

Let us now define a new operator, $\bar{X}^a(x)$, which is multiplicatively renormalisable and its on–shell matrix elements vanish in the continuum limit, then we get [46],

$$\bar{X}^a(x) = X^a(x) + \bar{\psi}(x) \{ \frac{\lambda^a}{2}, \bar{m} \} \gamma_5 \psi(x) + (Z_A - 1) \partial_\mu A_\mu^a, \tag{3.39}$$

where $Z_A$ is the axial vector current renormalisation and $\bar{m}$ is a matrix in flavour space. Inserting $\bar{X}^a(x)$ into Eq. 3.38 gives,

$$Z_A \langle |\alpha| \nabla^\mu A_\mu^a | \beta \rangle = \langle \alpha | \left[ \bar{\psi}(x) \{ \frac{\lambda^a}{2}, m - \bar{m} \} \gamma_5 \psi(x) \right] | \beta \rangle + \langle \alpha | \bar{X}^a | \beta \rangle. \tag{3.40}$$

Using the fact that we defined on shell matrix elements $\bar{X}^a$ to vanish in the continuum, we get the continuum limit equation,

$$Z_A\langle|\alpha|\partial_\mu A^a_\mu|\beta\rangle = \langle\alpha|\left[\bar{\psi}(x)\{\frac{\lambda^a}{2}, m-\bar{m}\}\gamma_5\psi(x)\right]|\beta\rangle. \tag{3.41}$$

The effect of the chiral symmetry breaking in Wilson quarks, is therefore an additive renormalisation of the mass $m \to m - \bar{m}$.

## 3.5 Ginsparg–Wilson Fermions

As discussed in the previous chapter (see Sections 2.2 and 2.3), the chiral symmetry of the QCD Lagrangian is explicitly broken by the quark masses, but for the light quarks whose masses are much less than $\Lambda_{\rm QCD}$, this symmetry holds approximately. An example of this effect is the light pseudo–scalar mesons of QCD, with masses which are small in comparison to $\Lambda_{\rm QCD}$, and which can be thought of as the pseudo–goldstone bosons of the approximate chiral symmetry. This symmetry allows us to treat the finite light quark masses as perturbations and we can construct an effective field theory called chiral perturbation theory.

Simple discretisations such as that proposed by Wilson break this approximate chiral symmetry still further. In fact Nielsen and Ninomiya proposed a no go theorem [47] which states that if the fermionic action satisfies the following properties,

- hermiticity
- locality
- translational invariance

then you cannot solve the doubling problem without explicitly breaking chiral symmetry.

The chiral symmetry is important for two reasons. Firstly in current lattice calculations, the quark masses are set to unphysically large values. As such, we need to extrapolate to the physical quark masses, and chiral perturbation theory provides a controlled way to do this. Secondly, renormalisation of operators in a chirally symmetric theory is simpler, as there is no mixing between operators of the opposite chirality.

To get around the no go theorem, Ginsparg and Wilson proposed that if the lattice Dirac operator obeyed the Ginsparg–Wilson relation, [48],

$$\{\gamma_5, D\} = 2aD\gamma_5 D, \tag{3.42}$$

then the theory is invariant under a lattice chiral symmetry [49]:

$$\begin{aligned}\delta\psi(x) &= i\epsilon\gamma_5 \sum_y (\delta_{xy} - \frac{a}{2} D_{xy})\psi(y), \\ \delta\bar{\psi}(x) &= i\epsilon \sum_y \bar{\psi}(y)(\delta_{yx} - \frac{a}{2} D_{yx})\gamma_5. \end{aligned} \tag{3.43}$$

Substituting Eqs. 3.43 into an action with a Ginsparg–Wilson lattice Dirac operator,

$$S^F_{GW} = \sum_{xy} \bar{\psi}(x)(D_{\text{latt}}(x,y) + m\delta_{xy})\psi(y), \tag{3.44}$$

yields a variation of the action, $\delta S^F_{GW}$, of:

$$\begin{aligned}\delta S^F_{GW} &= i\epsilon a^4 \sum_x \left(F(x) + 2m\bar{\psi}(x)\gamma_5\psi(x) + \bar{\Delta}(x)\right), \\ F(x) &= (\bar{\psi}D)(x)\gamma_5\psi(x) + \bar{\psi}(x)\gamma_5(D\psi)(x) - a(\bar{\psi}D)(x)\gamma_5(D\psi)(x), \\ \bar{\Delta}(x) &= -\frac{ma}{2}\left((\bar{\psi}D)(x)\gamma_5\psi(x) + \bar{\psi}(x)\gamma_5(D\psi)(x)\right). \end{aligned} \tag{3.45}$$

Using Eqs. 3.42 and 3.45 gives,

$$\delta S^F_{GW} = \sum_{x,y} \bar{\psi}(x)\left[\{\gamma_5, D\} - aD\gamma_5 D\right](x,y)\psi(y) + \mathcal{O}(m). \tag{3.46}$$

So in the limit of massless quarks, chiral symmetry is conserved.

The solution to the Ginsparg–Wilson relation is not unique, and the Dirac operator chosen must also eliminate species doubling. Any matrix of the form:

$$D = \frac{1}{a}(1 - V), \tag{3.47}$$

where,

$$V^\dagger V = \gamma_5 V \gamma_5 V = 1, \tag{3.48}$$

satisfies the Ginsparg–Wilson relation. Neuberger suggested an explicit expression for D giving rise to overlap fermions [50],

$$V = A(A^\dagger A)^{-\frac{1}{2}}, \tag{3.49}$$

$$A = 1 - a(D^W_{\text{latt}} + m), \tag{3.50}$$

where $D^W_{\text{latt}}$ is just the Wilson Dirac operator from Eq. 3.24.

## 3.6 Domain Wall Fermions

Another type of Ginsparg–Wilson fermions are Domain Wall Fermions. In order to simulate chiral fermions, Kaplan [51] suggested a method to recover a chiral gauge theory in $2n$ dimensions, by simulating a gauge theory of massive fermions in $2n+1$ dimensions. So to simulate a 4–dimensional chiral fermions, we need a gauge theory of massive 5–dimensional fermions. This idea was further refined by Furman and Shamir [52] where the fermions in this framework are now known as Domain Wall Fermions (DWF).

The basic idea is to introduce a space–dependent mass term to the fermionic action with a domain wall defect. Shamir's DWF action [53] is given by:

$$\begin{aligned} S_{\mathrm{DWF}} &= S_{\mathrm{F}} + S_{\mathrm{PV}}, \\ S_{\mathrm{F}} &= \sum_{i=1}^{3} \sum_{x,s;y,s'} \bar{\psi}(x,s) \left[ D^{\dagger}_{\mathrm{DWF}}(m_i;x,s,y,s') D_{\mathrm{DWF}}(m_i;x,s,y,s') \right]^{\frac{1}{2}} \psi(y,s') \\ S_{\mathrm{PV}} &= \sum_{i=1}^{3} \sum_{x,s;y,s'} \phi^{\dagger}(x,s) \left[ D^{\dagger}_{\mathrm{DWF}}(1;x,s,y,s') D_{\mathrm{DWF}}(1;x,s,y,s') \right]^{\frac{1}{2}} \phi(y,s'). \end{aligned} \tag{3.51}$$

$D_{\mathrm{DWF}}(m;x,s,y,s')$ is the DWF Dirac operator for one flavour of fermion with mass $m$, $x$ and $y$ represent traditional four–dimensional space time co-ordinates, while $s$ and $s'$ represent fifth–dimensional co-ordinates and $1 \leq s,s' \leq N_5$. $N_5$ is therefore the size of the 5th dimension. $D_{\mathrm{DWF}}(m;x,s,y,s')$ is also a function of the domain wall height $M$ and will be defined shortly. $S_F$ is the fermionic term, where the fermion fields $\bar{\psi},\psi$ are now 5–dimensional fields. Every 5–dimensional field describes one light 4–dimensional field, and $N_5-1$ 4–dimensional fields whose mass is of the order of the cutoff [52]. $S_{PV}$ is the Pauli–Villars term [54], this contains bosonic field variables $\phi$ and $\phi^{\dagger}$, and is introduced to cancel the $N_5-1$ unwanted massive fields, which would otherwise dominate the effective action in the limit $N_5 \to \infty$.

$D_{\mathrm{DWF}}(m;x,s,y,s')$ is defined as follows:

$$\begin{aligned} D_{\mathrm{DWF}}(m;x,s,y,s') &= D^{\parallel}(x,y)\delta_{ss'} + D^{\perp}(m;s,s')\delta_{xy}, \\ D^{\parallel}(x,y) &= \sum_{\mu} \frac{1}{2} \Big( ((1+\gamma_\mu)U_{x\mu}\delta_{x+\hat{\mu},y}) + (1-\gamma_\mu)U^{\dagger}_{y\mu}\delta_{x-\hat{\mu},y} \Big) + (M-4)\delta_{xy}, \\ D^{\perp}(m;s,s') &= \begin{cases} P_R\delta_{2s'} - mP_L\delta_{N_5 s'} - \delta_{1s'}, & \text{if} \quad s=1, \\ P_R\delta_{s+1,s'} + P_L\delta_{s-1,s'} - \delta_{ss'}, & \text{if} \quad 1<s<N_5, \\ -mP_R\delta_{1s'} + P_L\delta_{N_5-1,s'} - \delta_{N_5 s'}, & \text{if} \quad s=N_5, \end{cases} \end{aligned} \tag{3.52}$$

where indices $\mu$ will run over only the four physical dimensions.

Five–dimensional fields are represented by $\psi$ and $\bar{\psi}$, and the physical four–dimensional quark

fields, $q$ and $\bar{q}$ are therefore given by:

$$\begin{aligned} q(x) &= P_L\psi(x,1) + P_R\psi(x,N_5), \\ \bar{q}(x) &= \bar{\psi}(x,N_5)P_L + \bar{\psi}(x,1)P_R. \end{aligned} \tag{3.53}$$

With this action, fermionic states of opposite chiralities are localised on opposite boundaries of the fifth dimension.

### 3.6.1 Chiral symmetry breaking in DWF

The full five–dimensional action is invariant under a global $U(N_f)$ symmetry with a five–dimensional conserved current given by,

$$\begin{aligned} j^a_\mu(x,s) &= \frac{1}{2}\left(\bar{\psi}_{x,s}U_{x,\mu}\lambda^a\psi_{x+\hat{\mu},s} - \bar{\psi}_{x+\hat{\mu},s}U^\dagger_{x,\mu}\lambda^a\psi_{x,s}\right), \\ j^a_5(x,s) &= \begin{cases} \bar{\psi}_{x,s}P_R\lambda^a\psi_{x,s+1} - \bar{\psi}_{x,s+1}P_L\lambda^a\psi_{x,s}, & \text{if} \quad 1 \le s < N_5, \\ \bar{\psi}_{x,N_5}P_R\lambda^a\psi_{x,1} - \bar{\psi}_{x,1}P_L\lambda^a\psi_{x,N_5}, & \text{if} \quad s = N_5, \end{cases} \end{aligned} \tag{3.54}$$

which satisfies a continuity equation:

$$\sum_\mu \Delta_\mu j^a_\mu = \begin{cases} -j^a_5(x,1) - mj^a_5(x,N_5), & \text{if} \quad s = 1, \\ -\Delta_5 j^a_5, & \text{if} \quad 1 < s < N_5, \\ j^a_5(x,N_5-1) + mj^a_5(x,N_5), & \text{if} \quad s = N_5, \end{cases} \tag{3.55}$$

and where the operator $\Delta$ is defined as,

$$\begin{aligned} \Delta_\mu f(x,s) &= f(x,s) - f(x-\hat{\mu},s), \\ \Delta_5 f(x,s) &= f(x,s) - f(x,s-1). \end{aligned} \tag{3.56}$$

We now define a four–dimensional vector and axial current. The vector current,

$$V^a_\mu(x) = \sum_{s=1}^{N_5} j^a_\mu(x,s), \tag{3.57}$$

is conserved due to the cancellation of the surface terms in Eq. 3.55.

For the axial current, we define the axial transformation as:

$$\begin{aligned} \delta^a_A\psi_{x,s} &= +iq(s)\lambda^a\psi_{x,s}, \\ \delta^a_A\bar{\psi}_{x,s} &= -iq(s)\bar{\psi}_{x,s}\lambda^a, \end{aligned} \tag{3.58}$$

with

$$q(s) = \begin{cases} 1, & \text{if} \quad 1 \leq s \leq \frac{N_5}{2}, \\ -1, & \text{if} \quad \frac{N_5}{2} < s \leq N_5. \end{cases} \tag{3.59}$$

Therefore the fermion fields have opposite charges in each half of the fifth dimension.

The corresponding axial currents are then,

$$A^a_\mu(x) = -\sum_{s=1}^{N_5} \text{sign}\left(\frac{N_5}{2} - s + \frac{1}{2}\right) j^a_\mu(x,s), \tag{3.60}$$

and these satisfy the divergence equation,

$$\Delta_\mu A^a_\mu(x) = 2m j^a_5(x, N_5) + 2 j^a_5(x, N_5/2). \tag{3.61}$$

Now we define,

$$\begin{aligned} J^a_5(x) &= j^a_5(x, N_5) = \bar{q}(x)\gamma_5\lambda^a q(x), \\ J^a_{5q}(x) &= j^a_5(x, N_5/2). \end{aligned} \tag{3.62}$$

$J^a_5(x)$ is therefore just the usual continuum axial current, while $J^a_{5q}(x)$ is an additional term not present in the continuum. If we define the residual mass $m_{\text{res}}$ as the ratio of $J^a_{5q}(x)$ to $J^a_5(x)$, i.e..

$$J^a_{5q}(x) = m_{\text{res}} J^a_5(x), \tag{3.63}$$

then Eq. 3.61 becomes,

$$\Delta_\mu A^a_\mu(x) = 2(m + m_{\text{res}}) j^a_5(x, N_5). \tag{3.64}$$

The residual mass can therefore be thought of as an additive quark mass renormalisation which parametrises the chiral symmetry breaking present in the DWF action.

### 3.6.2 Reducing $m_{\text{res}}$

It has been shown in Ref. [55], that,

$$m_{\text{res}} \approx \frac{c_e \mathrm{e}^{-\lambda N_5}}{N_5} + \frac{c_l}{N_5}. \tag{3.65}$$

The first term on the RHS arises from the contribution of extended modes, while the second term is from the local modes of the DWF Dirac operator. $\lambda$ is an eigenvalue of the DWF Dirac operator and the constants $c_e$ and $c_l$ depend on the density of extended and localised eigenvalues of the DWF Dirac operator respectively.

In the limit $N_5 \to \infty$, $m_{\text{res}} \to 0$ and the chiral symmetry is exact, with no overlap between

the left and right handed quark fields on the boundaries of the fifth dimension. However, simulating with an $N_5$ high enough to reduce $m_{\text{res}}$ to machine precision is costly, so instead, studies in Ref. [55] show that for the lattices I shall be using, $m_{\text{res}}$ can be reduced to an acceptable level by choosing $N_5 \geq 16$. At this level, any systematic error due to chiral symmetry breaking will be much less than other systematic and statistical errors.

## 3.7 Renormalisation of Lattice Operators

As we saw in Section 2.5, the QCD Lagrangian is a function of running parameters, and as such any operators we calculate must be renormalised to some scale $\mu$. In the continuum this renormalisation is done perturbatively, and this same approach can be used when we move to a lattice theory.

By expanding out the link variables in the Lagrangian, we get terms involving multiple gauge and fermion fields. Exactly as in the continuum, these terms can be represented graphically as $n$–point diagrams with increasing numbers of loops.

The first problem with lattice perturbation theory is the addition of non–physical vertices, for example the two–quark, two–gluon vertex, which do not appear in continuum perturbation theory. These lattice artifacts appear with additional positive powers of the lattice spacing, and so disappear in the continuum limit, reproducing the correct continuum results. However, their appearance serves to complicate the perturbative expansion.

A second problem, is that our lattice theory, and hence the operators we wish to renormalise, can break certain continuum symmetries. In general when renormalised, operators will mix with all operators with the same symmetries. If a symmetry is broken on the lattice, then that means that some operators which could not mix in the continuum, are now free to do so. Of particular importance is the inexact chiral symmetry on the lattice. However, the exponentially accurate chiral symmetry of the domain wall fermion action should suppress the mixing between operators of different chirality.

The final problem is that in cases where the results from lattice perturbation theory, can be checked using non-perturbative methods, there is generally a significant discrepancy, see Ref. [56]. This is due to the poor convergence of lattice perturbation theory.

To get around these problems, we instead use a non–perturbative renormalisation (NPR) procedure, which is described in detail in Section 6.4.

# Chapter 4

# Lattice Methods

## 4.1 Monte Carlo Methods

In order to calculate the expectation value of observables we need to evaluate the integral given in Eq. 3.4, but to do this requires the integration over a large number of integration variables which make this practically impossible. For a $10^4$ lattice there are approximately $4 \times 10^4$ link variables, and each is a function of 8 real parameters, hence there are of the order of 320,000 integrations to be done [57].

The integral must therefore be evaluated using statistical methods, where the expectation value of an observable $\langle \mathcal{O} \rangle$ is approximated by,

$$\frac{1}{N} \sum_i \mathcal{O}_i \xrightarrow[N \to \infty]{} \langle \mathcal{O} \rangle \,, \tag{4.1}$$

where $\mathcal{O}_i$ represents the value of $\mathcal{O}$ calculated on the $i$th of a set of $N$ configurations. A configuration is a set of values for the fields at each point on the lattice. These configurations must be selected with a probability according to their weight ($\mathrm{e}^{-S}$) in the path integral in Eq. 3.4.

There are therefore two stages to the calculation of an observable. First, configurations of link variables must be produced with the correct probability, then the value of an observable must be calculated on each configuration.

### 4.1.1 The Hybrid Monte Carlo algorithm

The Hybrid Monte Carlo (HMC) Algorithm [58] combines the molecular dynamics [59, 60] and Metropolis [61] algorithms in a series of alternating steps. A molecular dynamics step is followed by a Metropolis step, which is then followed by another molecular dynamics step etc.

For the molecular dynamics step, we introduce fictitious momenta $P_l$, conjugate to the

variables we wish to integrate. In our case these variables are link variables $U_l$ for the bosons in our theory (fermions are treated slightly differently as shown in Section 4.2). The link variables are $SU(3)$ matrices, and the conjugate momenta belong to the Lie algebra of $SU(3)$. We can then write a Hamiltonian,

$$\mathcal{H}[U,P] = \sum_l \dot{U}_l P_l - \mathcal{L}[U], \tag{4.2}$$

where $\mathcal{L}[U]$ is the Lagrangian for our bosonic variables. We evolve the link variables and momenta for time $\tau$ (known as the trajectory length) using Hamilton's equations of motion, which requires the use of a numerical integrator such as a leapfrog integrator (see Section 4.1.2).

After the molecular dynamics step, we arrive at a new configuration of link variables and momenta, which is then accepted or rejected with probability,

$$P = \min\left(1, \frac{\mathrm{e}^{\tilde{\mathcal{H}}[U',P']}}{\mathrm{e}^{\tilde{\mathcal{H}}[U,P]}}\right). \tag{4.3}$$

This is known as a Metropolis accept/reject step and eliminates the systematic error introduced by a finite time step in the molecular dynamics step.

In summary, the algorithm is as follows [57],

- Choose a starting $SU(3)$ link matrix configuration $U_l$,
- Refresh the momenta $P_l$. I.e. choose momenta $P_l$ from the Gaussian distribution with Boltzmann factor $\mathrm{e}^{-\frac{1}{2}\sum_l P_l^2}$.
- Allow the link matrices and canonical momenta to evolve for time $\tau$ using Hamilton's equations of motion:

$$\dot{U}_l = iP_lU_l, \tag{4.4}$$
$$\dot{P}_l = -\frac{\partial S}{\partial U_l}. \tag{4.5}$$

- Accept the new configuration $\{U', P'\}$ with probability,

$$P = \min\left(1, \frac{\mathrm{e}^{\mathcal{H}[U',P']}}{\mathrm{e}^{\mathcal{H}[U,P]}}\right). \tag{4.6}$$

- Store the new or old configuration as appropriate, and then start again from the second step.

### 4.1.2 Leapfrog integrators

The time evolution of the $SU(3)$ link variables and their momenta (which belong to the Lie algebra of $SU(3)$) in the third step of the algorithm is realised by using a leapfrog integration technique [57]. We first introduce a time–step, $\epsilon$, and expand the fields $U_l(\tau+\epsilon)$ and their momenta $P_l(\tau+\epsilon)$ in a Taylor series giving,

$$U_l(\tau+\epsilon) = U_l(\tau) + \epsilon\dot{U}_l(\tau) + \frac{\epsilon^2}{2}\ddot{U}_l(\tau) + \mathcal{O}(\epsilon^3), \tag{4.7}$$

$$P_l(\tau+\epsilon) = P_l(\tau) + \epsilon\dot{P}_l(\tau) + \frac{\epsilon^2}{2}\ddot{P}_l(\tau) + \mathcal{O}(\epsilon^3). \tag{4.8}$$

From Hamiltons equations of motion we get,

$$\dot{U}_l(\tau) = P_l(\tau), \tag{4.9}$$

$$\ddot{U}_l(\tau) = \dot{P}_l(\tau) = -\frac{\partial S}{\partial U_l(\tau)}, \tag{4.10}$$

$$\begin{aligned}\ddot{P}_l(\tau) &= -\sum_m \frac{\partial^2 S}{\partial U_l(\tau)\partial U_m(\tau)} P_m(\tau) \\ &= \frac{1}{\epsilon}\left(\frac{\partial S}{\partial U_l(\tau+\epsilon)} - \frac{\partial S}{\partial U_l(\tau)}\right) + \mathcal{O}(\epsilon).\end{aligned} \tag{4.11}$$

These expressions involve differentiating the action (a scalar) by a link variable (an $SU(3)$ matrix), for example:

$$\dot{P}_l^{ij} = \frac{\partial S[U]}{\partial U_l^{ij}}. \tag{4.12}$$

The $i,j$th element of the matrix $\dot{P}$ is given by the differential of $S$ by the $i,j$th element of the matrix $U$.

Taylor expanding $P_l(\tau+\frac{\epsilon}{2})$ and substituting from Eq. 4.10 implies the following,

$$\begin{aligned}P_l(\tau+\frac{\epsilon}{2}) &= P_l(\tau) + \frac{\epsilon}{2}\dot{P}_l + \mathcal{O}(\epsilon^2) \\ &= P_l(\tau) - \frac{\epsilon}{2}\frac{\partial S}{\partial U_l(\tau)} + \mathcal{O}(\epsilon^2).\end{aligned} \tag{4.13}$$

Substituting Eqs. 4.9-4.11 into Eqs. 4.7 and 4.8, then using Eq 4.13 gives,

$$U_l(\tau+\epsilon) = U_l(\tau) + \epsilon P_l(\tau+\frac{\epsilon}{2}) + \mathcal{O}(\epsilon^3), \tag{4.14}$$

$$P_l(\tau+\frac{3\epsilon}{2}) = P_l(\tau+\frac{\epsilon}{2}) - \epsilon\frac{\partial S}{\partial U_l(\tau+\epsilon)} + \mathcal{O}(\epsilon^3). \tag{4.15}$$

When iterated this amounts to integrating the equations of motion, with an error of $\mathcal{O}(\epsilon^2)$.

$\dot{P}_l(\tau) = -\partial S/\partial U_l(\tau)$ is known as the force term. As the force increases, the updates to

the link momenta (and hence to the link variables) become larger and so the acceptance of the Metropolis step decreases for fixed step–size.

Decreasing the step–size will decrease the step–size error, which has the effect of increasing the percentage of steps which are accepted by the Metropolis accept-reject step of the HMC algorithm. The cost of this is that neighbouring trajectories are more correlated.

## 4.2 Pseudofermions

The HMC algorithm is only suitable for producing sets of bosonic field variables, but our action also contains fermionic fields which must be treated separately. The following discussion is based upon arguments in Ref. [57]. The fermionic fields can be integrated out of Eq. 3.4 to give,

$$\int [D\bar{\psi}][D\psi][DU]\mathcal{O}\,\mathrm{e}^{-S[\psi,\bar{\psi},U]} = \int [DU]\mathcal{O}_{\mathrm{eff}}\,\mathrm{e}^{-S_{\mathrm{eff}}[U]}, \tag{4.16}$$

where the effective action $S_{\mathrm{eff}}[U]$ is given by,

$$S_{\mathrm{eff}}[U] = S_G[U] - \ln\left[\det(D_{\mathrm{DWF}}[U])\right], \tag{4.17}$$

and we must therefore evaluate the determinant of the DWF Dirac matrix. This matrix can be very large, so the determinant would be expensive to compute exactly.

In the quenched approximation, the fermionic determinant is set to 1, which has the effect of reducing the amount of computing power required to perform the simulation. However, the cost is that we are no longer simulating full QCD, but ignoring all fermions in the vacuum (i.e.. no sea quarks), this introduces difficult–to–estimate systematic errors. All the results presented in this thesis will be unquenched, but we will compare with previous quenched determinations.

For an even number of degenerate flavours, the effective action can be written,

$$S_{\mathrm{eff}}[U] = S_G[U] - \frac{N_f}{2}\ln\left(\det(Q[U])\right), \tag{4.18}$$

where,

$$Q[U] = \tilde{D}^{\dagger}_{\mathrm{DWF}}[U]\tilde{D}_{\mathrm{DWF}}[U], \tag{4.19}$$

and $\tilde{D}^{\dagger}_{\mathrm{DWF}}[U]$ is the DWF Dirac matrix for a single flavour. This is important as it means that $Q[U]$ is a positive hermitian matrix, with positive determinant and we can therefore take its logarithm. For an odd number of flavours, the determinant is no longer guaranteed to be positive, and so we must use a modified algorithm (see Section 4.2.1).

We can now replace $\det Q$ with the integral,

$$\det Q = \int D\phi D\phi^{*}\mathrm{e}^{-\sum_{nm}\phi^{*}_{n}\tilde{Q}^{-2}_{nm}\phi_{m}}, \tag{4.20}$$

This integral is now over bosonic degrees of freedom, known as pseudo–fermion fields. We therefore have an effective action, involving $Q^{-2}$, which can be evaluated using the HMC algorithm.

### 4.2.1 Rational HMC

We wish to simulate with 2 degenerate light quarks and one strange quark (known as a 2+1 flavour simulation). Traditionally, odd numbers of quark flavours have been simulated using the R algorithm [62], but this is not an exact algorithm, i.e the results depend on the step size in the numerical integrator. HMC would be an exact algorithm, but the pseudo–fermion trick introduced in Section 4.2 can only work with an even number of quark flavours.

The solution is to use the rational hybrid monte carlo (RHMC) algorithm from Refs. [63, 64, 65]. In the RHMC algorithm we take fractional powers of the Dirac matrix itself, rather than its square, and then replace the non–local Dirac matrix by a rational approximation, $r(D)$, such that:

$$\det(D^{\alpha}) \approx \int D\phi D\phi^{*} \mathrm{e}^{-\phi^{*} r(D) \phi}, \tag{4.21}$$

where $\alpha$ is a fractional number.

### 4.2.2 Pseudofermions and the 2+1 flavour Domain Wall action

For the case of the DWF Dirac operator defined in Eq. 3.52, integrating out the fermionic fields as in Ref. [66] gives the following ratios of determinants,

$$\frac{\det\left[D^{\dagger}_{\mathrm{DWF}}(m_l) D_{\mathrm{DWF}}(m_l)\right]}{\det\left[D^{\dagger}_{\mathrm{DWF}}(1) D_{\mathrm{DWF}}(1)\right]} \frac{\det^{\frac{1}{2}}\left[D^{\dagger}_{\mathrm{DWF}}(m_s) D_{\mathrm{DWF}}(m_s)\right]}{\det^{\frac{1}{2}}\left[D^{\dagger}_{\mathrm{DWF}}(1) D_{\mathrm{DWF}}(1)\right]}, \tag{4.22}$$

with $D_{\mathrm{DWF}}(m)$ the DWF Dirac operator with quark mass $m = m_l$ for the degenerate light quarks and $m = m_s$ for the strange quark. The required determinants are calculated using the RHMC algorithm. The terms in the denominator result from integrating out the Pauli–Villars fields.

## 4.3 Correlation Functions

For our calculations, the relevant observables (see Eq. 3.4) are N–point correlation functions,

$$\begin{aligned} G^{(N)}(x_1 \ldots x_N) &= \langle 0 | T\left\{\mathcal{O}(x_1) ... \mathcal{O}(x_N)\right\} | 0 \rangle \\ &= \prod_{i=1}^{N} \left(-\frac{\partial}{\partial J(x_i)}\right) Z[J] \Big|_{J=0}, \end{aligned} \tag{4.23}$$

with $Z[J]$ the generating functional,

$$Z[J] = \frac{\int D\phi \mathrm{e}^{-\left(S + \int d^4x J(x)\mathcal{O}(x)\right)}}{\int D\phi \mathrm{e}^{-S}}, \tag{4.24}$$

which is normalised so that Z[0] = 1.

We shall calculate 2 and 3–point correlation functions, where the operators $\mathcal{O}(x_i)$ are meson, baryon, or other interpolating operators. As an example, consider the pseudo–scalar meson correlation function,

$$\langle \mathcal{O}_M(x)\bar{\mathcal{O}}_M(y)\rangle, \tag{4.25}$$

where $\mathcal{O}_M(x) = q(x)\gamma_5\bar{q}(x)$ and with $q(x)$ a quark field at position $x$. The source of the correlation function is the position of the last operator, in this case $y$ and is often set to the origin. Similarly the sink is the position of the first operator, in this case $x$. In three point functions, there is also an intermediate operator at some position $x'$.

We can simplify the expressions for $G^{(N)}(x_1 \ldots x_N)$ by using Wick's theorem. The contraction of two quark fields yields the propagator,

$$S_{ab,\alpha\beta}(y-x)\delta_{fg} = \overbrace{q_{af\alpha}(y)\bar{q}_{bg\beta}}(x), \tag{4.26}$$

where the quark fields have now been explicitly labelled with spin index $\alpha, \beta$, colour $a, b$ and flavour $f, g$. Wick's theorem states that the product of operators in Eq. 4.23 can be replaced by a sum over all sets of contractions between the quark and anti–quark fields. For the pseudo–scalar meson correlation function we have,

$$G_2(x,y) = \langle \sum_{\text{contr}} (S(x-y)\gamma_5 S^\dagger(x-y)\gamma_5)\rangle, \tag{4.27}$$

where the sum is over all sets of contractions. In order to calculate any N–point correlation function, we therefore need to calculate the quark propagators (in this case $S(x-y)$).

The quark propagator is the inverse of the Dirac matrix, which as we noted before in Section 4.2 is a very large sparse matrix. This inverse can be calculated from the equation,

$$D[x,y,U]S(y,z) = \delta(x-z). \tag{4.28}$$

This is a large system of equations, which is solved using the conjugate gradient algorithm [67].

The conjugate gradient algorithm is an iterative method. The more iterations the closer the solution comes to the exact solution, but the greater the computational cost.

## 4.4 Smearing

Instead of using local functions of the fields $q(x)$ in correlation functions, we could also use extended or smeared fields,

$$q(x) \to \Psi q(x). \tag{4.29}$$

This can have the effect of improving the overlap of the correlation function with the state we are interested in, often the ground state. We can smear quark fields at the source and the sink of our correlation function. For the smearing of quark fields at the source, this is equivalent to solving Eq. 4.28 using an extended operator instead of the delta function on the right hand side.

The types of smearing and sources we shall use are discussed in [68, 69, 70, 71], they are Gaussian smearing (G), Hydrogen–like wavefunction smearing (H), Wall smearing (W), Box smearing (B) and Kenway sources (K).

### 4.4.1 Gaussian Smearing

For Gaussian smearing [68], the quark fields are smeared with the function,

$$\Psi = \left(1 - \frac{\sigma^2}{4n}\nabla^2\right)^n, \tag{4.30}$$

$$\nabla^2 q(x) = \sum_\mu 2q(x) - U_\mu(x)q(x+\hat{\mu}) - U_\mu^\dagger(x-\hat{\mu})q(x-\hat{\mu}). \tag{4.31}$$

This tends to a Gaussian in the limit $n \to \infty$,

$$\Psi \to \mathrm{e}^{-\frac{\sigma^2\nabla^2}{4}}. \tag{4.32}$$

The radius of this Gaussian function, $\sigma$ can be tuned, with a larger radius smearing out the field over a larger spatial volume. The factor $n$ is another parameter, though in this case all that is required is that $n$ is sufficiently large such that the approximation in Eq. 4.32 holds.

### 4.4.2 Hydrogen–like wavefunction smearing

For some operators, a better overlap can be found from smearing the quark fields to look more like the $n$th hydrogen wavefunction [69],

$$\Psi_n(x) = \sum_{r=0}^{N}\left(r+\frac{1}{2}\right)^2 \phi_n(x) \sum_\mu \left[\prod_{m=0}^{r-1} U_\mu(x+n\mu)\right], \tag{4.33}$$

with the spatial dependence in $\phi_n(x)$ chosen to resemble the hydrogenic wavefunction,

$$\begin{aligned} \phi_n(x) &\propto \mathrm{e}^{-|\tilde{x}|} L_n(\tilde{x}), & (4.34)\\ \tilde{x} &= \frac{|x|}{(n+1)r_0}, & (4.35)\\ L_n(\tilde{x}) &= \frac{e^{\tilde{x}}}{n!}\frac{d^n}{d\tilde{x}^n}\left(\tilde{x}^n \mathrm{e}^{-\tilde{x}}\right). & (4.36) \end{aligned}$$

The $L_n$ are the Laguerre polynomials and $r_0$ is the radius. This radius and the value of $n$ can be tuned, in order to maximise the overlap with the states we are interested in.

### 4.4.3 Box and Wall smearing and sources

For box smearing, the quark fields are smeared with a function which is just a spatial box of size $n^3$:

$$\Psi(x) = \sum_{y_1=0}^{n}\sum_{y_2=0}^{n}\sum_{y_3=0}^{n} \delta(\vec{x}-\vec{y}). \tag{4.37}$$

Wall smearing is similar, but with a box the size of the entire lattice.

Similarly a box source is just an extended source term, replacing the delta function on the right hand side of Eq. 4.28 with a spatial box of size $n^3$:

$$D[x,y,U]S(y,z) = \sum_{x_1'=0}^{n}\sum_{x_2'=0}^{n}\sum_{x_3'=0}^{n} \delta(x-z-x'). \tag{4.38}$$

A Wall source is again similar, but instead of a spatial box of size $n^3$, we use a spatial box with a size equal to the spatial volume of the entire lattice.

### 4.4.4 Momentum and Kenway sources

For a momentum source, we replace the source in Eq. 4.28, by a momentum based phase,

$$D[x,y,U]S(y,z) = \mathrm{e}^{i\vec{p}.(\vec{z}-\vec{x})}. \tag{4.39}$$

This has the effect of giving the quark field a spatial momentum $\vec{p}$. Notice that for $\vec{p}=0$, this phase is constant, and hence this is equivalent to a wall source.

Often we will fix the gauge of a momentum source to Coulomb gauge where,

$$\nabla.A = 0. \tag{4.40}$$

Where we do not fix the gauge, we will call this a Kenway source.

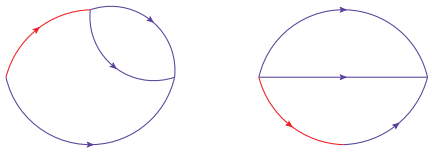

Figure 4.1: Two diagrams of a 3–point function for proton decay to a pion. The left hand diagram is a spatially oriented diagram with a proton on the right decaying to a meson on the left. The right hand diagram is rotated to show the 2–point–like function for the same process, involving two normal propagators and one sequential propagator. In both diagrams the blue lines represent quark propagators, while the red line represents the extended part of the sequential propagator.

### 4.4.5 Sequential Propagators

We will want to evaluate 3–point functions which are products of four propagators and are given by the expression,

$$G^{(3)}(x,y,0) = \mathrm{Tr}\left[S(x-y)\gamma_5 S(y-0)\Gamma S(x-0)\Gamma' S(x-0)\right] \; + \; \text{other contractions}, \tag{4.41}$$

where $\Gamma$ and $\Gamma'$ are two index spin matrices, the exact spin structure and all possible contractions for the three point functions we are interested in are given in Appendix B.

Diagrammatically, these 3–point functions look a lot like a 2–point functions with an extended propagator, see Figure 4.1. Instead of a 3–point function with source at position 0, sink at position $y$ and intermediate operator at position $x$, we instead treat this as a 2–point function with source and sink at 0 and $x$ respectively.

One of the propagators in this 2–point–like diagram contains the insertion point for the intermediate operator at position $y$, and this is known as the extended propagator or sequential propagator.

Going back to the example 3–point function given in equation 4.41, if we define a sequential propagator as:

$$S_{\mathrm{seq}}(x-0) = S(x-y)\gamma_5 S(y-0), \tag{4.42}$$

then we can rewrite Eq. 4.41 as,

$$S(y-0)\Gamma S(x-y)S(x-0)S(x-0) = S_{\mathrm{seq}}(x-0)\Gamma S(x-0)\Gamma' S(x-0). \tag{4.43}$$

This sequential propagator can be calculated by using a propagator, multiplied by any required spin structure $\Gamma$, as the source in Eq. 4.28. Expressions involving propagators can be

written in terms of this sequential propagator,

$$S_{\text{seq}}(z-y) = \sum_x S(y-x)\Gamma S(x-z)\mathrm{e}^{i\vec{p}.\vec{x}}. \tag{4.44}$$

where $\Gamma$ represents the spin structure required and $\vec{p}$ is the momentum inserted at the extension point.

### 4.4.6 Gauge smearing

Gauge smearing, or link smearing [70, 71] is the process of smoothing out the gauge fields by averaging over several neighbouring link configurations. When calculating observables, anytime we need to use a link $U_\mu(x)$, we can average together this, with the 6 spatial "staples" around it:

$$U_\mu(x) \to U'_\mu(x) = cU_\mu(x) + \sum_{\nu\neq\mu} U_\nu(x)U_\mu(x+\nu)U^\dagger_\nu(x+\mu), \tag{4.45}$$

see Figure 4.2. This new link $U'_\mu(x)$ must then be projected back onto the gauge group $SU(3)$. The ratio of the original link to the smeared links is parametrised by the constant $c$. The smearing can be carried out multiple ($N$) times, with the factor $N$ also a parameter which can be tuned.

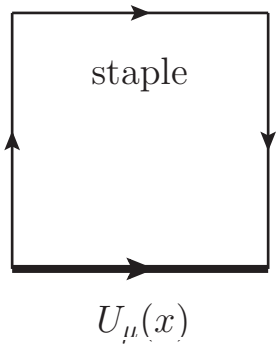


Figure 4.2: Showing one of the six possible staples around a link $U_\mu(x)$

Studies into the effects of gauge smearing have been carried out by [72], the effect is to increase the stability and speed of the inversion of the Dirac operator by removing eigenvalues of the Dirac operator close to 0.

## 4.5 Autocorrelations and thermalisation

Each gauge configuration is an update of the previous gauge configuration, therefore neighbouring gauge configurations are heavily correlated. We wish to average our data into bins, such

that each bin is sufficiently separated that it can be considered independent.

The integrated autocorrelation time [73] for an observable $\mathcal{O}(t)$ is,

$$\rho(t) = \frac{1}{N_{\text{data}} - t} \sum_{t'=1}^{N_{\text{data}}-t} \left(\mathcal{O}(t') - \bar{\mathcal{O}}\right)\left(\mathcal{O}(t'+t) - \bar{\mathcal{O}}\right), \tag{4.46}$$

where,

$$\bar{\mathcal{O}} = \sum_{t'=1}^{N_{\text{data}}} \mathcal{O}(t'), \tag{4.47}$$

and can be used to judge how quickly the gauge configurations decorrelate. The integrated autocorrelation time depends upon the observable being studied, and upon the lattice parameters in the simulation.

For our ensembles, the integrated autocorrelation time of the pseudo–scalar two–point correlation function was studied in Ref. [66]. See Section 5.4 for details of pseudo–scalar correlation functions. We define $\tau_{\text{int}} = \rho(12)$ to be the integrated autocorrelation time on time–slice 12 (a typical time–slice used in our fits, see Section 4.6), Ref. [66] plotted the integrated autocorrelation time as a function of separation between bins of configurations, this plot is shown in 4.3, and shows a plateau at a separation of around 20–25 trajectories, meaning that the configurations for our pseudo–scalar correlation function become decorrelated after a separation of approximately $2\tau_{\text{int}} = 40 - 50$ trajectories. The propagators for our n–point correlation functions shall therefore be measured at some frequency (for example every 10 configurations) and then binned to be in groups separated by at least 40 configurations.

We will also discard the first several gauge configurations until they have become thermalised. Ref [66] shows that for the plaquette, this happens after roughly 500 configurations, see Figure 4.4. We will therefore always discard at least the first 500 configurations of each ensemble.

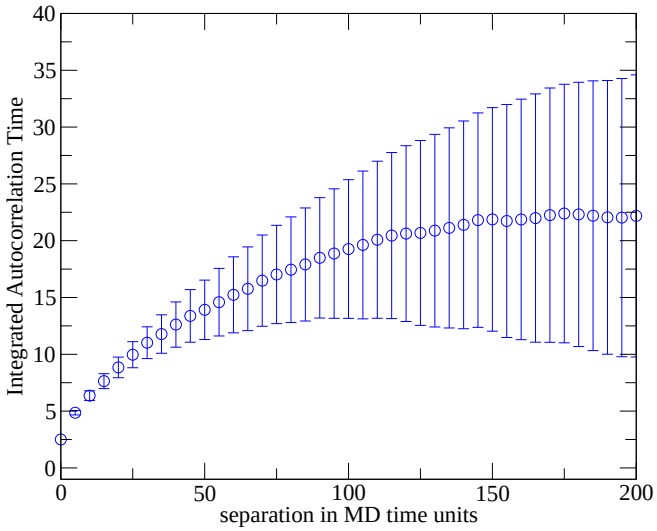


Figure 4.3: Integrated auto–correlation time for the two–point pseudo–scalar correlation function at timeslice 12 as a function of separation between neighbouring bins. The correlation function was calculated on the $am_u = 0.01, 16^3$ ensemble described in Section 5.2. Figure taken from [66].

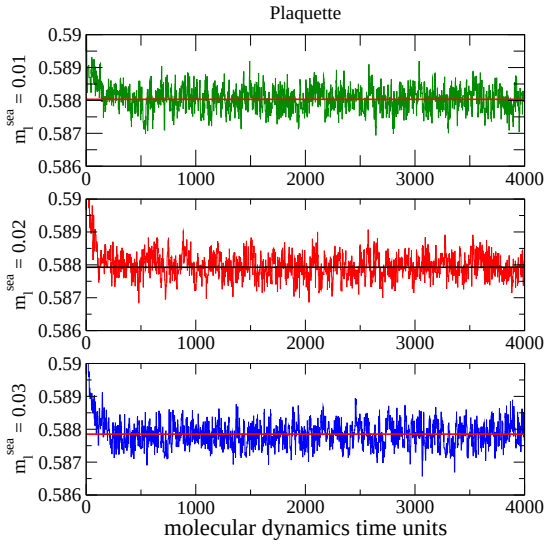


Figure 4.4: Evolution history of the plaquette calculated on the $am_u = 0.01, 0.02$ and $0.03$, $V = 16^3 \times 32$ ensembles described in Section 5.2. The horizontal lines are the ensemble average from configurations 2000–4000 for each ensemble. Figure taken from [66].

## 4.6 Fitting

We can generate data for two and three–point functions as in Eq. 4.27, Fourier transformed in $\vec{x}$, with momentum $\vec{p}$. As an example, the two–point pseudo–scalar correlation function with momentum $\vec{p} = 0$ is,

$$f(t) = \sum_{\vec{x}} \mathrm{Tr}\left[\langle \bar{q}(\vec{x},t)\gamma_5 q(\vec{x},t)\bar{q}(\vec{0},0)\gamma_5 q(\vec{0},0)\rangle\right], \tag{4.48}$$

where the trace is over spin and colour indices. This has time dependence (see Chapter 5 for details),

$$f(t) = \sum_n G_n \left[\mathrm{e}^{-m_n t} + \mathrm{e}^{-m_n(T-t)}\right], \tag{4.49}$$

where the sum over $n$ represents a sum over states with different energies $m_n$ and amplitudes $G_N$. $T$ is the time extent of the lattice. $m_n$ and $G_n$ are parameters of the pion correlation function which we wish to measure. Specifically, $m_0$ is the pseudo–scalar ground state mass and to find this we can form an effective mass,

$$m_{\mathrm{eff}}(t) = \cosh^{-1}\left(\frac{f(t+1)+f(t-1)}{f(t)}\right) \to m_\pi \quad 0 \ll t \ll T. \tag{4.50}$$

This effective mass tends to the ground state mass $m_\pi$ when the excited states from the sum in Eq. 4.49 have died away. Statistical noise will mean that the resulting data is not exactly constant, so in order to find the constant value, we will have to perform a fit to the data, over a time–range starting after the data becomes constant.

For other quantities we will use functions, or ratios of correlation functions to cancel the time dependence. The aim will always be to reduce the fitting procedure to one where we only need to fit to a constant.

### 4.6.1 Fitting to a constant

Suppose we start with a series of $N_{\mathrm{t}}$ distributions of values $\{f_i(t)\}$, where $i = 1 \ldots N_{\mathrm{conf}}$, and $t = 1 \ldots N_{\mathrm{t}}$, which we wish to fit to a constant $p$. We can do this by minimising $\chi^2$ where,

$$\chi^2(p) = \sum_{t,t'} \left(\bar{f}(t) - p\right)\left(\sigma_{t,t'}\right)^{-1}\left(\bar{f}(t') - p\right), \tag{4.51}$$

where $\bar{f}(t) = \frac{1}{N_{\mathrm{conf}}}\sum_i f_i(t)$ and $\sigma_{t,t'}$ is the covariance matrix (more detail about the computation of the covariance matrix can be found in Section 4.6.3). This can be minimised by setting

$\frac{d\chi^2(p)}{dp} = 0$,

$$\begin{aligned} 0 &= \frac{d}{dp}\left(\sum_{t,t'}\left(\bar{f}(t)-p\right)\left(\sigma_{t,t'}\right)^{-1}\left(\bar{f}(t')-p\right)\right) \\ &= \frac{d}{dp}\left(\sum_{t,t'}\bar{f}(t)\left(\sigma_{t,t'}\right)^{-1}\bar{f}(t') + p^2\left(\sigma_{t,t'}\right)^{-1} - \bar{f}(t)\left(\sigma_{t,t'}\right)^{-1}p - p\left(\sigma_{t,t'}\right)^{-1}\bar{f}(t')\right) \\ &= 2p\sum_{t,t'}\left(\sigma_{t,t'}\right)^{-1} - 2\sum_{t,t'}\bar{f}(t)\left(\sigma_{t,t'}\right)^{-1}, \end{aligned} \tag{4.52}$$

and solving for p, giving:

$$p_{\text{fit}} = \frac{\sum_{t,t'}\left(\sigma_{t,t'}\right)^{-1}\bar{f}(t')}{\sum_{t,t'}\left(\sigma_{t,t'}\right)^{-1}}. \tag{4.53}$$

The $\chi^2$ of this fit can then be calculated by substituting $p = p_{\text{fit}}$ in Eq. 4.51.

### 4.6.2 Error Bars

The above gives us a central value for a fit, but no error bar. The error on the fitted value can be calculated using a bootstrap resampling scheme [74]. Again, we start off with a series of $N_{\text{t}}$ distributions of values $\{f_i(t)\}$, where $i = 1 \ldots N_{\text{conf}}$, and $t = 1 \ldots N_{\text{t}}$. We can form a bootstrap sample by taking $N_{\text{conf}}$ random elements from within $\{f_i(t)\}$ allowing repeats, thus sampling the distribution $\{f_i(t)\}$ with a uniform probability. If we do this $\text{N}_{\text{boot}}$ times then this forms a distribution of distributions $\{f_j^b(t)\}$, with $j = 1 \ldots N_{\text{conf}}$, and $b = 1 \ldots N_{\text{boot}}$. On each bootstrap sample we can now calculate $\chi_b^2(p^b)$,

$$\chi_b^2(p^b) = \sum_{t,t'}\left(\bar{f}^b(t) - p^b\right)\left(\sigma_{t,t'}^b\right)^{-1}\left(\bar{f}^b(t') - p^b\right), \tag{4.54}$$

which is minimised by,

$$p_{\text{fit}}^b = \frac{\sum_{t,t'}\left(\sigma_{t,t'}^b\right)^{-1}\bar{f}^b(t')}{\sum_{t,t'}\left(\sigma_{t,t'}^b\right)^{-1}}. \tag{4.55}$$

Now we have a distribution of values for $p_{\text{fit}}$, and the width of this distribution is an estimate of the variance of the fitted value.

### 4.6.3 Correlations

The covariance matrix $\sigma_{t,t'}^b$ contains any information about how correlated the data we are fitting is. For uncorrelated data, the covariance matrix will be diagonal, with elements equal to the variance of each datapoint. In general however, the data we generate will contain correlations

between timeslices, which we must take into account when fitting. Unfortunately, we do not know the exact covariance matrix, we must estimate it from the sample data.

In order to do this we have three options

- Ignore any correlations completely, by using a diagonal covariance matrix

$$\sigma^b_{t,t'} = \begin{cases} \frac{1}{N_{\rm boot}} \sum_b (\bar{f}^b(t) - \langle \bar{f}(t) \rangle)(\bar{f}^b(t') - \langle \bar{f}(t') \rangle), & \text{if } t = t' \ , \\ 0, & \text{otherwise,} \end{cases} \tag{4.56}$$

  where,

$$\langle \bar{f}(t) \rangle = \frac{1}{N_{\rm boot}} \sum_b \bar{f}^b(t) = \frac{1}{N_{\rm boot}} \frac{1}{N_{\rm conf}} \sum_b \sum_j f^b_j(t). \tag{4.57}$$

- Estimate the covariance matrix from all of the original data and use this same covariance matrix for each bootsample,

$$\sigma_{t,t'} = \frac{1}{N_{\rm boot}} \sum_b (\bar{f}^b(t) - \langle \bar{f}(t) \rangle)(\bar{f}^b(t') - \langle \bar{f}(t') \rangle). \tag{4.58}$$

  This is known as a frozen covariance matrix.

- Use only the data contained in each bootsample to estimate the covariance matrix. The covariance matrix will therefore be different for each bootsample. To do this we need to form a secondary bootstrap sample from our data. Starting from the distribution of distributions $\{f^b_j(t)\}$ for each b we take $N_{\rm conf}$ random elements, allowing repeats as before. Doing this $N_{\rm boot}$ times gives $\{f^{bb'}_k(t)\}$ where $k = 1 \ldots N_{\rm conf}$ and $b/b' = 1 \ldots N_{\rm boot}$. Then the covariance matrix is

$$\sigma^b_{t,t'} = \frac{1}{N_{\rm boot}} \sum_{b'} (\bar{f}^{bb'}(t) - \langle \bar{f}^b(t) \rangle)(\bar{f}^{bb'}(t') - \langle \bar{f}^b(t') \rangle), \tag{4.59}$$

  where,

$$\bar{f}^{bb'}(t) = \frac{1}{N_{\rm conf}} \sum_k f^{bb'}_k(t), \tag{4.60}$$

$$\langle \bar{f}^b(t) \rangle = \frac{1}{N_{\rm boot}} \sum_{b'} \bar{f}^{bb'}(t) = \frac{1}{N_{\rm boot}} \frac{1}{N_{\rm conf}} \sum_{b'} \sum_k f^{bb'}_k(t). \tag{4.61}$$

  This is known as an unfrozen covariance matrix.

As we are dealing with correlated data, it is unsatisfactory to use an uncorrelated fit. If possible we wish to use correlated fits. For estimating the covariance matrix, [75] shows that the unfrozen estimate has a smaller bias, so this is the method we shall use. However, [76] warns of

the dangers of using correlated fits with insufficient data. For $N$ data samples and a fit function with $D$ parameters [76] suggests not using correlated fits unless $N > \max(D^2, 10(D+1))$. For our case, where we typically fit to a constant ($D = 1$), we therefore require $N > 20$. The drawback of using an unfrozen covariance matrix is that the condition number of the covariance matrix can be higher than that of the frozen covariance matrix, and so the numerical inversion which we require to perform the fit can be more unstable. Where this is the case, we shall use an uncorrelated fit.

### 4.6.4 Fitting real data

We will be interested in fitting data which is a function of one or more parameters, often involving an exponential decay. There are algorithms which can fit directly to a function of data but in some cases it may be beneficial to find a function of the data which is either constant, or tends to a constant, and to fit to that using the algorithm outlined in Section 4.6.1 above.

As already mentioned, for the example of the pion, we can isolate the ground state mass by forming an effective mass as shown in Eq. 4.50 and explained in detail in Section 5.4. In general, if there is a function $g[f(\{p_i\}; t)] \to p_j$ at large times, then we can fit to this to find one parameter instead of using a more complicated algorithm to find all the parameters at once.

### 4.6.5 Fit Algorithm Summary

The full fitting algorithm, using an unfrozen covariance matrix to fit a constant to a function of the raw data, is summarised below in Figure 4.5.

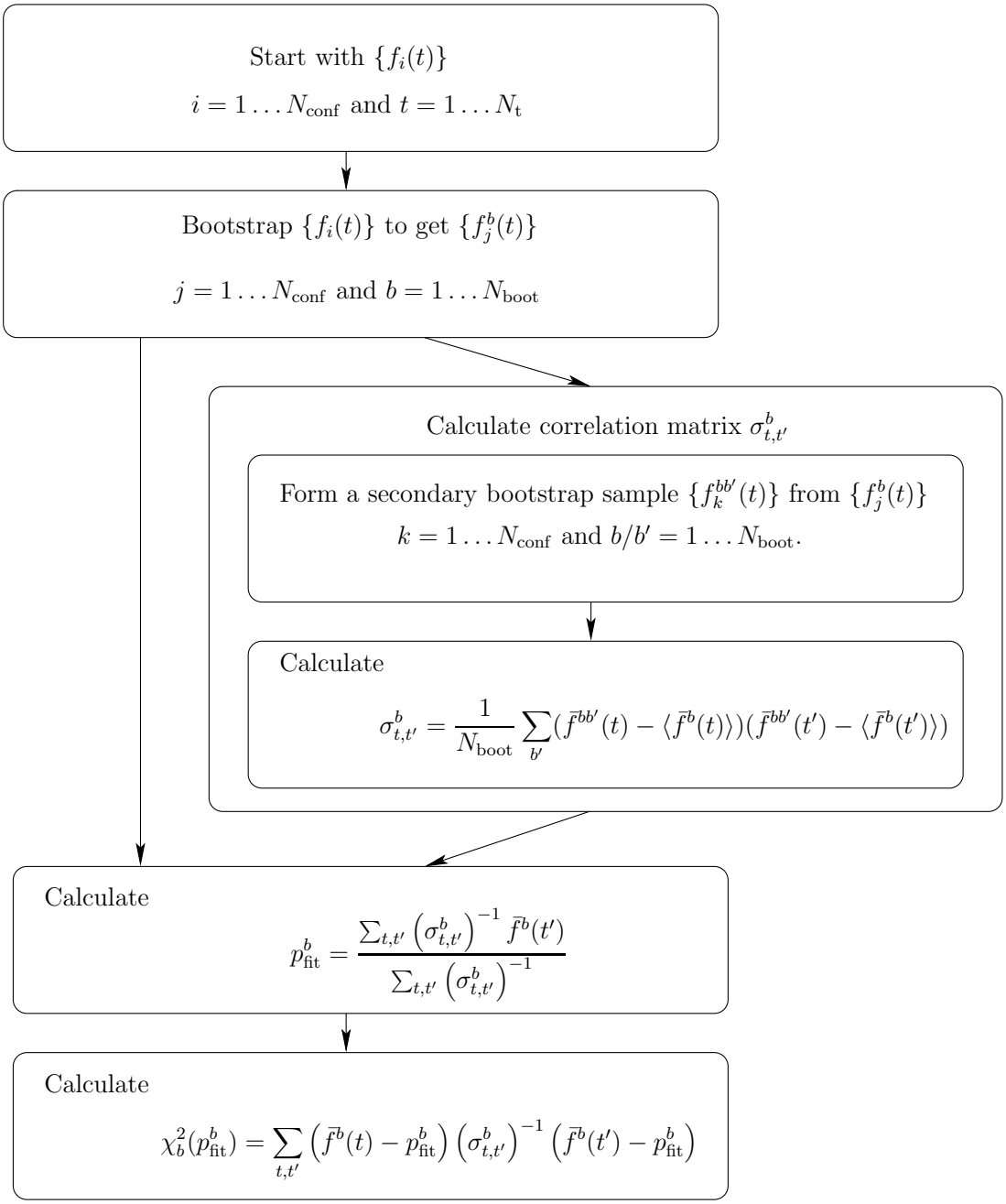


Figure 4.5: An algorithm for fitting a constant to some data

# Chapter 5

# Meson and Baryon Results

In this chapter, I shall give results for baryon and meson 2–point functions. Although not directly related to proton decay, some of these results are required to properly normalise the proton decay matrix elements, as shown Chapter 6. First I shall give some general notation for two–point functions in Section 5.1, then I shall describe the ensembles we used in the baryon and meson calculations in Section 5.2. Next I will talk about baryon correlation functions, specifically the proton correlation function and its mass and amplitude in Section 5.3. Finally I will discuss pseudo–scalar meson correlation functions in Section 5.4.

## 5.1 General Notation

At this stage, it is useful to define two general classes of operators. Firstly a three quark operator,

$$\mathcal{O}^{\Gamma_m\Gamma_n}_{q_iq_jq_k} = \epsilon_{abc}(q_i^{aT}C\Gamma_m q_j^b)\Gamma_n q_k^c, \tag{5.1}$$

and secondly a two quark operator,

$$\mathcal{O}^{\Gamma_n}_{q_iq_j} = (\bar{q}_i^a\Gamma_n q_j^a). \tag{5.2}$$

In both cases $\Gamma_n$ are 2 index spin matrices and $q_i^a$ are quark fields with flavour $i$ and colour $a$. The matrix $C = \gamma_2\gamma_4$ is the charge conjugation matrix. Note that all spin indices have been suppressed. We have already seen operators of the type in Eq. 5.1 when discussing the baryon number violating operators in Section 2.4.

We also introduce a labelling for the possible spin matrices, $\Gamma_n$, which is shown in Table 5.1.

We can form 2–point correlation functions from these operators

$$f^{A,B}(t) = \sum_{\vec{x}} \mathrm{e}^{i\vec{p}.\vec{x}}\mathrm{Tr}\left[S_{\mathrm{proj}}\langle\mathcal{O}^A(\vec{x},t)\bar{\mathcal{O}}^B(\vec{0},0)\rangle\right], \tag{5.3}$$

| Label | Spin structure |
|---|---|
| $S$ | $1$ |
| $P$ | $\gamma_5$ |
| $V$ | $\gamma_\mu$ |
| $A$ | $\gamma_\mu\gamma_5$ |
| $T$ | $\sigma_{\mu\nu} = \frac{1}{2}[\gamma_\mu, \gamma_\nu]$ |
| $\tilde{T}$ | $\gamma_5\sigma_{\mu\nu}$ |
| $L$ | $P_L = \frac{1}{2}(1-\gamma_5)$ |
| $R$ | $P_R = \frac{1}{2}(1+\gamma_5)$ |

Table 5.1: Labelling of combinations of spin matrices

with $A, B$ collective indices representing the flavour and spin structure of either 2 quark or 3 quark operators and the trace is over all spin and colour indices. This is a 2–point function for a hadron created at the origin, and then annihilated at $(\vec{x}, t)$. $S_{\text{proj}}$ is a spin projection matrix. In baryons $S_{\text{proj}} = \frac{1}{2}(1+\gamma_4)$ projects out the positive parity state, while $S_{\text{proj}} = \frac{1}{2}(1-\gamma_4)$ gives the negative parity state. The pseudo–scalar meson states have negative parity, so there is no need for a parity projection and we use $S_{\text{proj}} = 1$. $\vec{p}$ is the momentum of the state we wish to study.

We sum over the spatial co-ordinate $\vec{x}$, to leave a two–point correlator as function of time. As we shall see later, the long time exponential fall off of this correlation function can be used to study the ground state mass.

## 5.2 Ensemble details

Gauge configurations were generated with the RHMC algorithm with a trajectory length of $\tau = 1$. These ensembles are the same as those described in [66] and [77]. There are ensembles for two different lattice volumes, $V = L_x^3 \times L_t \times L_5 = 16^3 \times 32 \times 16$, and $24^3 \times 64 \times 16$, with $L_x$ the size of the lattice in each of the three spatial directions, $L_t$ the size in the time direction and $L_5$ the size in the 5th dimension. Both of these lattices have a fixed inverse lattice spacing of $a^{-1} = 1.73(3)$ GeV. For each volume, ensembles with light sea quark masses of $am_{ud} = 0.01, 0.02, 0.03$ were produced, while on the $24^3 \times 64 \times 16$ volume lattice, we produced an additional ensemble with sea quark mass $am_{ud} = 0.005$. The mass of the strange quark in the sea remained fixed in each ensemble at $am_s = 0.04$.

Quark propagators were then calculated on configurations separated by $\Delta$ gauge configurations, such that there were no significant autocorrelations (see Section 4.5). The exact configuration ranges and $\Delta$ for the ensembles used to generate nucleon and meson correlation functions are given in Tables 5.2 and 5.3 respectively. The propagators were calculated using valence quark masses equal to either the light sea quark mass, or the strange sea quark mass as

appropriate. These propagators were then combined and contracted with the appropriate spin / colour structure to form the two–point correlation functions. For the case of the $24^3 \times 64 \times 16$ lattice, there are two independent propagator runs for each light quark mass.

| $V \times L_s$ | $am_{ud}$ | $N_{\text{traj}}$ | $\Delta$ | $N_{\text{cfg}}$ | $N_{\text{src}}$ | $N_{\text{bin}}$ | Smearing |
|---|---|---|---|---|---|---|---|
| | 0.01 | 500-4000 | 10 | 175 | 4 | 8 | LL, GL, GG |
| $16^3 \times 32 \times 16$ | 0.02 | 500-4000 | 10 | 175 | 4 | 8 | LL, GL, GG |
| | 0.03 | 500-7580 | 10 | 177 | 2 | 8 | LL, GL, GG |
| | 0.005 | 900-4500 | 10 | 90 | 2 | 8 | LL, HL |
| | | | 10 | 90 | $2 \times 2$ | 8 | G'L, G'G' |
| $24^3 \times 64 \times 16$ | 0.01 | 1500-3860 | 10 | 59 | 2 | 8 | LL, GL |
| | | | 40 | 59 | 2 | 2 | G'L |
| | 0.02 | 1800-3600 | 10 | 45 | 2 | 8 | LL, HL |
| | | | 40 | 45 | 2 | 2 | G'L |
| | 0.03 | 1020-3060 | 20 | 51 | 1 | 2 | LL, HL |
| | | | 40 | 51 | 1 | 1 | G'L |

Table 5.2: RHMC 2+1 flavour datasets used for the proton mass and amplitude calculations. $V$ is the space-time volume of the lattice, $L_s$ is the extent of the fifth dimension, $am_{ud}$ is the light sea quark mass ($am_s$ is kept fixed at 0.04), $N_{\text{traj}}$ is the lowest to highest trajectories analysed with correlation functions calculated every $\Delta$ trajectories, $N_{\text{cfg}}$ is the number of configurations, $N_{\text{src}}$ is the number of quark propagators solved with different source locations and $N_{\text{bin}}$ is the bin size. For the $24^3 \times 64 \times 16$ data, there are two independent runs for each of the sea quark masses. These independent runs used different smearings, $\Delta$, source locations and $N_{\text{src}}$. Smearing shows the multiple different smearing of the quark fields used. Each smearing is a 2 letter code to denote the smearing of the three quark fields at the source and sink respectively, $L$ is for local smearing, $G$ and $G'$ are Gaussian smearing with different smearing radii, $H$ is hydrogen–like wavefunction smearing.

The abbreviations for the different smearings given in Tables 5.2 and 5.3 correspond to the smearing at source and sink. In all cases all of the quarks at the source or sink are smeared in the same way, this is the same convention as used in [78]. For the baryon correlation functions, this abbreviation is always a two letter code, with the first letter referring to source smearing and the second to sink smearing. $L$ refers to local or unsmeared quark fields, $G$ and $G'$ both refer to Gaussian smeared quark fields, but with a different smearing radius, $H$ refers to Hydrogen–like wavefunction smearing. For the meson correlation functions, $GK$ corresponds to a Gaussian smeared Kenway source, while the third letter, $L$ or $G$, corresponds to either Local or Gaussian sink smearing. We have used different smearing parameters for the Gaussian smearing of the meson and baryon fields. For details of each of these smearing functions, see Section 4.4.

| $V \times L_s$ | $am_{ud}$ | $N_{\rm traj}$ | $\Delta$ | $N_{\rm cfg}$ | $N_{\rm src}$ | $N_{\rm bin}$ | Smearing |
|---|---|---|---|---|---|---|---|
| $24^3 \times 64 \times 16$ | 0.005 | 900-4350 | 50 | 70 | 1 | 1 | GKL, GKG |
| | 0.01 | 1540-7500 | 80 | 75 | 1 | 1 | GKL, GKG |
| | 0.02 | 1620-3600 | 40 | 50 | 1 | 1 | GKL, GKG |
| | 0.03 | 1260-3040 | 40 | 45 | 1 | 1 | GKL, GKG |

Table 5.3: RHMC 2+1 flavour datasets used for the pseudo–scalar meson mass and amplitude calculations. $V$ is the space-time volume of the lattice, $L_s$ is the extent of the fifth dimension, $am_{ud}$ is the light sea quark mass ($am_s$ is kept fixed at 0.04), $N_{\rm traj}$ is the lowest to highest trajectories analysed with correlation functions calculated every $\Delta$ trajectories, $N_{\rm cfg}$ is the number of configurations, $N_{\rm src}$ is the number of quark propagators solved with different source locations and $N_{\rm bin}$ is the bin size. All propagators used are solved with a gaussian smeared Kenway source, denoted $GK$. The sink smearing is either Local $L$, or Gaussian $G$.

## 5.3 The proton correlation function

We wish to calculate the proton correlation function, $f^{PS,PS}_{udu,udu}$, which involves the operators $\mathcal{O}^{PS}_{udu}$. For momentum $\vec{p} = 0$ and writing all fields and indices explicitly we get,

$$f^{PS,PS}_{udu,udu} = \sum_{\vec{x}} \epsilon^{abc}\epsilon^{def}\frac{1}{2}\left(1+\gamma_4\right)_{\delta\gamma} \tag{5.4}$$

$$\left\langle u^a_\alpha(x)(C\gamma_5)_{\alpha\beta}d^b_\beta(x)u^c_\gamma(x)\bar{u}^d_\delta(0)\bar{d}^e_\epsilon(0)\overline{(C\gamma_5)}_{\epsilon\zeta}\bar{u}^f_\zeta(0)\right\rangle . \tag{5.5}$$

See Appendix A for details. The sum over all possible Wick contractions between quark and antiquark fields gives two different sets,

$$\left\langle u^a_\alpha(x)d^b_\beta(x)u^c_\gamma(x)\bar{u}^d_\delta(0)\bar{d}^e_\epsilon(0)\bar{u}^f_\zeta(0)\right\rangle = u^a_\alpha(x)d^b_\beta(x)u^c_\gamma(x)\bar{u}^d_\delta(0)\bar{d}^e_\epsilon(0)\bar{u}^f_\zeta(0)$$

$$+ \; u^a_\alpha(x)d^b_\beta(x)u^c_\gamma(x)\bar{u}^d_\delta(0)\bar{d}^e_\epsilon(0)\bar{u}^f_\zeta(0). \tag{5.6}$$

We exchange pairs of quark fields until each contraction is between quark fields which appear next to each other in Eq. 5.6. Each interchange introduces a minus sign, as the quark fields anticommute. The first set of contractions requires an odd number of interchanges, while the second requires an even number.

We are then left with a series of contractions, each contraction gives us a propagator, e.g..

$$\overbrace{u^a_\alpha(x)\bar{u}^b_\beta(0)} = S^{ab}_{\alpha\beta}(x). \tag{5.7}$$

Substituting these contractions back into Eq. 5.5 gives:

$$f^{PS,PS}_{udu,udu} = \sum_{\vec{x}} \frac{1}{2}(1+\gamma_4)_{\delta\gamma}\epsilon^{abc}\epsilon^{def}(C\gamma_5)_{\alpha\beta}\overline{(C\gamma_5)}_{\epsilon\zeta} \left[S^{af}_{\alpha\zeta}(x)S^{be}_{\beta\epsilon}(x)S^{cd}_{\gamma\delta}(x) - S^{ad}_{\alpha\delta}(x)S^{bf}_{\beta\zeta}(x)S^{ce}_{\gamma\epsilon}(x)\right]. \quad (5.8)$$

Although some of the propagators are between up quarks/antiquarks and some between down quarks/antiquarks, from now on we ignore this distinction as the masses of the up and down quarks in our simulation are equal, and therefore the propagators are the same.

On each ensemble, a propagator was calculated with a valence quark mass equal to the light quark mass in the sea. This propagator was then used multiple times, and its loose spin and colour indices contracted together in the appropriate ways as in Eq. 5.8 to form $f^{PS,PS}_{udu,udu}$.

The time dependence of the proton correlation function can be found if we substitute,

$$\langle \mathcal{O}_N(x)\bar{\mathcal{O}}_N(x)\rangle = \sum_k \mathrm{e}^{ik.x}\langle \mathcal{O}_N(k)\bar{\mathcal{O}}_N(k)\rangle, \quad (5.9)$$

and insert a complete set of states,

$$1 = \frac{1}{2E(\vec{k})}\sum_n\sum_s |n(k,s)\rangle\langle n(k,s)|\,, \quad (5.10)$$

to give:

$$\begin{aligned} f^{PS,PS}_{udu,udu}(t) &= \mathrm{Tr}\sum_k\sum_{\vec{x}} S_{\mathrm{proj}}\mathrm{e}^{i\vec{k}.\vec{x}-E(k)t}\langle \mathcal{O}_N(k,s)\frac{1}{2E(k)}\sum_n |n(k,s)\rangle\langle n(k,s)|\,\bar{\mathcal{O}}_N(k,s)\rangle \\ &= \mathrm{Tr}\sum_k \delta(\vec{k})S_{\mathrm{proj}}\mathrm{e}^{-E(k)t}\langle \mathcal{O}_N(k,s)\frac{1}{2E(k)}\sum_n |n(k,s)\rangle\langle n(k,s)|\,\bar{\mathcal{O}}_N(k,s)\rangle \\ &= \sum_k \frac{1}{2E(k)}\mathrm{e}^{-E(k)t}\mathrm{Tr}S_{\mathrm{proj}}\langle \mathcal{O}_N(k,s)|0\rangle\langle 0|\bar{\mathcal{O}}_N(k,s)\rangle\delta(\vec{k}) \\ &= \sum_k \frac{1}{2E(k)}\mathrm{e}^{-E(k)t}\mathrm{Tr}S_{\mathrm{proj}}G_N(k)u(k,s)G_N(k)\bar{u}(k,s)\delta(\vec{k}), \end{aligned} \quad (5.11)$$

where we have defined the proton amplitude $G_N(k)$,

$$\langle \mathcal{O}_N(k,s)|0\rangle = G_N(k)u(k,s). \quad (5.12)$$

Now tracing over the spin indices using,

$$\mathrm{Tr}\left[u(k,s)\bar{u}(k,s)\right]\delta(\vec{k}) = \left[\gamma_\mu k_\mu + E(k)\right]\delta(\vec{k}) = \left[1+\gamma_4\right]E(k)\delta(\vec{k}), \quad (5.13)$$

and inserting $S_{\rm proj} = \frac{1}{2}(1+\gamma_4)$ we get,

$$\begin{aligned} f^{PS,PS}_{udu,udu}(t) &= \sum_k \frac{1}{2E(k)} G_N^2(k) \mathrm{e}^{-E(k)t} \mathrm{Tr} \frac{E(k)}{2} (1+\gamma_4)(1+\gamma_4) \\ &= 2\sum_k G_N^2(k) \mathrm{e}^{-E(k)t}. \end{aligned} \tag{5.14}$$

We can split the sum over energies into two, a sum over positive energies, and another over negative energies. The negative energy states can be thought of as a backwards propagating positive energy states, and therefore we write the correlation function as,

$$f^{PS,PS}_{udu,udu}(t) = 2\sum_k (G_p)^2 \mathrm{e}^{-E(k)t} + \left(G'_p\right)^2 \mathrm{e}^{-E'(k)(T-t)}. \tag{5.15}$$

For $0 \ll t \ll T/2$, only the forward propagating ground state will contribute leaving,

$$f^{PS,PS}_{udu,udu}(t) \to 2 (G_N)^2 \mathrm{e}^{-m_N t}. \tag{5.16}$$

$m_N$ is the mass of ground state and $G_N$ is the ground state amplitude. The aim of this section shall be to calculate the ground state mass and amplitude, $m_N$ and $G_N$.

### 5.3.1 The proton mass

$m_N$ can be found by considering an effective mass,

$$m_{\rm eff} = log\left(\frac{C(t)}{C(t+1)}\right) \to m_N \quad 0 \ll t \ll T/2. \tag{5.17}$$

Over the appropriate time range, this effective mass should tend to a constant, we will call this flat region a plateau. We can therefore perform a fit to the effective mass over a window between timeslices $t_{\rm min}$ and $t_{\rm max}$, with an unfrozen correlation matrix using the algorithm described in Section 4.6.

$t_{\rm max}$ is chosen so that the contribution from the backwards propagating state does not contaminate the signal from the forward propagating state we are trying to measure. In practice, the signal in a baryon correlation function is statistically noisy, and this noise increases with $t$, so any signal has degenerated into noise well before the backward propagating state has any sizeable effect. Therefore, any reasonable choice of $t_{\rm max}$ does not greatly affect the fit. However, it is important to cut off the fit range at a point when the error bars are still reasonable, as otherwise a poor fit to the first few points in the fit window, can be disguised by the large errors (and hence small contributions to $\chi^2$/d.o.f) on the final few points in the fit window.

$t_{\rm min}$ must be high enough such that the excited state contributions have died out from the sum in Eq. 5.15. Obviously the choice of $t_{\rm min}$ will affect the fitted value for the effective mass.

As the plateau is approached from above, fitting to a timeslice which is too early will tend to increase the fitted value for the mass. The stability of the fit to sensible variations in the fit range is an important test of the accuracy of the fit itself. For each fit, we will check that the fitted value does not change noticeably within $t_{\min} \pm 1$.

The effective mass of the proton correlation function, with the number of configurations we have generated, can be very noisy. The result of this is that the fitted value for the proton mass will have a large statistical error. However, it also makes determining the exact location of the plateau difficult, thus increasing the systematic error. To overcome these problems, we can perform a simultaneous fit to the effective mass of multiple correlation functions with the same exponential time dependence. As the data just tends to a constant, this is simple to do, and does not introduce any additional fit parameters. Firstly, the operator $\mathcal{O}^{PS}_{udu}$, which appears in the correlation function $f^{PS,PS}_{udu,udu}$, is only one possible operator. Another choice is the operator $\mathcal{O}^{A_4S}_{udu}$, with a correlation function $f^{A_4S,A_4S}_{udu,udu}$ which has the same exponential time dependence. Secondly we can fit to multiple correlation functions with different smearing combinations, as described in Section 4.4. The types of smearing we have used for each ensemble are given in Table 5.4. All of these additional correlation functions will be correlated, as they are all calculated on the same gauge configurations. We will call each operator / smearing combination a fit channel.

One extra possible advantage of different channels is that they can have a different (and hopefully better) overlap with the ground state than the unsmeared $f^{PS,PS}_{udu,udu}$ correlation function. A better overlap means that the excited states die out sooner and the plateau begins at an earlier timeslice, allowing a fit to more datapoints. To fully maximise this possible benefit, it is important to choose fit ranges separately for each channel.

Results for the proton mass calculated on each of the ensembles described in Section 5.2 are given in Table 5.5 and example effective mass plateaus are shown in Figure 5.1. The different channels and the corresponding time ranges used in each fit are given in Table 5.5.

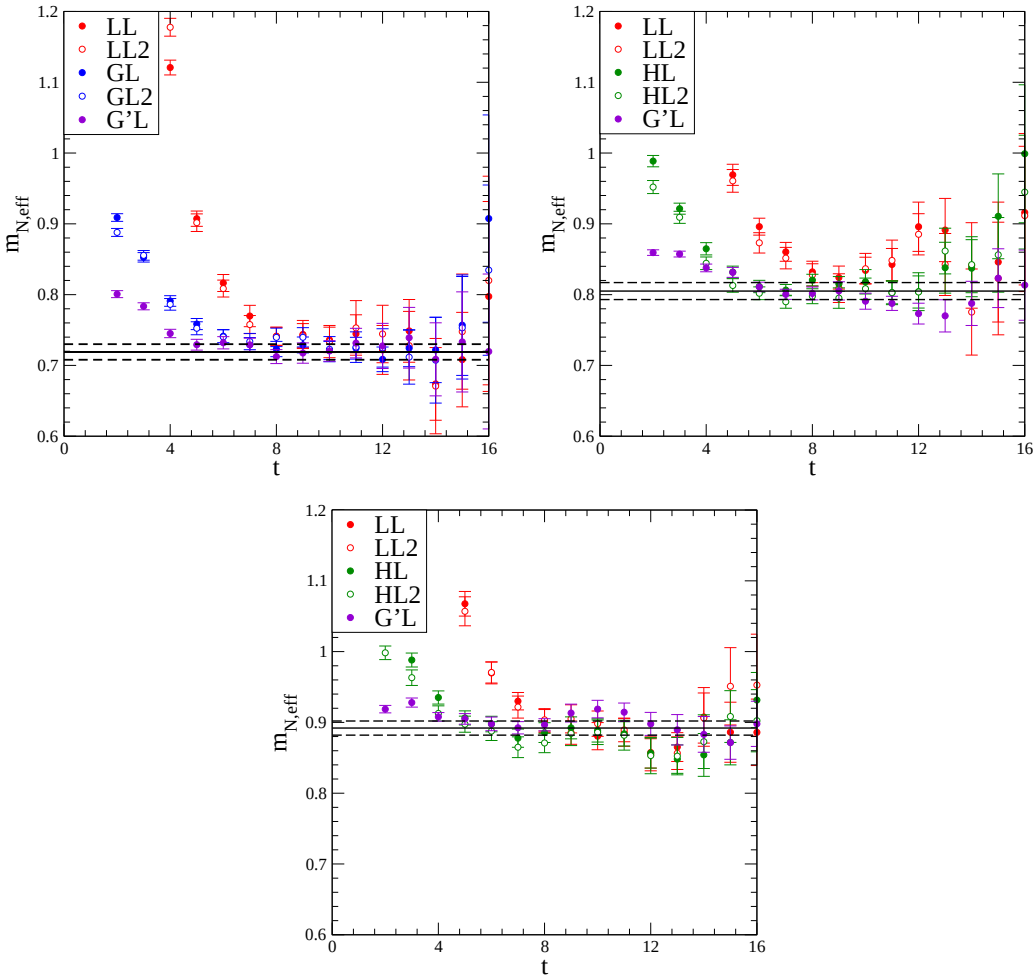


Figure 5.1: Effective mass (Eq. 5.17) plots for the $24^3 \times 64$ ensemble with different light valence quark masses. (a) is for $am_u = 0.01$, (b) is for $am_u = 0.02$ and (c) is for $am_u = 0.03$. The different colours correspond to different smearings. Those datasets labelled with a 2 use the operator $f^{A_4S,A_4S}_{udu,udu}(t)$, the rest use $f^{PS,PS}_{udu,udu}(t)$. Horizontal lines show the fit to the plateau.

| $m_u$ | $V = 16^3 \times 32$ | | | | $V = 24^3 \times 64$ | | | |
|---|---|---|---|---|---|---|---|---|
| | | | Fit Range | | | | Fit Range | |
| | Smearing | $O^{\Gamma\Gamma}$ | $m_N$ | $G_N$ | Smearing | $O^{\Gamma\Gamma}$ | $m_N$ | $G_N$ |
| 0.005 | | | | | LL | $O^{PS}$ | - | 9-12 |
| | | | | | HL | $O^{PS}$ | 6-12 | - |
| | | | | | HL | $O^{A_4S}$ | 6-12 | - |
| | | | | | G'L | $O^{PS}$ | 6-12 | - |
| | | | | | G'G' | $O^{PS}$ | 6-12 | - |
| 0.01 | LL | $O^{PS}$ | 9-12 | 9-12 | LL | $O^{PS}$ | 9-12 | 9-12 |
| | LL | $O^{A_4S}$ | 9-12 | - | LL | $O^{A_4S}$ | 9-12 | - |
| | GL | $O^{PS}$ | 9-12 | - | GL | $O^{PS}$ | 8-12 | - |
| | GL | $O^{A_4S}$ | 9-12 | - | GL | $O^{A_4S}$ | 8-12 | - |
| | | | | | G'L | $O^{PS}$ | 7-12 | - |
| 0.02 | LL | $O^{PS}$ | 9-12 | 9-12 | LL | $O^{PS}$ | 9-10 | 9-12 |
| | LL | $O^{A_4S}$ | 9-12 | - | LL | $O^{A_4S}$ | 9-10 | - |
| | GL | $O^{PS}$ | 8-12 | - | HL | $O^{PS}$ | 9-11 | - |
| | GL | $O^{A_4S}$ | 8-12 | - | HL | $O^{A_4S}$ | 9-11 | - |
| | GG | $O^{PS}$ | 8-11 | - | G'L | $O^{PS}$ | 9-11 | - |
| | GG | $O^{A_4S}$ | 8-11 | - | | | | |
| 0.03 | LL | $O^{PS}$ | 10-12 | 9-12 | LL | $O^{PS}$ | 10-12 | 9-12 |
| | LL | $O^{A_4S}$ | 10-12 | - | LL | $O^{A_4S}$ | 10-12 | - |
| | GL | $O^{PS}$ | 8-12 | - | HL | $O^{PS}$ | 9-12 | - |
| | GL | $O^{A_4S}$ | 8-12 | - | HL | $O^{A_4S}$ | 9-12 | - |
| | GG | $O^{PS}$ | 8-12 | - | G'L | $O^{PS}$ | 8-12 | - |
| | GG | $O^{A_4S}$ | 8-12 | - | | | | |

Table 5.4: Smearings, operators and fit ranges used for the calculation of nucleon masses and amplitudes. The smearing is a two letter code denoting smearing at the source and sink respectively, with L for Local smearing, G and G' for Gaussian smearing with different smearing radii, and H for Hydrogen–like wavefunction smearing.

| $V \times L_s$ | $am_{ud}/am_s$ | $am_N$ | $G_N$ |
|---|---|---|---|
| $16^3 \times 32 \times 16$ | 0.03/0.04 | 0.908(6) | 0.01387(36) |
| | 0.02/0.04 | 0.819(8) | 0.01198(35) |
| | 0.01/0.04 | 0.722(19) | 0.00996(22) |
| | $\chi^{\mathrm{ral}}$ | 0.606(24) | 0.00745(50) |
| $24^3 \times 64 \times 16$ | 0.03/0.04 | 0.892(10) | 0.01362(41) |
| | 0.02/0.04 | 0.805(12) | 0.01156(57) |
| | 0.01/0.04 | 0.720(10) | 0.00990(31) |
| | 0.005/0.04 | 0.671(5) | 0.00789(24) |
| | $\chi^{\mathrm{ral}}$ | 0.588(9) | 0.00651(36) |

Table 5.5: Results from fits to the nucleon mass and amplitude, as a function of the quark masses and lattice volume. Also shown are the results of the linear extrapolation of the nucleon mass and amplitude to the chiral limit.

### 5.3.2 The proton mass: error scaling

For the case of the $am_u = 0.005$ ensemble on the $24^3 \times 64$ lattice, the plateau was not stable within variations of $t_{\text{min}}$, see Figure 5.2. To account for this additional source of error, we fitted across a large time range spanning the multiple potential plateau. The incompatibility of the multiple plateau is reflected in a poor value for $\chi^2$ per degree of freedom of 4.3. We then rescaled the errors on each datapoint by $\sqrt{\chi^2/\text{d.o.f}}$ and performed a second fit to this rescaled data. This gave a $\chi^2$/d.o.f of 1, as expected, and a fitted mass compatible with the all of the previous best fit values, but with a larger error. This larger error reflects both the statistical error and the additional systematic error of choosing the correct plateau region. The fits to the effective mass on this ensemble before and after rescaling are shown in Figure 5.2. This fitted value from the rescaled data is the one given in Table 5.5.

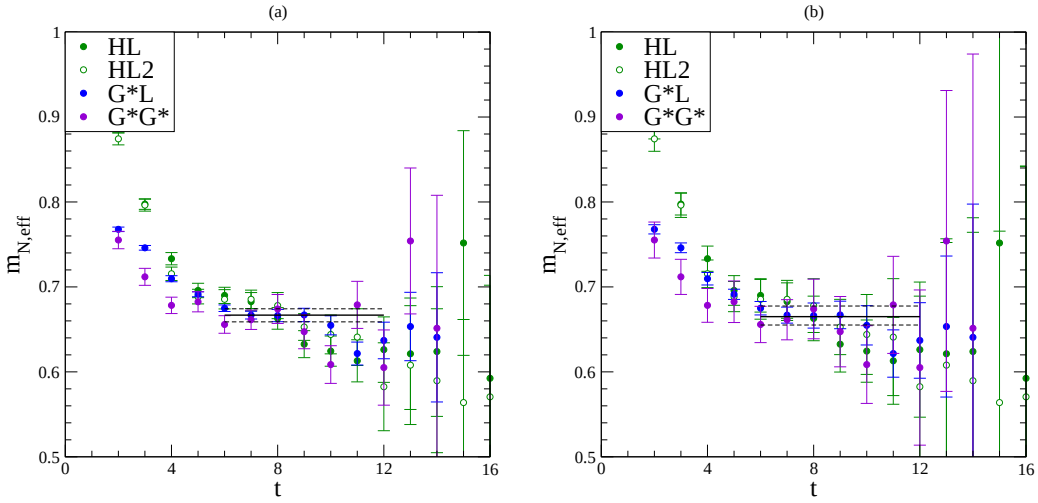


Figure 5.2: Effective mass (Eq. 5.17) plots for the $24^3 \times 64$ ensemble with different light valence quark masses $am_u = 0.005$. (a) shows the fit across the two incompatible choices for the plateau (b) shows the fit to the combined plateau after rescaling the errors. The different colours correspond to different smearings. Those datasets labelled with a 2 use the operator $f^{A_4S,A_4S}_{udu,udu}(t)$, the rest use $f^{PS,PS}_{udu,udu}(t)$.

### 5.3.3 The proton mass: extrapolation

The proton masses for the different ensembles, are compatible with a linear extrapolation in the quark mass,

$$m_N = A(m_u + m_{\text{res}}) + B. \tag{5.18}$$

The value of the proton mass in the chiral limit defined as the value of $m_N$ at $a(m_u + m_{\text{res}}) = 0$. Graphs of these extrapolations are shown in Figure 5.3 and the value of the proton mass in the chiral limit is shown in Table 5.5. Within errors, the proton mass calculated on ensembles with the same valence quark mass are compatible, as are the extrapolated values.

We can calculate the proton mass in the chiral limit in physical units by multiplying our result in lattice units by the inverse lattice spacing $a^{-1} = 1.73(3)$GeV. This gives $m_N = 1.04(4)$GeV and 1.02(2)GeV for the $16^3 \times 32 \times 16$ and $24^3 \times 64 \times 16$ lattices respectively. The error quoted does not include any additional systematic errors, but is already close to agreement with the experimentally measured values for the nucleon mass $m_N = 0.938272013(23)$GeV.

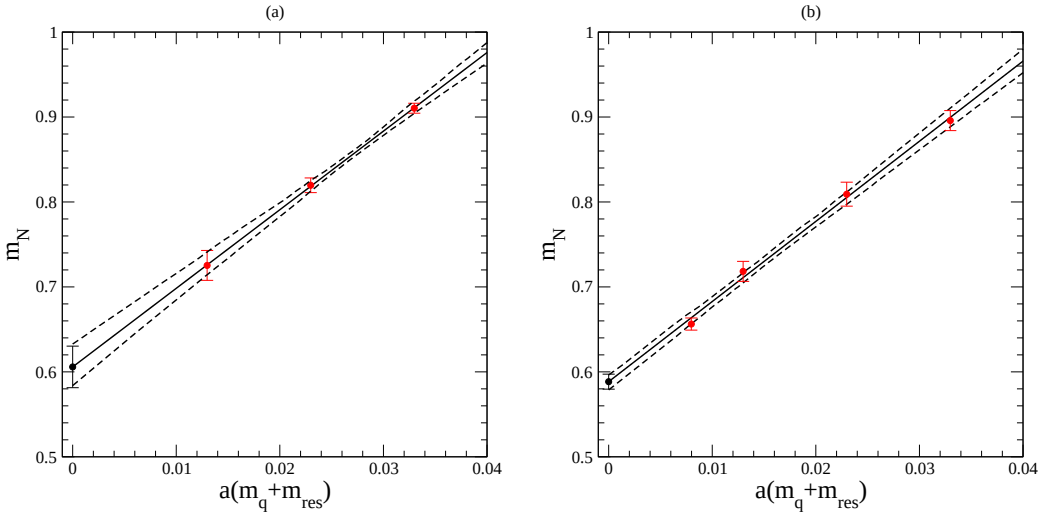


Figure 5.3: Chiral extrapolations of the proton mass for (a) the $16^3 \times 32$ lattice and (b) the $24^3 \times 64$ lattice. The results on both lattices (both on individual data points, and in the chiral limit) are compatible within errors.

### 5.3.4 The proton amplitude

The proton amplitude $G_N$, can now be calculated by considering an effective amplitude,

$$G^2_{N,\text{eff}}(t) = \frac{1}{2} f^{PS,PS}_{udu,udu}(t) \mathrm{e}^{m_N t}, \tag{5.19}$$

where $m_N$ is the proton ground state mass that we just calculated. In this case, the different smearings and operators we used to calculate the mass cannot be used, as they will each have different amplitudes. Apart from this difference, we can perform a fit to this effective amplitude in the same way as for the effective mass, choosing an appropriate time range for the fit as before.

Results for the proton amplitude calculated on each of the ensembles described in Section 5.2 are given in Table 5.5 and example effective amplitude plateaus are shown in Figure 5.4. The different channels and the corresponding time ranges used in each fit are given in Table 5.4.

Again we see that the proton amplitude is consistant with a linear extrapolation

$$G_N = A(m_u + m_{\text{res}}) + B. \tag{5.20}$$

This extrapolation is shown in Figure 5.5. Within errors, the amplitudes calculated on ensembles with the same valence quark mass are compatible, as are the extrapolated values.

Values for the nucleon amplitude in the chiral limit, $(am_u + am_{\text{res}}) = 0$, are given in Table 5.5.

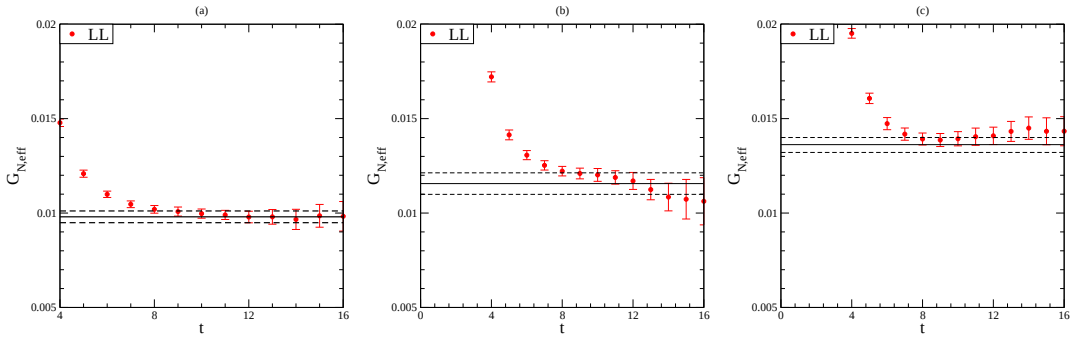


Figure 5.4: Effective amplitude (Eq. 5.19) plots for the $24^3 \times 64$ ensemble with different light valence quark masses. (a) is for $am_u = 0.01$, (b) is for $am_u = 0.02$ and (c) is for $am_u = 0.03$. Horizontal lines show the fit to the plateau.

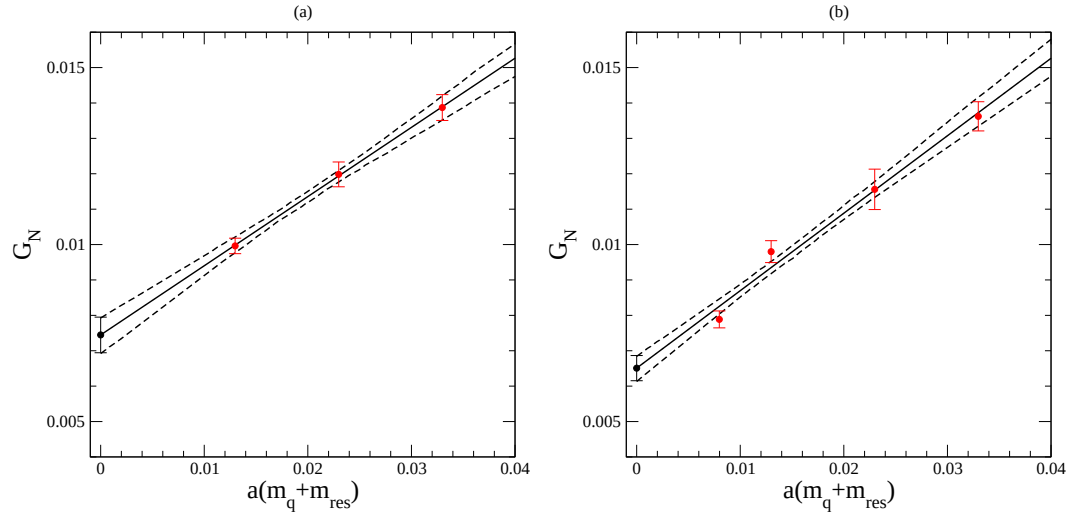


Figure 5.5: Chiral extrapolations of the proton amplitude for (a) the $16^3 \times 32$ lattice and (b) the $24^3 \times 64$ lattice.

## 5.4 Mesons

### 5.4.1 The meson correlation function

For a pseudo–scalar meson correlation function we use the operator $\mathcal{O}^P_{q_iq_j}$. We divide these mesons into two types, pion correlation functions and kaon correlation functions. For pions $q_i$ and $q_j$ are both light quark fields (i.e. up / down). For kaons, $q_i$ is a light quark field and $q_j$ is a strange quark field.

In the same way as for the proton correlation function, we write out the pseudo–scalar meson correlation function explicitly, but this time we add a momentum $\vec{p}$,

$$f^{P,P}_{q_iq_j,q_iq_j} = -\sum_{\vec{x}} \mathrm{e}^{i\vec{p}.\vec{x}} \left\langle q^{ai}_\alpha(x)(\gamma_5)_{\alpha\beta}\bar{q}^{aj}_\beta(x)\bar{q}^{bi}_\gamma(0)\overline{(\gamma_5)}_{\gamma\delta}q^{bj}_\delta(0)\right\rangle . \tag{5.21}$$

There is therefore only one contraction we can make,

$$\left\langle q^{ai}_\alpha(x)\bar{q}^{aj}_\beta(x)\bar{q}^{bi}_\gamma(0)q^{bj}_\delta(0)\right\rangle = \overbrace{q^{ai}_\alpha(x)\bar{q}^{aj}_\beta(x)\bar{q}^{bi}_\gamma(0)q^{bj}_\delta(0)}. \tag{5.22}$$

So in terms of propagators, the meson correlation function is,

$$f^{P,P}_{q_iq_j,q_iq_j} = \mathrm{tr}\left[\sum_{\vec{x}} \mathrm{e}^{i\vec{p}.\vec{x}} S^{ab}_j(x)\gamma_5 S^{ab}_i(x)\gamma_5\right]. \tag{5.23}$$

We now make a distinction between the flavour of the quark propagator, as some will be between strange quarks and some between light quarks. We produce one propagator with a mass equal to the light quark mass in the sea and one propagator with the mass equal to the strange quark mass in the sea. These can then be combined, with the appropriate spin / colour structure, to produce either a two–point function with two light propagators (a pion correlation function) or a two–point function with one light and one heavy propagator (a kaon correlation function). We still make no distinction between up and down type correlation functions, and hence the different pion correlation functions (i.e.. $\pi^{\pm,0}$) are all equal.

The time dependence of the meson correlation function is given by,

$$f^{P,P}_{q_iq_j,q_iq_j}(t) = \sum_n \frac{(G_n)^2}{2E_n}\left(\mathrm{e}^{-E_nt} \pm \mathrm{e}^{-E_n(T-t)}\right), \tag{5.24}$$

where the $\pm$ sign depends on the transformation under parity of the operator $\mathcal{O}^P_{q_iq_j}$ in $f^{P,P}_{q_iq_j,q_iq_j}$. The pseudo–scalar operator is odd under time reversal, so the pseudo–scalar correlation function is even, and we have a + sign.

In a similar way as for the nucleon correlation function, in the limit $0 \ll t \ll T$ this looks

like,

$$f^{P,P}_{q_iq_j,q_iq_j}(t) \to \frac{(G_M)^2}{2E_M}\left(\mathrm{e}^{-E_M t} + \mathrm{e}^{-E_M(T-t)}\right), \tag{5.25}$$

where $G_M \equiv G_0$ is the ground state meson amplitude and $E_M \equiv E_0$ is the ground state meson energy. The pion correlation function has a momentum $\vec{p}$, so $E_0^2 = m_0^2 + \vec{p}^2$.

### 5.4.2 The meson ground state energy

To find the ground state energy, we can form an effective energy,

$$E_{\mathrm{eff}}(t) = \cosh^{-1}\left(\frac{f^{P,P}_{q_iq_j,q_iq_j}(t+1) + f^{P,P}_{q_iq_j,q_iq_j}(t-1)}{f^{P,P}_{q_iq_j,q_iq_j}(t)}\right) \to E_M \quad 0 \ll t \ll T. \tag{5.26}$$

We use mesons with three different momenta, $\vec{p} = \frac{2\pi}{L}(0,0,0)$, $\frac{2\pi}{L}(1,0,0)$ and $\frac{2\pi}{L}(1,1,0)$. We use multiple smearings and fit to the plateau over appropriate time ranges, see Table 5.6 for details. Examples of the plateau are shown in Figure 5.6 while the results for the meson mass are given in Tables 5.7 and 5.8.

| | | | Fit Range | | | |
|---|---|---|---|---|---|---|
| $m_u/m_s$ | Momentum | Smearing | $E_\pi$ | $G_\pi$ | $E_K$ | $G_K$ |
| 0.005 / 0.04 | $\frac{2\pi}{L}(0,0,0)$ | GKL,GKG | 6-20 | 6-20 | 6-20 | 6-20 |
| | $\frac{2\pi}{L}(1,0,0)$ | GKL,GKG | 6-20 | 6-20 | 6-20 | 6-20 |
| | $\frac{2\pi}{L}(1,1,0)$ | GKL,GKG | 6-15 | 6-15 | 6-15 | 6-15 |
| 0.01 / 0.04 | $\frac{2\pi}{L}(0,0,0)$ | GKL,GKG | 6-20 | 6-20 | 6-20 | 6-20 |
| | $\frac{2\pi}{L}(1,0,0)$ | GKL,GKG | 7-20 | 7-20 | 8-20 | 8-20 |
| | $\frac{2\pi}{L}(1,1,0)$ | GKL,GKG | 6-15 | 6-15 | 6-15 | 6-15 |
| 0.02 / 0.04 | $\frac{2\pi}{L}(0,0,0)$ | GKL,GKG | 5-20 | 5-20 | 5-20 | 5-20 |
| | $\frac{2\pi}{L}(1,0,0)$ | GKL,GKG | 7-20 | 7-20 | 7-20 | 7-20 |
| | $\frac{2\pi}{L}(1,1,0)$ | GKL,GKG | 5-15 | 5-15 | 7-15 | 7-15 |
| 0.03 / 0.04 | $\frac{2\pi}{L}(0,0,0)$ | GKL,GKG | 6-20 | 6-20 | 6-20 | 6-20 |
| | $\frac{2\pi}{L}(1,0,0)$ | GKL,GKG | 6-20 | 6-20 | 6-20 | 6-20 |
| | $\frac{2\pi}{L}(1,1,0)$ | GKL,GKG | 6-15 | 6-15 | 6-15 | 6-15 |

Table 5.6: Fit ranges used for the calculation of pseudo–scalar meson masses and amplitudes. All on the $V = 24^3 \times 64 \times 16$ lattice, with the smearing, momenta and valence quark masses shown.

In practice, the results for meson energies where the mesons have large momenta can be noisy. We can calculate the ground state energy for $\vec{p} = (0,0,0)$ as above, then use the dispersion relation $E^2 = m^2 + \vec{p}^2$ to get the energies at higher momenta, these are shown in Tables 5.7 and 5.8, and have smaller error bars than the results from when the energy is computed directly from the correlation function with momentum. For this reason, these values of the meson energy are preferred, and used to calculate the meson amplitude below.

| $m_u/m_s$ | Momentum | $E_\pi$ | $\sqrt{m_\pi^2+\vec{p}^2}$ | $G_\pi$ |
|---|---|---|---|---|
| 0.03 / 0.04 | $\frac{2\pi}{L}(0,0,0)$ | 0.3896(8) | 0.3896(8) | 0.2538(34) |
| | $\frac{2\pi}{L}(1,0,0)$ | 0.4714(14) | 0.4694(7) | 0.2544(36) |
| | $\frac{2\pi}{L}(1,1,0)$ | 0.5430(23) | 0.5375(6) | 0.2554(33) |
| 0.02 / 0.04 | $\frac{2\pi}{L}(0,0,0)$ | 0.3242(10) | 0.3242(10) | 0.2310(32) |
| | $\frac{2\pi}{L}(1,0,0)$ | 0.4162(16) | 0.4167(8) | 0.2312(36) |
| | $\frac{2\pi}{L}(1,1,0)$ | 0.5020(28) | 0.4921(7) | 0.2326(38) |
| 0.01 / 0.04 | $\frac{2\pi}{L}(0,0,0)$ | 0.2433(8) | 0.2433(8) | 0.2062(22) |
| | $\frac{2\pi}{L}(1,0,0)$ | 0.3588(25) | 0.3574(6) | 0.2095(28) |
| | $\frac{2\pi}{L}(1,1,0)$ | 0.4557(41) | 0.4430(5) | 0.2119(37) |
| 0.005 / 0.04 | $\frac{2\pi}{L}(0,0,0)$ | 0.1924(10) | 0.1924(10) | 0.1944(23) |
| | $\frac{2\pi}{L}(1,0,0)$ | 0.3384(30) | 0.3249(7) | 0.1915(31) |
| | $\frac{2\pi}{L}(1,1,0)$ | 0.4331(59) | 0.4172(5) | 0.1960(48) |
| $\chi^{\rm ral}$ | $\frac{2\pi}{L}(0,0,0)$ | 0.0020(16) | | 0.1754(35) |
| | $\frac{2\pi}{L}(1,0,0)$ | 0.1959(49) | | 0.1910(51) |
| | $\frac{2\pi}{L}(1,1,0)$ | 0.3202(81) | | 0.2036(69) |

Table 5.7: Results for the pseudo–scalar pion masses ($E_\pi$) and amplitudes ($G_\pi$) for pion correlation functions with light quark masses $am_u = 0.005, 0.01, 0.02$ and 0.03. The final three rows contain the results of an extrapolation to the chiral limit. The $\sqrt{m_\pi^2+\vec{p}^2}$ column shows the result of the pion mass calculated using the dispersion relation $E^2 = \vec{p}^2 + m^2$.

The pseudo–scalar pion and kaon masses are consistant with linear extrapolations in the square root of the light quark mass,

$$E_{PS} = A\sqrt{m_u + m_{\rm res}} + B. \tag{5.27}$$

The results of these extrapolations are shown in Figure 5.7. Values of the meson masses in the chiral limit, $am_u + am_{\rm res} = 0$ are given in Tables 5.7 and 5.8. Note that chiral perturbation theory predicts that in the chiral limit the pion mass should go to 0, this behaviour can be seen in the plots.

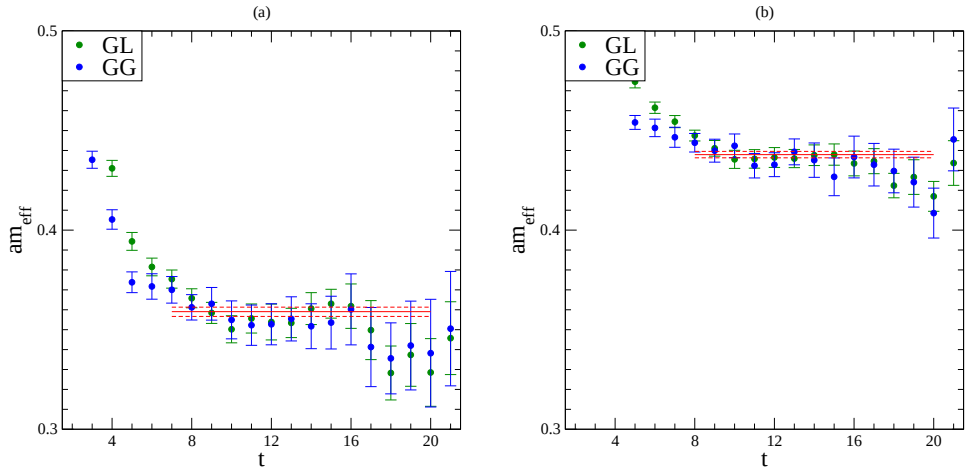


Figure 5.6: Pseudo–scalar effective energy (Eq. 5.26) plots for the $24^3 \times 64$ ensemble with light valence quark masses $am_u = 0.01$, strange valence quark mass $am_s = 0.04$ and momentum $\vec{p} = \frac{2\pi}{L_x}(1,0,0)$. (a) is from a pion pseudo–scalar correlation function with two light propagators, (b) is from a kaon pseudo–scalar correlation function with one light and one heavy propagator. The different colours correspond to different smearings. Horizontal lines show the fit to the plateau.

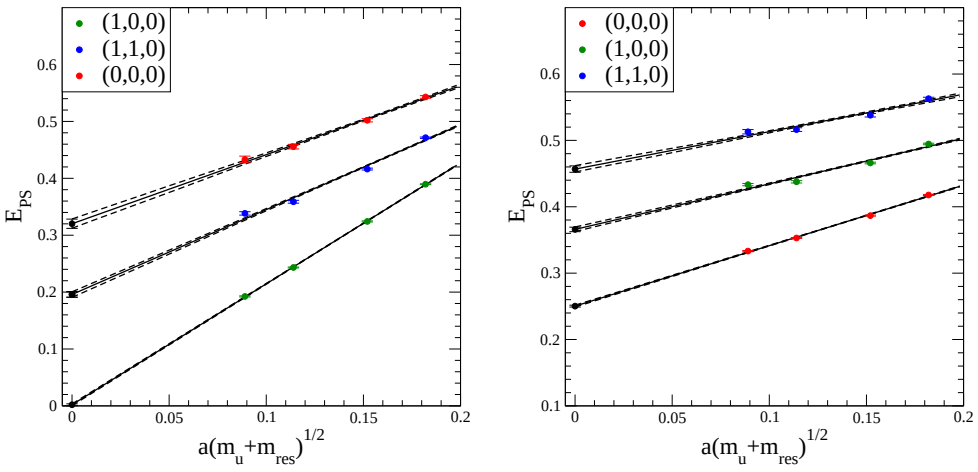


Figure 5.7: A linear extrapolation of the pseudo–scalar meson masses to the chiral limit. Both plots show results from the $24^3 \times 64$ ensembles with strange valence quark mass $am_s = 0.04$. The different colours represent the different momenta $\vec{p} = \frac{2\pi}{L_x}(0,0,0)$, $\frac{2\pi}{L_x}(1,0,0)$ and $\frac{2\pi}{L_x}(1,1,0)$. (a) is from a pion pseudo–scalar correlation function with two light propagators, (b) is from a kaon pseudo–scalar correlation function with one light and one heavy propagator.

| $m_u/m_s$ | Momentum | $E_K$ | $\sqrt{m_K^2+\vec{p}^2}$ | $G_K$ |
|---|---|---|---|---|
| 0.03 / 0.04 | $\frac{2\pi}{L}(0,0,0)$ | 0.4177(8) | 0.4177(8) | 0.2608(35) |
| | $\frac{2\pi}{L}(1,0,0)$ | 0.4945(12) | 0.4930(7) | 0.2619(35) |
| | $\frac{2\pi}{L}(1,1,0)$ | 0.5629(21) | 0.5582(6) | 0.2630(34) |
| 0.02 / 0.04 | $\frac{2\pi}{L}(0,0,0)$ | 0.3867(8) | 0.3867(8) | 0.2450(33) |
| | $\frac{2\pi}{L}(1,0,0)$ | 0.4660(13) | 0.4670(7) | 0.2455(34) |
| | $\frac{2\pi}{L}(1,1,0)$ | 0.5379(27) | 0.5353(6) | 0.2467(37) |
| 0.01 / 0.04 | $\frac{2\pi}{L}(0,0,0)$ | 0.3529(7) | 0.3529(7) | 0.2269(24) |
| | $\frac{2\pi}{L}(1,0,0)$ | 0.4376(18) | 0.4394(6) | 0.2305(24) |
| | $\frac{2\pi}{L}(1,1,0)$ | 0.5163(28) | 0.5115(5) | 0.2317(26) |
| 0.005 / 0.04 | $\frac{2\pi}{L}(0,0,0)$ | 0.3332(9) | 0.3332(9) | 0.2141(23) |
| | $\frac{2\pi}{L}(1,0,0)$ | 0.4334(16) | 0.4237(7) | 0.2119(23) |
| | $\frac{2\pi}{L}(1,1,0)$ | 0.5130(33) | 0.4981(6) | 0.2180(30) |
| $\chi^{\rm ral}$ | $\frac{2\pi}{L}(0,0,0)$ | 0.2503(14) | | 0.2014(33) |
| | $\frac{2\pi}{L}(1,0,0)$ | 0.3659(34) | | 0.2122(34) |
| | $\frac{2\pi}{L}(1,1,0)$ | 0.4568(48) | | 0.2226(50) |

Table 5.8: Results for the pseudo–scalar kaon masses and amplitudes for kaon correlation functions with light quark masses $am_u = 0.005, 0.01, 0.02$ and $0.03$ the final three rows contain the results of an extrapolation to the chiral limit. The $\sqrt{m_K^2+\vec{p}^2}$ column shows the result of the pion mass calculated using the dispersion relation $E^2 = \vec{p}^2 + m^2$.

### 5.4.3 The meson amplitude

We could find the meson amplitude from a fit to an effective amplitude of the unsmeared correlation function, as we did for the proton amplitude in Section 5.3. However, we can also find the amplitude from a ratio of smeared correlation functions.

Consider two meson correlation functions $f^{SS}$ and $f^{SL}$, the first with some smearing $S$ at the source and the same smearing at the sink and the second with $S$ smearing at the source but no smearing at the sink (labelled with $L$ for $L$ocal smearing),

$$f^{SL} \to \frac{(G_M^S G_M^L)}{2E_M}\left(\mathrm{e}^{-E_M t} + \mathrm{e}^{-E_M(T-t)}\right) \quad 0 \ll t \ll T, \tag{5.28}$$

$$f^{SS} \to \frac{(G_M^S G_M^S)}{2E_M}\left(\mathrm{e}^{-E_M t} + \mathrm{e}^{-E_M(T-t)}\right) \quad 0 \ll t \ll T. \tag{5.29}$$

$$\tag{5.30}$$

In both cases we can form effective amplitudes,

$$G_{\rm eff}^{SL}(t) = 2E_M f^{SL}\left(\mathrm{e}^{-E_M t} + \mathrm{e}^{-E_M(T-t}\right)^{-1} \to G_M^S G_M^L \quad 0 \ll t \ll T, \tag{5.31}$$

$$G_{\rm eff}^{SS}(t) = 2E_M f^{SS}\left(\mathrm{e}^{-E_M t} + \mathrm{e}^{-E_M(T-t}\right)^{-1} \to G_M^S G_M^S \quad 0 \ll t \ll T, \tag{5.32}$$

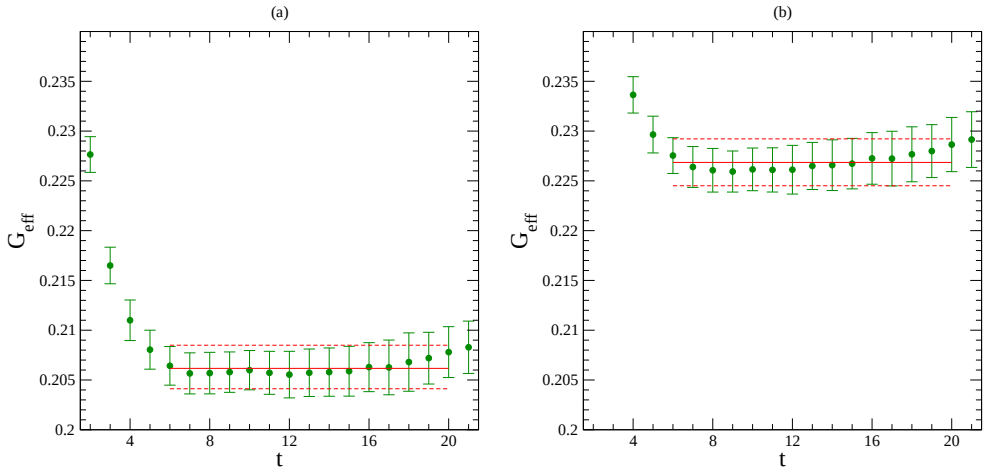


Figure 5.8: Pseudo–scalar effective amplitude (Eq. 5.33) plots for the $24^3 \times 64$ ensemble with light valence quark masses $am_u = 0.01$, strange valence quark mass $am_s = 0.04$ and momentum $\vec{p} = \frac{2\pi}{L_x}(0,0,0)$. (a) is from a pion pseudo–scalar correlation function with two light propagators, (b) is from a kaon pseudo–scalar correlation function with one light and one heavy propagator. Horizontal lines show the fit to the plateau.

so that the ratio,

$$G_{\text{eff}}(t) = \sqrt{2E_M}\frac{G^{SL}_{\text{eff}}(t)}{\sqrt{G^{SS}_{\text{eff}}(t)}} \to G^L_M \quad 0 \ll t \ll T, \tag{5.33}$$

can be used to find the unsmeared amplitude that we are looking for.

We use this method, with the smearing and fit ranges given in Table 5.6, to find the meson amplitude. Example plateau are shown in Figure 5.8, while the results are given in Tables 5.7 and 5.8.

The pion and kaon amplitudes on each of the ensembles are plotted in Figure 5.9. Both pion and kaon amplitudes are consistant with a linear extrapolation

$$G_{PS} = A(m_u + m_{\text{res}}) + B. \tag{5.34}$$

The extrapolations are shown in Figure 5.9. The values of the meson amplitudes in the chiral limit, $am_u + am_{\text{res}} = 0$ are given in Tables 5.7 and 5.8.

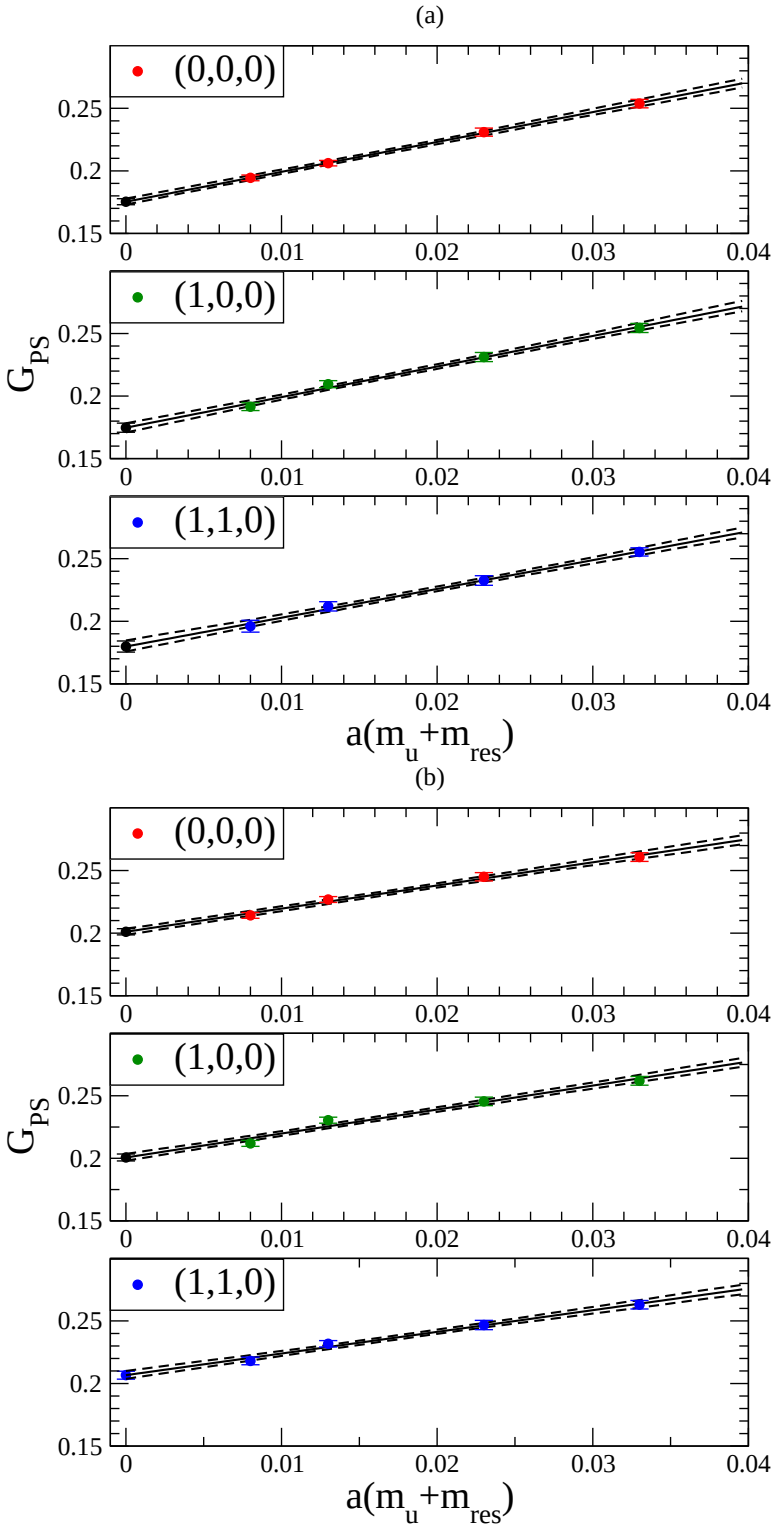


Figure 5.9: A linear extrapolation of the pseudo–scalar meson amplitudes to the chiral limit. Both plots show results from the $24^3 \times 64$ ensembles with strange valence quark mass $am_s = 0.04$. The different colours represent the different momenta $\vec{p} = \frac{2\pi}{L_x}(0,0,0)$, $\frac{2\pi}{L_x}(1,0,0)$ and $\frac{2\pi}{L_x}(1,1,0)$. (a) is from a pion pseudo–scalar correlation function with two light propagators, (b) is from a kaon pseudo–scalar correlation function with one light and one heavy propagator.

# Chapter 6

# Matrix Element Results

We can now calculate the matrix elements relevant for proton decay. As shown previously in Eq. 2.45,

$$\Gamma(N \to M + l) = \frac{m_N}{32\pi}\left(1 - \left(\frac{m_M}{m_N}\right)^2\right)^2 \left|\sum_i C^i W_0^i(N \to M + l)\right|^2 . \tag{6.1}$$

So the proton decay width can be decomposed into a sum of products of Wilson coefficients and QCD matrix elements. The Wilson coefficients contain the high energy GUT–scale physics and will in general depend on the particular GUT being considered. The matrix elements contain the low energy hadronic physics, are the same for all GUTs and can be calculated in Lattice QCD.

There are two methods we can use to calculate these matrix elements. In the *direct* method, we calculate a three–point correlation function involving a baryon number violating operator. In the *indirect* method, we use $\chi$PT (see Sections 2.3 and 2.4.2) and the relations from Table 2.1 to relate the three–point function to the two low–energy constants from the baryon number violating sector of the chiral lagrangian. As we shall see, these low–energy constants can be calculated from proton–to–vacuum two–point functions.

In the following sections we first give the details of the ensembles used to calculate the proton decay matrix elements in Section 6.1, we then use both methods to calculate the matrix elements, firstly using the *indirect* method in Section 6.2 and then using the *direct* method in Section 6.3.

## 6.1 Ensemble details

For the indirect matrix elements, the ensembles used are the same as those used to calculate the proton mass and amplitude, and are given in Table 5.2.

The ensembles used to calculate the direct matrix elements are given in Table 6.1.

The ensembles used for the NPR calculation are given in Table 6.2. In this case, our main

results are calculated using the ensembles generated on the lattice with volume $V = 16^3 \times 32 \times 16$ and the lattice with volume $V = 24^3 \times 64 \times 16$ was used to check for finite volume effects.

| $V \times L_s$ | $am_{ud}$ | $N_{\text{traj}}$ | $\Delta$ | $N_{\text{cfg}}$ | $N_{\text{src}}$ | $N_{\text{bin}}$ | Smearing |
|---|---|---|---|---|---|---|---|
| $24^3 \times 64 \times 16$ | 0.005 | 900-8500 | 50 | 155 | 1 | 1 | GKL, GKG |
| | 0.01 | 1540-7500 | 40 | 75 | 1 | 2 | GKL, GKG |
| | 0.02 | 1620-3600 | 40 | 50 | 1 | 1 | GKL, GKG |
| | 0.03 | 1260-3040 | 40 | 45 | 1 | 1 | GKL, GKG |

Table 6.1: RHMC 2+1 flavour datasets used for the pseudo–scalar meson mass and amplitude calculations. $V$ is the space-time volume of the lattice, $L_s$ is the extent of the fifth dimension. The light quark mass is $am_{ud}$, correlation functions with two values of the strange valence quark mass $am_s = 0.04, 0.0343$ were calculated for each light quark mass. The strange sea quark mass is kept fixed at 0.04. $N_{\text{traj}}$ is the lowest to highest trajectories analysed with correlation functions calculated every $\Delta$ trajectories, $N_{\text{cfg}}$ is the number of configurations, $N_{\text{src}}$ is the number of quark propagators solved with different source locations and $N_{\text{bin}}$ is the bin size. All propagators used are solved with a gaussian smeared Kenway source, denoted $GK$. The sink smearing as Local $L$.

| | | NPR | | | | |
|---|---|---|---|---|---|---|
| $V \times L_s$ | $am_{ud}$ | $N_{\text{traj}}$ | $\Delta$ | $N_{\text{cfg}}$ | $N_{\text{src}}$ | $N_{\text{bin}}$ |
| $16^3 \times 32 \times 16$ | 0.01 | 1000-4000 | 40 | 75 | 4 | 1 |
| | 0.02 | 1000-4000 | 40 | 75 | 4 | 1 |
| | 0.03 | 1000-4000 | 40 | 75 | 4 | 1 |

Table 6.2: RHMC 2+1 flavour datasets used for the non-perturbative renormalization. $V$ is the space-time volume of the lattice, $L_s$ is the extent of the fifth dimension, $am_{ud}$ is the up sea quark mass (the strange sea quark mass is kept fixed at 0.04), $N_{\text{traj}}$ is the lowest to highest trajectories analysed with matrix elements calculated every $\Delta$ trajectories, $N_{\text{cfg}}$ is the number of configurations, $N_{\text{src}}$ is the number of quark propagators solved with different source locations and $N_{\text{bin}}$ is the bin size. $24^3 \times 64 \times 16$ data were generated for the non-perturbative renormalization calculation, however, it was only used as a check for finite volume errors and so does not appear here.

## 6.2 The indirect method

The discussion and results from the indirect method are based upon work published in Ref. [1]. There have been many previous calculations of the proton decay matrix elements using the indirect method. For example, Refs. [37, 79] use quenched Wilson fermions while Ref. [80] uses domain wall fermions with both quenched and 2 flavours of dynamical quarks. This work is the first to use 2+1 flavours of dynamical domain wall fermions.

Table 2.1 shows the relations between matrix elements and the low energy constants (LECs) $\alpha$ and $\beta$. For example,

$$\langle \pi^0 | \mathcal{O}^{RL}_{udu} | p \rangle = \frac{\alpha}{\sqrt{2} f}(1 + D + F). \tag{6.2}$$

The aim in this section shall be to calculate these LECs so that the matrix elements can be reconstructed.

The advantage of the *indirect* method is that it only requires the calculation of two low energy constants from two–point functions. This is much simpler, and computationally cheaper, than the full calculation of the three–point functions which is required for the *direct* method.

The disadvantage of the *indirect* method is that the $\chi$PT introduces an additional source of systematic error. In previous studies (e.g.. Ref. [80]), there has been seen to be a considerable discrepancy of up to a factor of 2, between the *direct* and *indirect* methods, with the *indirect* approach tending to underestimate the matrix elements. For example, in Ref. [80], $\langle \pi^0 | \mathcal{O}^{RL}_{udu} | p \rangle = -0.060(18)$ for the direct measurement, while the indirect reconstruction of the same matrix element gives $-0.125(15)$.

Expanding the baryon violating terms from the chiral lagrangian in Eq. 2.48 to zeroth order in the meson fields, shows that the low–energy constants $\alpha$ and $\beta$ can be determined from the proton to vacuum matrix elements:

$$\begin{aligned} \langle 0 | \mathcal{O}^{RL}_{udu} | N(k,s) \rangle &= \alpha P_L u(k,s), & (6.3) \\ \langle 0 | \mathcal{O}^{LL}_{udu} | N(k,s) \rangle &= \beta P_L u(k,s). & (6.4) \end{aligned}$$

Using the same notation from Section 5.1, we can form two–point functions involving the operators $\mathcal{O}^{R/L\,L}_{udu}$:

$$\begin{aligned} f^{RL,PS}_{udu,udu}(t) &\to G_N \alpha \mathrm{e}^{-m_N t} \quad t \gg 0, & (6.5) \\ f^{LL,PS}_{udu,udu}(t) &\to G_N \beta \mathrm{e}^{-m_N t} \quad t \gg 0, & (6.6) \end{aligned}$$

where $G_N$ is the proton amplitude as defined in Eq. 5.12. As these have the same timedependence as the nucleon two–point correlation function, we can find $\alpha$ and $\beta$ by forming the ratios,

$$\begin{aligned} R_\alpha(t) &= 2G_N \frac{f^{RL,PS}_{udu,udu}(t)}{f^{PS,PS}_{udu,udu}(t)} \to \alpha \quad t \gg 0, \\ R_\beta(t) &= 2G_N \frac{f^{LL,PS}_{udu,udu}(t)}{f^{PS,PS}_{udu,udu}(t)} \to \beta \quad t \gg 0. & (6.7) \end{aligned}$$

In order to calculate the ratio, we therefore need to use the values for the proton amplitude, calculated in Section 5.3.4.

The two point functions $f^{RL,PS}_{udu,udu}$ and $f^{LL,PS}_{udu,udu}$ contain the same quark fields as the proton two–point correlation function, $f^{PS,PS}_{udu,udu}$, that we used in Section 5.3. Because of this, the contractions are the same as in Eq. 5.6, all that changes is the spin structure. With momentum $\vec{p} = (0,0,0)$, the two–point function is given by,

$$\begin{aligned} f^{R/L\,L,PS}_{udu,udu} &= \frac{1}{2}(1+\gamma_4)_{\delta\gamma}\epsilon^{abc}\epsilon^{def}(CP_{R/L})_{\alpha\beta}(P_L)_{\gamma\iota}\overline{(C\gamma_5)}_{\epsilon\zeta} \\ &\quad \sum_{\vec{x}}\left[S^{af}_{\alpha\zeta}(x)S^{be}_{\beta\epsilon}(x)S^{cd}_{\iota\delta}(x) - S^{ad}_{\alpha\delta}(x)S^{bf}_{\beta\zeta}(x)S^{ce}_{\gamma\epsilon}(x)\right]. \end{aligned} \tag{6.8}$$

Again, we compute propagators with mass equal to the light sea quark mass, and contract the spin and colour indices together as in Eq. 6.8 to form the two point functions.

We shall compute the matrix elements at $\vec{p} = \vec{k} = 0$ and hence $q^2 = m_N^2 - m_M^2$. Therefore, especially for the case of the proton to pion matrix elements, the required inequality $q^2 \ll m_N^2$ does not hold well. We will come back to this source of systematic error when we compare the two methods of estimating the matrix elements in Section 7.3.

### 6.2.1 Results for the low energy constants

The denominator of the ratios from Eq. 6.7, is the proton correlation function $f^{PS,PS}_{udu,udu}$, and is chosen so as to cancel the time dependence in the numerator. E.g.. for the low energy constant $\alpha$,

$$\begin{aligned} R_\alpha(t) &= 2G_N\frac{f^{RL,PS}_{udu,udu}(t)}{f^{PS,PS}_{udu,udu}(t)} \\ &\rightarrow 2G_N\frac{G_N\alpha e^{-m_N t}}{2G_N^2 e^{-m_N t}} = \alpha \quad t \gg 0. \end{aligned} \tag{6.9}$$

Therefore fitting to a constant using the algorithm in Section 4.6 will yield the low energy constants $\alpha$ and $\beta$.

Again, we fit to multiple smearings and choose time ranges appropriately. The smearings and time ranges used are given in Table 6.3. Note that in general, the fit ranges for this ratio start earlier than for the proton and meson effective mass and amplitude calculations. This is because the contributions from excited states in the numerator of the ratio from Eq. 6.7 are also present in the denominator and hence both should cancel each other out. However, the results are also in general more noisy, and so the maximum fit range is earlier too.

Results for the low energy constants are given in Table 6.4 and example plateaus for $\alpha$ and $\beta$ are shown in Figures 6.1 and 6.2 respectively.

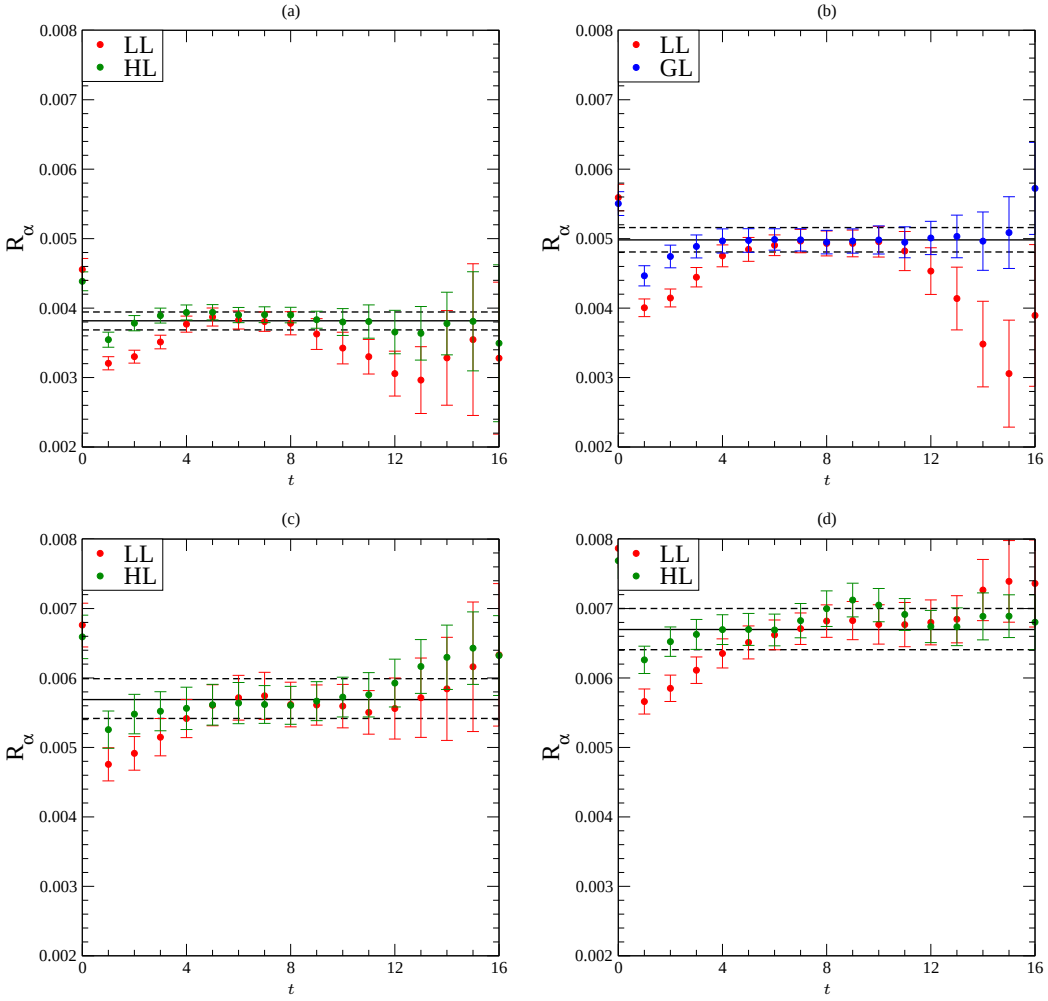


Figure 6.1: The ratio $R_\alpha$ in Eq. 6.7 for the $24^3 \times 64$ dataset with $am_u = 0.005, 0.01, 0.02$ and 0.03 respectively. The different colours correspond to different source smearing. Horizontal lines show the fit to the plateau.

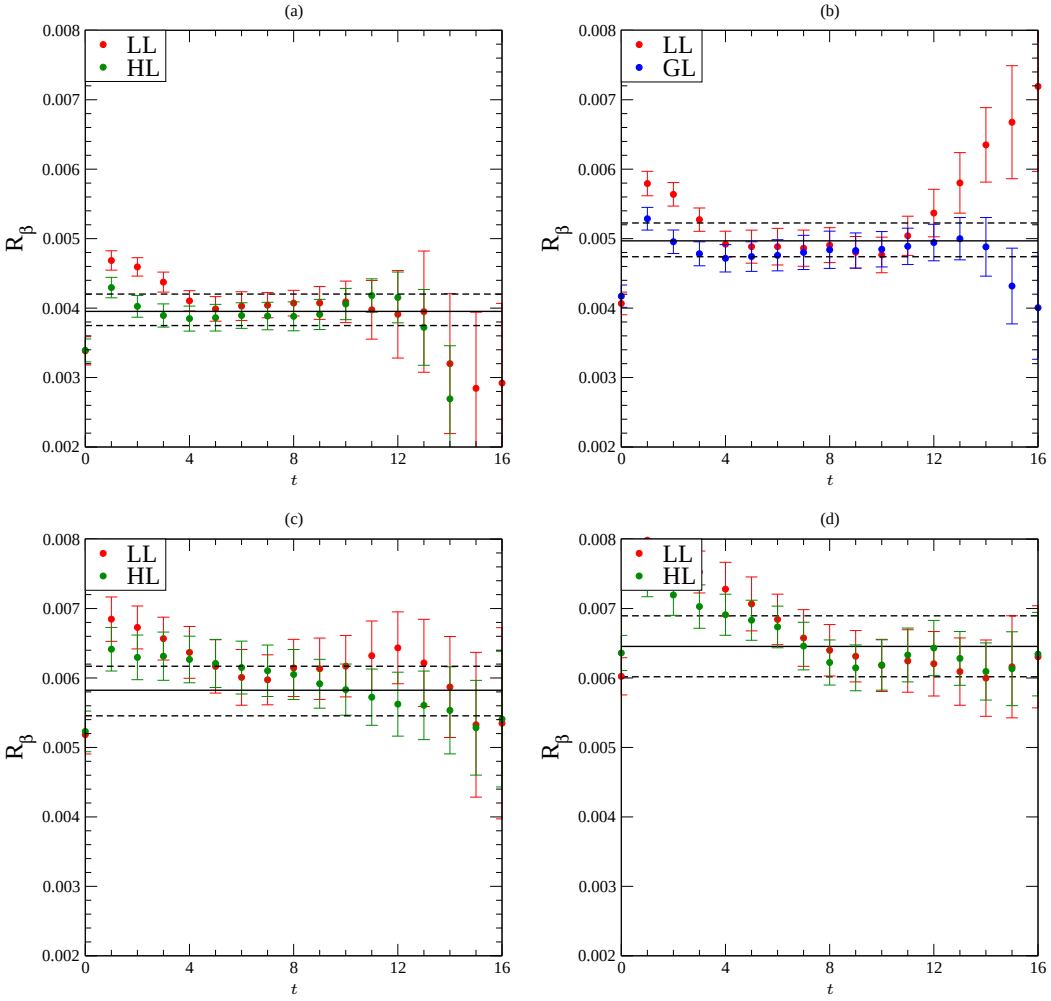


Figure 6.2: The ratio $R_\beta$ from Eq. 6.7 for the $24^3 \times 64$ dataset with $am_u = 0.005, 0.01, 0.02$ and 0.03 respectively. The different colours correspond to different source smearing. Horizontal lines show the fit to the plateau.

| $m_u$ | $V = 16^3 \times 32$ | Fit Range | | $V = 24^3 \times 64$ | Fit Range | |
|---|---|---|---|---|---|---|
| | Smearing | $\alpha$ | $\beta$ | Smearing | $\alpha$ | $\beta$ |
| 0.005 | | | | LL | 5-8 | 5-9 |
| | | | | HL | 4-10 | 4-9 |
| 0.01 | LL | 5-8 | 5-8 | LL | 7-11 | 5-10 |
| | GL | 3-8 | 3-8 | GL | 7-11 | 4-10 |
| 0.02 | LL | 6-12 | 5-12 | LL | 7-11 | 5-10 |
| | GL | 6-10 | 4-14 | HL | 7-11 | 7-10 |
| 0.03 | LL | 7-11 | 6-11 | LL | 9-13 | 9-11 |
| | GL | 7-11 | 8-12 | HL | 9-13 | 9-11 |

Table 6.3: Smearings and fit ranges used for the calculation of the low energy constants $\alpha$ and $\beta$.

| $V \times L_s$ | $am_{ud}/am_s$ | $a^3\alpha$ | $a^3\beta$ |
|---|---|---|---|
| $16^3 \times 32 \times 16$ | 0.03/0.04 | -0.00695(19) | 0.00719(21) |
| | 0.02/0.04 | -0.00605(31) | 0.00606(30) |
| | 0.01/0.04 | -0.00478(43) | 0.00511(47) |
| | chiral | -0.00349(64) | 0.00369(63) |
| $24^3 \times 64 \times 16$ | 0.03/0.04 | -0.00689(33) | 0.00621(38) |
| | 0.02/0.04 | -0.00571(32) | 0.00598(38) |
| | 0.01/0.04 | -0.00508(29) | 0.00486(28) |
| | 0.005/0.04 | -0.00397(18) | 0.00400(22) |
| | chiral | -0.00326(27) | 0.00348(32) |

Table 6.4: Results from fits to the LECs $\alpha$ and $\beta$, reported as a function of the quark masses, for two different lattice volumes. The results of linear chiral extrapolations are also reported. All the results are given in units of the lattice spacing $a \approx 0.12$ fm.

Again we can perform a linear fit for both of the low energy constants,

$$\text{LEC} = A(m_u + m_{\text{res}}) + B. \tag{6.10}$$

The results of this fit as well as an extrapolation to the chiral limit, $a(m_u + m_{\text{res}}) = 0$, are shown in Figure 6.3. The values from this chiral extrapolation are also given in Table 6.4.

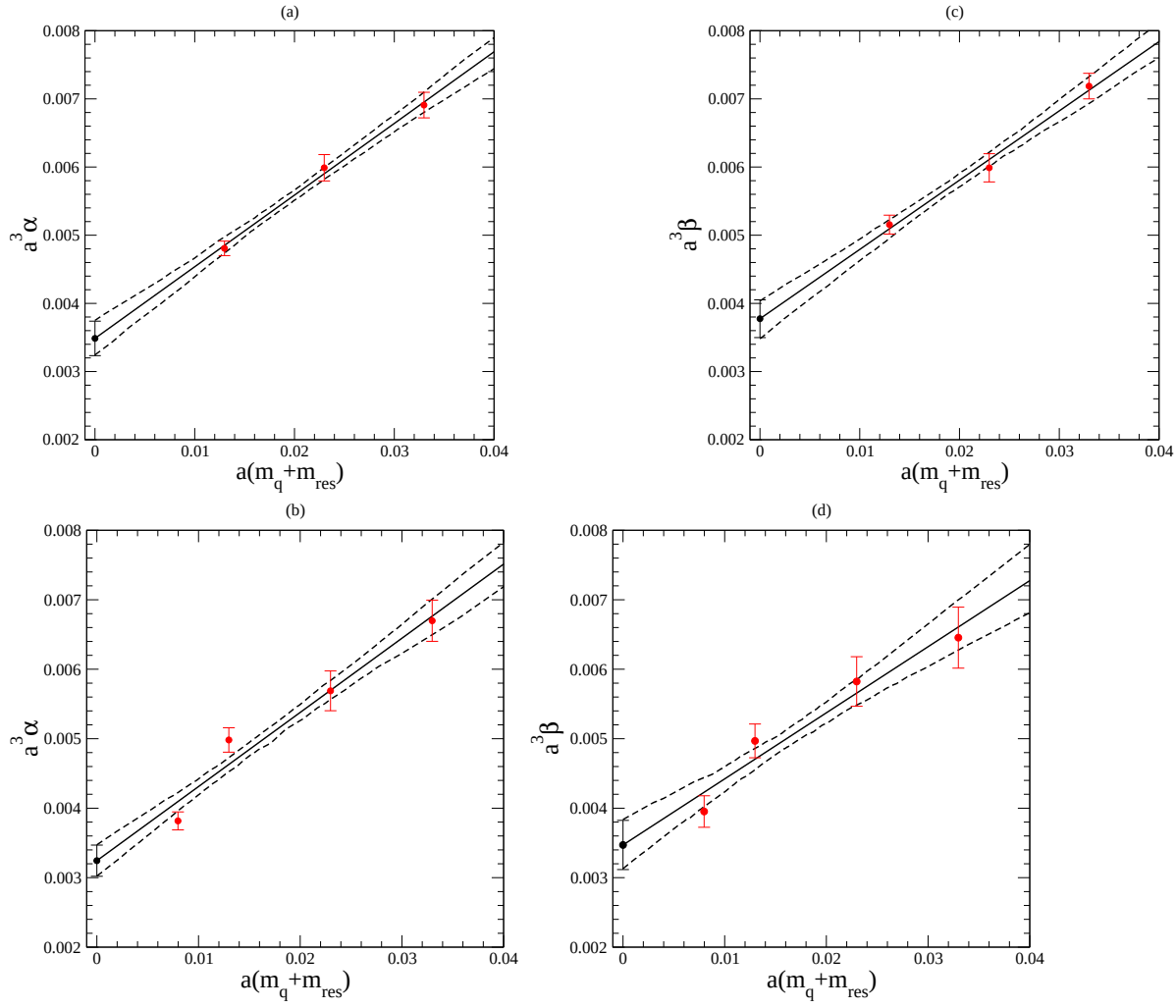


Figure 6.3: Linear chiral extrapolation for the ratios $R_\alpha$ and $R_\beta$ for the $16^3 \times 32$ and $24^3 \times 64$ datasets.

### 6.2.2 Systematic Errors on the LECs

The errors on the LECs have so far been purely statistical. From the results in Table 6.4 we can see that for the statistics available, there are no significant finite volume effects in either $\alpha$ or $\beta$ as the results on both volumes agree within errors. Figure 6.4 shows the agreement for $\alpha$ between the two volumes.

As already described in Section 5.3.2, there were problems with determining the plateau position for the nucleon mass on the $V = 24^3 \times 64 \times 16$, $am_u = 0.005$ ensemble. Through the nucleon amplitude calculation, this result indirectly effects the calculation of $\alpha$ and $\beta$. For a conservative analysis we performed a chiral extrapolation for $\alpha$ and $\beta$ both with and without this lightest point. This gave a result which differed by 18% for $\alpha$ and 17% for $\beta$ as shown in Figure 6.5. We use this as an estimate of the error in extrapolating to the chiral limit.

It should be noted that in our simulation, the strange quark mass is held fixed and hence in the extrapolation, only the light quarks are taken to the chiral limit. However, if we compare our result with the $N_f = 2$ results from Ref [80] we see there is very good agreement $\alpha_{N_f=2} = -0.0100(19)$, $\beta_{N_f=2} = 0.0108(21)$. For $N_f = 2$, the strange quark mass is effectively infinite, so this agreement signifies that $\alpha$ and $\beta$ have little dependence on the strange sea quark mass.

Working at fixed lattice spacing, we are not able to present a continuum extrapolation for the LECs. Nonetheless, it should be noted that DWFs are automatically O(a) improved and are therefore expected to have a good scaling behaviour.

We leave a final numerical value for the LECs, with all systematic errors included, until after we have calculated the non–perturbative renormalisation in Section 6.4 and its associated systematic and statistical errors.

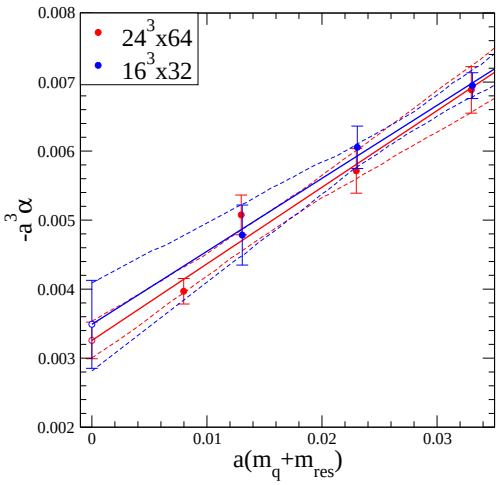


Figure 6.4: The LEC $\alpha$ measured on the two different volumes. There are no noticeable finite size effects. The chiral extrapolations from the two volumes are shown as white filled circles and also agree within errors.

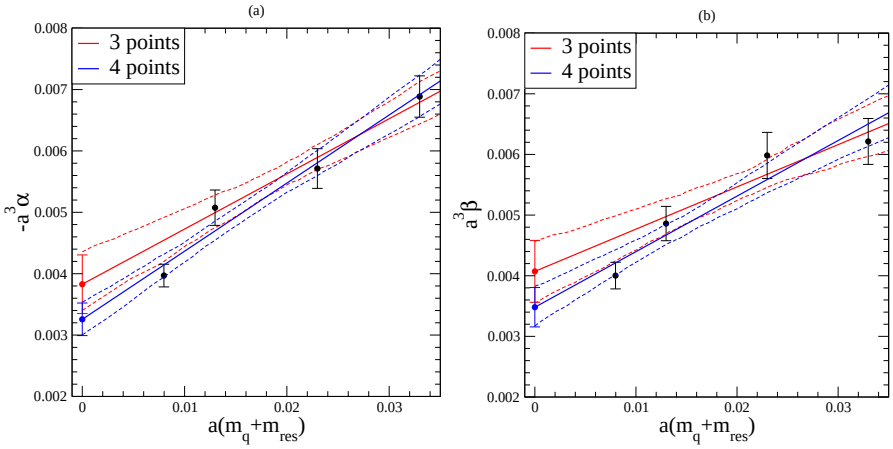


Figure 6.5: An extrapolation for $\alpha$ and $\beta$ on the $V = 24^3 \times 64 \times 16$ ensembles both with and without the value from the lightest valence quark mass point ($am_u = 0.005$). This gives results differing by 18% for $\alpha$ and 17% for $\beta$.

## 6.3 The direct method

We can define three point correlation functions $C_\mu^A(q^2)$ of the form,

$$\begin{aligned}
C_4^A(q^2) &= \mathrm{tr}\left[\frac{1}{2}(1+\gamma_4)\sum_{\vec{x}_1\vec{x}} \mathrm{e}^{i\vec{p}.(\vec{x}_1-\vec{x})}\langle \mathcal{O}^P_{q_iq_j}(\vec{x}_1,t_1)\mathcal{O}^A(\vec{x},t)\bar{\mathcal{O}}^{PS}_{udu}(\vec{0},t_0)\rangle\right] \\
&= \frac{G_N G_M}{2E_M}\mathrm{e}^{-E_M(t_1-t)}\mathrm{e}^{-m_N(t-t_0)}\left(W_0^A(q^2)+(m_N-E_M)\,W_q^A(q^2)\right), \\
C_i^A(q^2) &= \mathrm{tr}\left[\frac{1}{2}(1+\gamma_4)\,\gamma_i\sum_{\vec{x}_1\vec{x}} \mathrm{e}^{i\vec{p}.(\vec{x}_1-\vec{x})}\langle \mathcal{O}^P_{q_iq_j}(\vec{x}_1,t_1)\mathcal{O}^A\bar{\mathcal{O}}^{PS}_{udu}(\vec{0},t_0)\rangle\right] \\
&= -\frac{G_N G_M}{2E_M}\mathrm{e}^{-E_M(t_1-t)}\mathrm{e}^{-m_N(t-t_0)} iq_i W_q^A(q^2), \qquad (6.11)
\end{aligned}$$

where the index $i$ runs from 1...3 only. $\mathcal{O}^A(\vec{x},t)$ are the baryon violating operators, where $A$ is a collective index for the the spin and flavour structure of the operator. $\mathcal{O}^{PS}_{udu}(\vec{0},t_0)$ are nucleon operators as in the proton correlation function and $\mathcal{O}^P_{q_iq_j}(\vec{x}_1,t_1)$ are meson operators as in the meson correlation function.

The flavour content of the nucleon is fixed, and the flavour content of the mesons will vary depending on whether we are considering a pion or kaon decay channel. The flavour content of the baryon violating operator is then chosen so that each of the quark/antiquark fields in the nucleon and meson operators are partnered with an antiquark/quark field of the same flavour. For some decay channels this choice is unique, but for others there may be multiple choices for the flavour content of the baryon violating operator. The full list of proton decay matrix elements, and their baryon number operator structure is given in Eqs. 2.33-2.39.

For the four quark / antiquark field pairs of varying flavour in our three point functions, there are 24 possible contractions, although only some of these will be non–zero for each specific flavour combination of the meson and baryon violating operators. The full list of contractions is given in Appendix B. As for the *indirect* method, we can make light and heavy propagators which can be tied together with the appropriate spin and colour structure to form the three point function. In this case, the mesons have an injected momenta, so we need to create propagators for each of the different momenta we wish to consider.

As shown in Appendix B, to calculate the three–point function we need two normal (non–sequential) propagators and one sequential propagator and the spin and colour indices are then contracted as appropriate. For the non–sequential propagators, we use a Gaussian smeared Kenway source, with smearing radius 5 and a local sink. For the sequential propagators, we take the non–sequential propagator and smear the Gaussian smear the sink with smearing radius 3. This lower smearing radius matches the smearing for the pion correlation functions we calculated in Section 5.4. This is then multiplied by the spin matrix $\gamma_5$ and Gaussian smeared

again, using the same smearing radius of 3. Finally we perform a second inversion of the Dirac operator using this smeared correlation function as a source.

In order to cancel the time dependence we also need to calculate the proton and pseudo–scalar correlation functions, which both require the calculation of non–sequential propagators with the same smearing as the propagators we used for the three point function. These propagators therefore have a Gaussian smeared Kenway source, and a local sink. The propagators that we will use to make the pseudo–scalar meson correlation function have Gaussian smearing with smearing radius 3, while the those we will use to make the proton correlation function use Gaussian smearing with smearing radius 5.

The matrix elements involving the $\eta$ contain disconnected loops. Although these can be evaluated in principle using Lattice QCD, in practice the disconnected loops lead to a very noisy signal. This is due to the fact that disconnected loops have constant variance as the spatial separation between the loop and the connected pieces of the matrix element increases. For this reason, we ignore the $N \to \eta$ decay channels, and concentrate solely on the remaining 10 matrix elements from Eqs. 2.33 and 2.35-2.38.

The three–point functions have time dependence which we wish to cancel by forming appropriate ratios with the proton and meson correlation functions,

$$R^{A}_{3\mathrm{pt},\mu}(q^2) = \frac{C^{A}_{\mu}(q^2)}{f^{P,P}_{q_iq_j,q_iq_j}(\vec{p}) f^{PS,PS}_{udu,udu}(\vec{k})} G_M G_N L^3. \tag{6.12}$$

Much like with the indirect method, we will use the nucleon amplitude $G_N$ and the pseudo-scalar meson amplitudes $G_M = G_\pi, G_K$ as calculated in Sections 5.3 and 5.4 respectively.

The momenta $\vec{p}$ and $\vec{k}$ of the pion and nucleon correlation functions in the denominator of Eq. 6.12 must match the values of $\vec{p}$ and $\vec{k}$ used in the three–point function in the numerator, in order to correctly cancel the time dependence. We therefore calculate the ratios for the same three values of momenta as we used in Section 5.4, $\vec{p} = \frac{2\pi}{L}(0,0,0)$, $\frac{2\pi}{L}(1,0,0)$ and $\frac{2\pi}{L}(1,1,0)$, the momenta of the nucleon is held fixed at $\vec{k} = 0$, so that the momentum transfer $\vec{q} = \vec{k} - \vec{p} = -\vec{p}$.

In order to extract the form factor $W_0$, we form the combination,

$$W_0^{R/LL}(q^2) = (R_{3\mathrm{pt},4}) + i\frac{q_4}{q_j}(iR_{3\mathrm{pt},j}), \tag{6.13}$$

and we use the values for $m_N$ and $E_M = E_\pi, E_K$ that we have calculated earlier in Sections 5.3 and 5.4, together with $iq_4 = m_N - E_M$. The factor of $q_j$ in the denominator of the fraction in Eq. 6.13 means we cannot calculate $W_0$ for $\vec{q} = -\vec{p} = \frac{2\pi}{L}(0,0,0)$. We will therefore calculate $W_0$ for $\vec{p} = \frac{2\pi}{L}(1,0,0)$ and $\frac{2\pi}{L}(1,1,0)$ only.

### 6.3.1 Form factor results and extrapolation

The ratios from Eq. 6.12 are chosen such that the time dependence is cancelled, e.g..

$$R^A_{3\mathrm{pt},4}(q^2) \to \left(W_0^A(q^2) + (m_N - E_M)\, W_q^A(q^2)\right) \quad t \gg 0. \tag{6.14}$$

Therefore each of the two terms on the RHS of Eq. 6.13 has had the time dependence cancelled,

$$(R_{3\mathrm{pt},4}) + i\frac{q_4}{q_j}\,(iR_{3\mathrm{pt},j}) \to W_0^A(q^2) \quad t \gg 0, \tag{6.15}$$

and hence the whole expression should again tend to a plateau, once contributions from any excited states have died away. We can fit simultaneously to the channels $W_0^{R/LL}$ and $-W_0^{L/RR}$, as these should be equal according to Eq. 2.32.

We can therefore fit a constant to the plateau, again using the fit algorithm of Section 4.6. However, when fitting to these form factors, it was found that the covariance matrix for an unfrozen correlated fit had a large condition number $> 10^6$. This meant that the numerical inversion of the matrix was unstable, and in some cases, the inversion algorithm (the SVD algorithm, [81]) would not converge at all. As a measure of the stability of the inversion, we calculated the following quantity,

$$\frac{1}{N^2}\left|MM^{-1} - 1\right|, \tag{6.16}$$

where $M$ is an $N \times N$ matrix. For an exact inversion with no rounding errors, this quantity should be exactly zero. For the least stable covariance matrices, this quantity was $\sim 10^{-5}$. At this level, the inaccuracies in the inversion were causing noticeable effects in the fitting algorithm, and a correlated fit was deemed inappropriate. Instead we performed an uncorrelated fit for all of the *direct* results presented in this section. The fit ranges used are given in Table 6.5 and examples of the plateau are shown in Figure 6.6. The results are given in Tables 6.6 to 6.9.

We perform the extrapolation in two stages, first we perform a linear fit in $q^2$,

$$W_0(m_u, q^2) = Aq^2 + B, \tag{6.17}$$

and then extrapolate or interpolate as appropriate to $q^2 = 0$. Examples of the momentum extrapolation are given in Figure 6.7.

Secondly, we perform a linear fit in the light quark mass to the $q^2 = 0$ data–points,

$$W_0(m_u, q^2 = 0) = C(m_u + m_{\mathrm{res}}) + D, \tag{6.18}$$

and extrapolate to the chiral limit, $a(m_u + m_{\mathrm{res}}) = 0$. Examples of the chiral extrapolation are given in Figure 6.8. The values of $W_0$ after the momentum and chiral extrapolations are given in Tables 6.6 to 6.9.

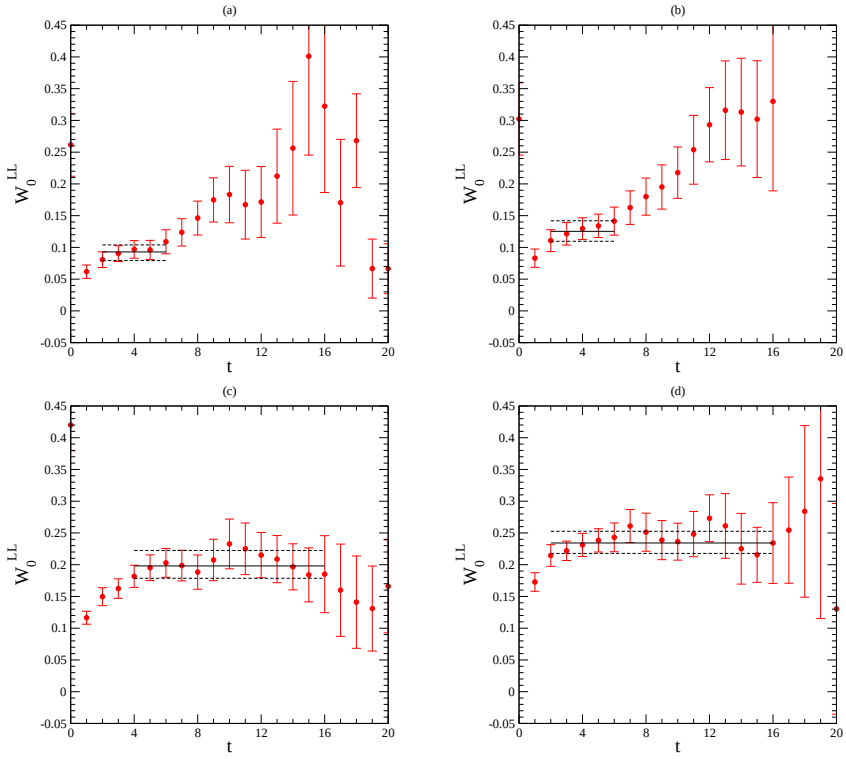


Figure 6.6: Example plateau for the form factor, $W^{LL}_{0;udu}(q^2)$ on the $24^3 \times 64$ datasets with $am_u = 0.005, 0.01, 0.02$ and $0.03$ for plots $(a)$, $(b)$, $(c)$ and $(d)$ respectively. The pion momenta is $a\vec{p} = \frac{2\pi}{L_x}(1,0,0)$ and the nucleon momenta is $a\vec{(k)} = \frac{2\pi}{L_x}(0,0,0)$.

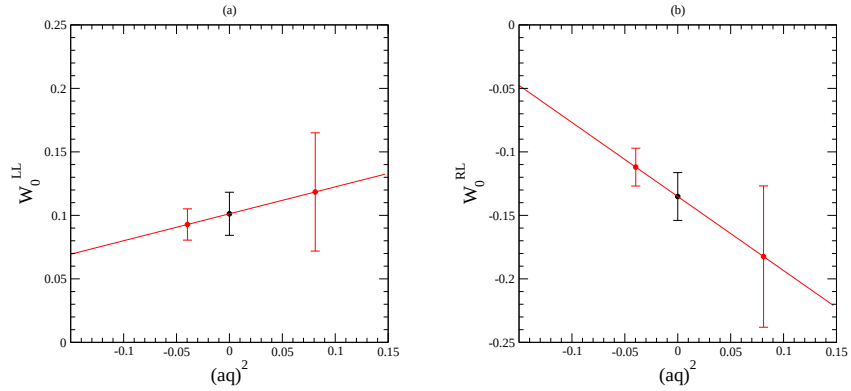


Figure 6.7: Plot (a) shows an example momentum interpolation of the form factor $W^{LL}_{0;udu}(q^2)$ to $(aq)^2 = 0$ and (b) shows an interpolation of the form factor $W^{RL}_{0;udu}(q^2)$. The form factors were calculated on the $24^3 \times 64$ lattice with $am_u = 0.005$.

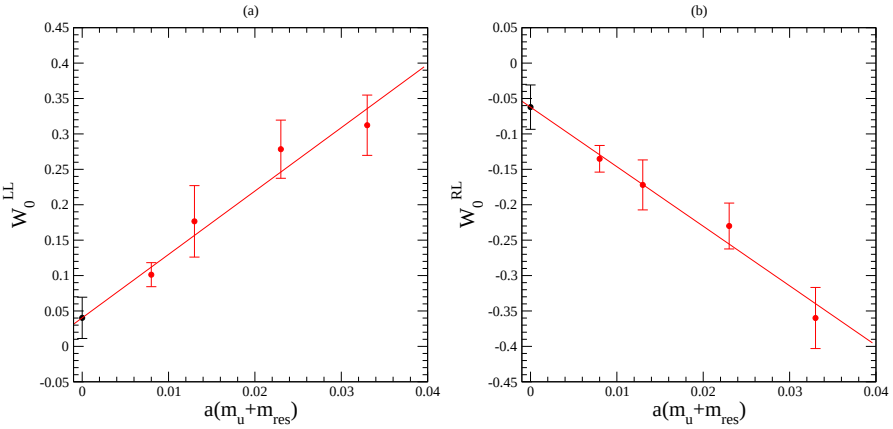


Figure 6.8: Example chiral extrapolation of the form factor $W^{LL}_{0;udu}$ to the chiral limit $a(m_u + m_{\rm res}) = 0$. The form factors were calculated on the $24^3 \times 64$ lattice and interpolated to $(aq)^2 = 0$.

| | $am_u$ | $(aq)^2$ | fitrange | $(aq)^2$ | fitrange |
|---|---|---|---|---|---|
| $W_{0;udu}^{LL}$ | 0.03 | −0.123 | 2-16 | 0.000 | 6-16 |
| | 0.02 | −0.095 | 4-16 | 0.029 | 8-16 |
| | 0.01 | −0.076 | 2-6 | 0.050 | 4-12 |
| | 0.005 | −0.040 | 2-6 | 0.081 | 3-8 |
| $W_{0;udu}^{RL}$ | 0.03 | −0.123 | 6-13 | 0.000 | 7-12 |
| | 0.02 | −0.095 | 4-15 | 0.029 | 5-12 |
| | 0.01 | −0.076 | 3-9 | 0.050 | 4-11 |
| | 0.005 | −0.040 | 3-13 | 0.081 | 8-13 |
| $W_{0;usu}^{LL}$ | 0.03 | −0.123 | 1-16 | 0.000 | 1-16 |
| | 0.02 | −0.095 | 5-16 | 0.029 | 2-9 |
| | 0.01 | −0.076 | 5-14 | 0.050 | 3-14 |
| | 0.005 | −0.040 | 7-11 | 0.081 | 1-10 |
| $W_{0;usu}^{RL}$ | 0.03 | −0.123 | 2-14 | 0.000 | 3-15 |
| | 0.02 | −0.095 | 5-16 | 0.029 | 6-14 |
| | 0.01 | −0.076 | 5-10 | 0.050 | 3-14 |
| | 0.005 | −0.040 | 9-14 | 0.081 | 2-12 |
| $W_{0;usd}^{LL}$ | 0.03 | −0.123 | 2-16 | 0.000 | 2-16 |
| | 0.02 | −0.095 | 5-16 | 0.029 | 6-16 |
| | 0.01 | −0.076 | 2-10 | 0.050 | 6-10 |
| | 0.005 | −0.040 | 7-11 | 0.081 | 3-10 |
| $W_{0;usd}^{RL}$ | 0.03 | −0.123 | 2-16 | 0.000 | 2-16 |
| | 0.02 | −0.095 | 5-16 | 0.029 | 6-16 |
| | 0.01 | −0.076 | 2-10 | 0.050 | 6-10 |
| | 0.005 | −0.040 | 2-11 | 0.081 | 2-8 |
| $W_{0;uds}^{LL}$ | 0.03 | −0.123 | 2-16 | 0.000 | 2-16 |
| | 0.02 | −0.095 | 6-16 | 0.029 | 2-16 |
| | 0.01 | −0.076 | 3-10 | 0.050 | 5-10 |
| | 0.005 | −0.040 | 7-11 | 0.081 | 3-11 |
| $W_{0;uds}^{RL}$ | 0.03 | −0.123 | 2-16 | 0.000 | 2-16 |
| | 0.02 | −0.095 | 6-16 | 0.029 | 2-16 |
| | 0.01 | −0.076 | 3-10 | 0.050 | 5-10 |
| | 0.005 | −0.040 | 6-14 | 0.081 | 3-11 |
| $W_{0;dsu}^{LL}$ | 0.03 | −0.123 | 2-16 | 0.000 | 2-16 |
| | 0.02 | −0.095 | 6-16 | 0.029 | 6-16 |
| | 0.01 | −0.076 | 2-10 | 0.050 | 6-11 |
| | 0.005 | −0.040 | 7-11 | 0.081 | 2-10 |
| $W_{0;dsu}^{RL}$ | 0.03 | −0.123 | 2-16 | 0.000 | 2-16 |
| | 0.02 | −0.095 | 6-16 | 0.029 | 6-16 |
| | 0.01 | −0.076 | 2-10 | 0.050 | 6-11 |
| | 0.005 | −0.040 | 2-12 | 0.081 | 2-12 |

Table 6.5: Fit ranges for the fits to the proton decay form factors $W_0$. $am_u$ is the light quark mass, the strange quark mass for all ensembles is 0.04. $q = k - p$ is the four momentum transfer between the nucleon and the meson.

| | $am_{ud}/am_s$ | $(aq)^2$ | $W_0$ | $(aq)^2$ | $W_0$ | $(aq)^2$ | $W_0$ |
|---|---|---|---|---|---|---|---|
| $W^{LL}_{0;udu}$ | 0.03/0.04 | $-0.123$ | 0.234(17) | 0.000 | 0.312(43) | 0 | 0.312(43) |
| | 0.02/0.04 | $-0.095$ | 0.198(22) | 0.029 | 0.303(53) | 0 | 0.278(41) |
| | 0.01/0.04 | $-0.076$ | 0.125(16) | 0.050 | 0.211(80) | 0 | 0.177(50) |
| | 0.005/0.04 | $-0.040$ | 0.093(12) | 0.081 | 0.118(47) | 0 | 0.101(17) |
| | $\chi^{\rm ral}$ | | | | | 0 | 0.040(29) |

| | $am_{ud}/am_s$ | $(aq)^2$ | $W_0$ | $(aq)^2$ | $W_0$ | $(aq)^2$ | $W_0$ |
|---|---|---|---|---|---|---|---|
| $W^{RL}_{0;udu}$ | 0.03/0.04 | $-0.123$ | -0.278(22) | 0.000 | -0.360(43) | 0 | -0.360(43) |
| | 0.02/0.04 | $-0.095$ | -0.211(22) | 0.029 | -0.236(40) | 0 | -0.230(32) |
| | 0.01/0.04 | $-0.076$ | -0.133(15) | 0.050 | -0.198(62) | 0 | -0.172(35) |
| | 0.005/0.04 | $-0.040$ | -0.112(15) | 0.081 | -0.182(56) | 0 | -0.135(19) |
| | $\chi^{\rm ral}$ | | | | | 0 | -0.062(31) |

Table 6.6: Results from fits to the form factor $W^{R/L\,L}_{0;udu}(q^2; p \to \pi^0)$ in lattice units. The three columns of results correspond to the form factor calculated at two values of $(aq)^2$, and then the extrapolation or interpolation to $(aq)^2 = 0$. The results are for the $24^3 \times 64 \times 16$ lattice with quark masses $am_u = 0.005$, 0.01, 0.02 and 0.03. Also shown is the extrapolation extrapolation of the $(aq)^2 = 0$ results to the chiral limit $a(m_u + m_{\rm res}) = 0$.

| | $am_{ud}/am_s$ | $(aq)^2$ | $W_0$ | $(aq)^2$ | $W_0$ | $(aq)^2$ | $W_0$ |
|---|---|---|---|---|---|---|---|
| $W^{LL}_{0;usu}$ | 0.03/0.04 | $-0.103$ | 0.063(5) | 0.015 | 0.100(12) | 0 | 0.095(11) |
| | 0.02/0.04 | $-0.057$ | 0.073(8) | 0.056 | 0.072(12) | 0 | 0.073(8) |
| | 0.01/0.04 | $-0.020$ | 0.051(10) | 0.086 | 0.076(22) | 0 | 0.056(9) |
| | 0.005/0.04 | 0.016 | 0.047(8) | 0.113 | 0.030(9) | 0 | 0.049(10) |
| | $\chi^{\rm ral}$ | | | | | 0 | 0.033(11) |

| | $am_{ud}/am_s$ | $(aq)^2$ | $W_0$ | $(aq)^2$ | $W_0$ | $(aq)^2$ | $W_0$ |
|---|---|---|---|---|---|---|---|
| $W^{RL}_{0;usu}$ | 0.03/0.04 | $-0.103$ | 0.185(12) | 0.015 | 0.246(23) | 0 | 0.239(21) |
| | 0.02/0.04 | $-0.057$ | 0.184(17) | 0.056 | 0.238(31) | 0 | 0.211(20) |
| | 0.01/0.04 | $-0.020$ | 0.137(13) | 0.086 | 0.201(32) | 0 | 0.149(13) |
| | 0.005/0.04 | 0.016 | 0.081(13) | 0.113 | 0.067(11) | 0 | 0.084(15) |
| | $\chi^{\rm ral}$ | | | | | 0 | 0.55(20) |

Table 6.7: Results from fits to the form factor $W^{R/L\,L}_{0;usu}(q^2; p \to K^0)$ in lattice units. The three columns of results correspond to the form factor calculated at two values of $(aq)^2$, and then the extrapolation or interpolation to $(aq)^2 = 0$. The results are for the $24^3 \times 64 \times 16$ lattice with quark masses $am_u = 0.005$, 0.01, 0.02 and 0.03. Also shown is the extrapolation extrapolation of the $(aq)^2 = 0$ results to the chiral limit $a(m_u + m_{\rm res}) = 0$.

| | $am_{ud}/am_s$ | $(aq)^2$ | $W_0$ | $(aq)^2$ | $W_0$ | $(aq)^2$ | $W_0$ |
|---|---|---|---|---|---|---|---|
| $W^{LL}_{0;uds}$ | 0.03/0.04 | $-0.103$ | 0.260(20) | 0.015 | 0.334(36) | 0 | 0.324(31) |
| | 0.02/0.04 | $-0.057$ | 0.245(23) | 0.056 | 0.316(42) | 0 | 0.281(30) |
| | 0.01/0.04 | $-0.020$ | 0.181(18) | 0.086 | 0.213(36) | 0 | 0.187(17) |
| | 0.005/0.04 | 0.016 | 0.121(16) | 0.113 | 0.106(22) | 0 | 0.124(18) |
| | $\chi^{\rm ral}$ | | | | | 0 | 0.072(25) |

| | $am_{ud}/am_s$ | $(aq)^2$ | $W_0$ | $(aq)^2$ | $W_0$ | $(aq)^2$ | $W_0$ |
|---|---|---|---|---|---|---|---|
| $W^{RL}_{0;uds}$ | 0.03/0.04 | $-0.103$ | -0.277(21) | 0.015 | -0.333(39) | 0 | -0.326(32) |
| | 0.02/0.04 | $-0.057$ | -0.247(20) | 0.056 | -0.275(41) | 0 | -0.261(30) |
| | 0.01/0.04 | $-0.020$ | -0.177(20) | 0.086 | -0.211(36) | 0 | -0.184(17) |
| | 0.005/0.04 | 0.016 | -0.090(9) | 0.113 | -0.095(17) | 0 | -0.089(10) |
| | $\chi^{\rm ral}$ | | | | | 0 | -0.028(20) |

Table 6.8: Results from fits to the form factor $W^{R/L\,L}_{0;uds}(q^2; p \to K^+)$ in lattice units. The three columns of results correspond to the form factor calculated at two values of $(aq)^2$, and then a linear extrapolation or interpolation to $(aq)^2 = 0$. The results are for the $24^3 \times 64 \times 16$ lattice with quark masses $am_u = 0.005$, 0.01, 0.02 and 0.03. Also shown is the extrapolation extrapolation of the $(aq)^2 = 0$ results to the chiral limit $a(m_u + m_{\rm res}) = 0$.

| | $am_{ud}/am_s$ | $(aq)^2$ | $W_0$ | $(aq)^2$ | $W_0$ | $(aq)^2$ | $W_0$ |
|---|---|---|---|---|---|---|---|
| $W^{LL}_{0;usd}$ | 0.03/0.04 | $-0.103$ | 0.097(7) | 0.015 | 0.109(18) | 0 | 0.108(15) |
| | 0.02/0.04 | $-0.057$ | 0.086(10) | 0.056 | 0.084(12) | 0 | 0.085(9) |
| | 0.01/0.04 | $-0.020$ | 0.067(8) | 0.086 | 0.067(18) | 0 | 0.067(9) |
| | 0.005/0.04 | 0.016 | 0.038(7) | 0.113 | 0.038(11) | 0 | 0.038(8) |
| | $\chi^{\rm ral}$ | | | | | 0 | 0.023(11) |

| | $am_{ud}/am_s$ | $(aq)^2$ | $W_0$ | $(aq)^2$ | $W_0$ | $(aq)^2$ | $W_0$ |
|---|---|---|---|---|---|---|---|
| $W^{RL}_{0;usd}$ | 0.03/0.04 | $-0.103$ | -0.114(10) | 0.015 | -0.149(18) | 0 | -0.145(15) |
| | 0.02/0.04 | $-0.057$ | -0.106(12) | 0.056 | -0.112(17) | 0 | -0.109(11) |
| | 0.01/0.04 | $-0.020$ | -0.077(9) | 0.086 | -0.099(21) | 0 | -0.081(8) |
| | 0.005/0.04 | 0.016 | -0.040(6) | 0.113 | -0.034(8) | 0 | -0.041(7) |
| | $\chi^{\rm ral}$ | | | | | 0 | -0.018(10) |

Table 6.9: Results from fits to the form factor $W^{R/L\,L}_{0;usd}(q^2; p \to K^+)$ in lattice units. The three columns of results correspond to the form factor calculated at two values of $(aq)^2$, and then a linear extrapolation or interpolation to $(aq)^2 = 0$. The results are for the $24^3 \times 64 \times 16$ lattice with quark masses $am_u = 0.005$, 0.01, 0.02 and 0.03. Also shown is the extrapolation extrapolation of the $(aq)^2 = 0$ results to the chiral limit $a(m_u + m_{\rm res}) = 0$.

| | $am_{ud}/am_s$ | $(aq)^2$ | $W_0$ | $(aq)^2$ | $W_0$ | $(aq)^2$ | $W_0$ |
|---|---|---|---|---|---|---|---|
| $W^{LL}_{0;dsu}$ | 0.03/0.04 | $-0.103$ | -0.162(12) | 0.015 | -0.221(24) | 0 | -0.214(20) |
| | 0.02/0.04 | $-0.057$ | -0.162(17) | 0.056 | -0.212(28) | 0 | -0.187(19) |
| | 0.01/0.04 | $-0.020$ | -0.115(12) | 0.086 | -0.145(23) | 0 | -0.121(11) |
| | 0.005/0.04 | 0.016 | -0.084(9) | 0.113 | -0.066(13) | 0 | -0.087(11) |
| | $\chi^{\rm ral}$ | | | | | 0 | -0.050(14) |

| | $am_{ud}/am_s$ | $(aq)^2$ | $W_0$ | $(aq)^2$ | $W_0$ | $(aq)^2$ | $W_0$ |
|---|---|---|---|---|---|---|---|
| $W^{RL}_{0;dsu}$ | 0.03/0.04 | $-0.103$ | -0.069(6) | 0.015 | -0.091(13) | 0 | -0.088(11) |
| | 0.02/0.04 | $-0.057$ | -0.079(10) | 0.056 | -0.108(19) | 0 | -0.093(11) |
| | 0.01/0.04 | $-0.020$ | -0.051(7) | 0.086 | -0.090(17) | 0 | -0.59(7) |
| | 0.005/0.04 | 0.016 | -0.032(5) | 0.113 | -0.031(8) | 0 | -0.032(5) |
| | $\chi^{\rm ral}$ | | | | | 0 | -0.020(8) |

Table 6.10: Results from fits to the form factor $W^{R/L\,L}_{0;dsu}(q^2; p \to K^+)$ in lattice units. The three columns of results correspond to the form factor calculated at two values of $(aq)^2$, and then a linear extrapolation or interpolation to $(aq)^2 = 0$. The results are for the $24^3 \times 64 \times 16$ lattice with quark masses $am_u = 0.005$, 0.01, 0.02 and 0.03. Also shown is the extrapolation extrapolation of the $(aq)^2 = 0$ results to the chiral limit $a(m_u + m_{\rm res}) = 0$.

### 6.3.2 Form factor systematic errors

So far the errors which we have presented for the form factors have been purely statistical. However, there are several sources of systematic error on our measurement and we shall now attempt to address each of these in turn.

As for the *indirect* method, our chiral extrapolation was an extrapolation in the light quark mass only, while the strange quark mass was held fixed. After the gauge configurations were generated with $am_s = 0.04$, analysis in Ref. [77] suggests the physical strange quark mass to be $am_s = 0.0343(16)$. We performed a second analysis with this value for the valence strange quark mass, while the sea quark mass was held fixed at 0.04. Figure 6.9 shows one example of the form factor $W^{LL}_{0;usu}(p \to K^0)$ in this case the difference between the fitted values is $< 2\%$. This is negligible when compared to the statistical error from the fit of $\sim 20\%$.

Ideally, we would perform a calculation at multiple lattice spacings, and extrapolate to the continuum limit. However, with only a single fixed lattice spacing we are unable to do this. Nonetheless, it should be noted that DWFs are automatically $\mathcal{O}(a)$ improved and are therefore expected to have a good scaling behaviour. Due to finite $L_s$ there are small $\mathcal{O}(a)$ errors, which, however are negligible compared to the other errors in this study.

Unlike for the *indirect* method, we have data for the *direct* method calculations on only a single lattice volume. Although we cannot perform a finite volume comparison, the lack of significant finite volume effects for the *indirect* method gives confidence that there will also be no significant finite volume effects in our results for the *direct* method.

Finally, we have performed only a simple linear chiral extrapolation to the chiral limit. To estimate the error in this approach, we can perform an extrapolation without the lightest point. Figure 6.10 shows an example for the form factor $W^{LL}_{0;udu}(p \to \pi^0)$. In this case the extrapolated value from both extrapolations are consistant within errors, this behaviour is typical of the extrapolations of all the matrix elements, due to the very large error on the extrapolated point from chiral extrapolations involving only 3 light quark masses.

In summary, all sources of systematic error that we have considered here are negligible when compared to the statistical error and so shall be ignored. We leave a full determination of the matrix elements in physical units until after we have discussed the renormalisation of these matrix elements in Section 6.4.

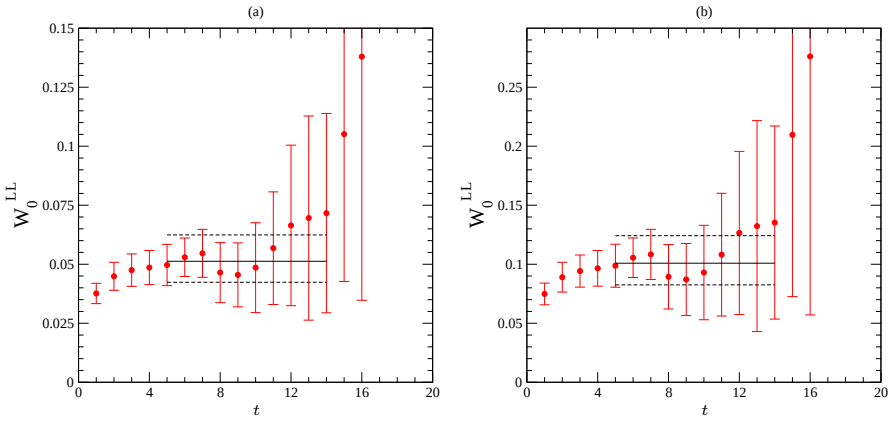


Figure 6.9: (a) and (b) show the form factor $W^{LL}_{0;usu}(p \to K^0)$ calculated with a strange valence quark mass of 0.04 and 0.0343 respectively.

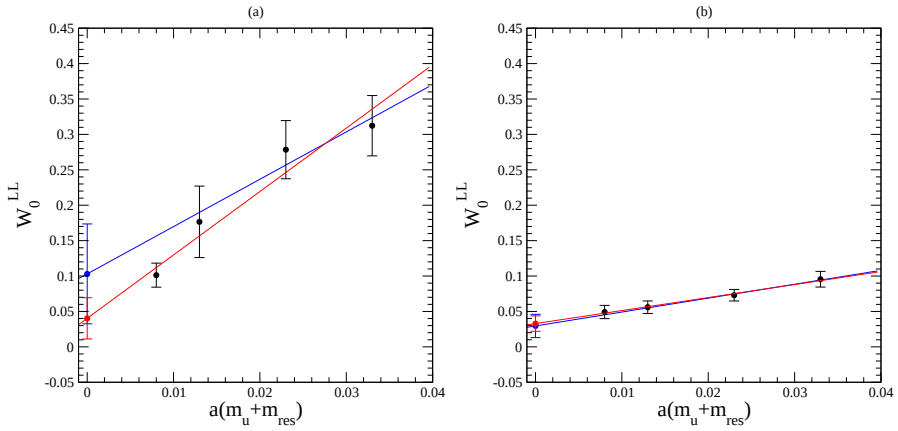


Figure 6.10: Chiral extrapolation of the form factors $W^{LL}_{0;udu}(p \to \pi^0)$ and $W^{LL}_{0;usu}(p \to K^0)$ for plots (a) and (b) respectively. The blue lines (and points) show the extrapolation (and extrapolated point in the chiral limit) for only the three heaviest valence quark masses. The red lines (and points) show the extrapolation (and extrapolated point in the chiral limit) from all four valence quark masses.

## 6.4 Non–perturbative Renormalisation

For the operator renormalisation (see Sections 2.5 and 3.7), we use the non–perturbative MOM–scheme renormalisation technique of the Rome–Southampton group [56]. This method has previously been used in Refs. [56, 80, 82] and the application of this method to the baryon number violating operators we have calculated is found in Ref. [80].

As the *direct* and *indirect* methods both use the same operators, the renormalisation is the same for both. Operators with different flavour structure (i.e.. $udu$, $uds$ etc.) also have the same renormalisation factor, which can be seen by noticing that the procedure we give below is identical, regardless of the flavour structure. For this reason we drop the flavour structure of the operators $\mathcal{O}^{\Gamma\Gamma'}_{q_i q_j q_k}$ and instead refer to the operators purely by the spin structure, LL, RL etc.

The renormalised operators $\mathcal{O}^A_{\text{ren}}$ are related to the lattice operators $\mathcal{O}^A_{\text{latt}}$ that we calculate by,

$$\mathcal{O}^A_{\text{ren}} = Z^{AB}_{\text{ND}} \mathcal{O}^B_{\text{latt}}, \tag{6.19}$$

where the compound index $A, B$ represents the spin structure of our operators, i.e. $A \equiv LL$, $RL$ etc. $Z_{\text{ND}}$ is a mixing matrix, which mixes the operators we are interested in with other operators with the same symmetries. Due to the exponentially accurate chiral symmetry afforded by domain wall fermions and the fact that our baryon number violating operators are chirally symmetric, the mixing between operators is expected to be small and so the off diagonal elements of this mixing matrix should also be small. The goal of this section is therefore to calculate the elements of this mixing matrix.

### 6.4.1 The parity and chirality bases

We can classify the baryon number violating operators into groups depending on their transformations under parity $\mathcal{P}$ and the isospin symmetry $\mathcal{S}$, the interchange of up and down quarks in the Lagrangian. The isospin symmetry holds because the up and down quarks in our simulation are degenerate in mass. Under this transformation, an operator will come back to itself with a possible change of sign, depending on the spin structure. Operators can therefore be categorised into $\mathcal{S}^+$ and $\mathcal{S}^-$ sectors, depending on if the sign either does or does not change under this switching symmetry. The classification of operators is shown in Table 6.11. This classification is important, as operators with different symmetry properties (i.e.. different blocks in Table 6.11) will not mix under renormalisation.

The operators in Table 6.11 are not the operators LL, RL that we have used earlier, but do form a complete basis known as the parity basis of operators. This basis is related to the

| | $\mathcal{S}^-$ | $\mathcal{S}^+$ |
|---|---|---|
| $\mathcal{P}^-$ | $SS$, $PP$, $AA$ | $VV$, $TT$ |
| $\mathcal{P}^+$ | $SP$, $PS$, $-AV$ | $-VA$, $T\tilde{T}$ |

Table 6.11: Classification of the $\mathcal{O}^{\Gamma\Gamma'}_{q_iq_jq_k}$ operators according to their transformation properties under parity and switching transformations.

baryon number violating operators we are interested in via the transformation,

$$LL = \frac{1}{4}(SS+PP) - \frac{1}{4}(SP+PS), \tag{6.20}$$

$$RL = \frac{1}{4}(SS-PP) - \frac{1}{4}(SP-PS), \tag{6.21}$$

$$A(LV) = \frac{1}{2}AA - \frac{1}{2}(-AV),, \tag{6.22}$$

where the basis of operators $LL$, $RL$ and $A(LV)$ is known as the chirality basis. The mixing matrix in the chirality basis, $Z_{\rm ND}$, and in the parity basis are therefore related via:

$$Z_{\rm ND} = \mathcal{T}\tilde{Z}_{\rm ND}\mathcal{T}^{-1}, \tag{6.23}$$

where

$$\mathcal{T} = \begin{pmatrix} 1/4 & 1/4 & 0 \\ 1/4 & -1/4 & 0 \\ 0 & 0 & 1/2 \end{pmatrix}. \tag{6.24}$$

In order to reconstruct the mixing matrix in the chirality basis, we therefore need only consider the operators in the $\mathcal{S}^-$ sector of the parity basis. Futher, we note that there is a one to one mapping between operators in the $\mathcal{P}^-$ and $\mathcal{P}^+$ sectors,

$$\mathcal{O}(\mathcal{P}^+) = \gamma_5\mathcal{O}(\mathcal{P}^-), \tag{6.25}$$

the renormalisation matrix for these two sectors is therefore identical, so we shall only calculate the renormalisation for the $\mathcal{O}(\mathcal{P}^-)$ sector.

The strategy shall therefore be to calculate the mixing matrix for the basis $SS$, $PP$, $AA$, then reconstruct the mixing matrix for the chirality basis using Eqs. 6.20-6.24.

### 6.4.2 NPR formulation

We start from the Green's function of the baryon number violating operator with three external quark states,

$$G^A(x_0,x_1,x_2,x_3) = \langle \mathcal{O}^A(x_0)\bar{u}(x_1)\bar{d}(x_2)\bar{s}(x_3)\rangle, \tag{6.26}$$

Here the $u$, $d$ and $s$ do not represent the physical flavours, but are used to differentiate the three different quarks. We then Fourier transform each external leg, with the same momentum $p$, and then amputate to define the vertex function, $\Lambda^A(p^2)$,

$$\begin{aligned}\Lambda^A(p^2) &= \left|\sum_x \mathrm{e}^{ip.x} G^A(x_0,x_1,x_2,x_3)\right|_{\mathrm{Amp}} \\ &= \epsilon^{abc}(C\Gamma\Gamma'\frac{\langle S_u(p)S_d(p)S_s(p)\rangle}{\langle S_u^{-1}(p)\rangle\langle S_d^{-1}(p)\rangle\langle S_s^{-1}(p)\rangle} \end{aligned} \tag{6.27}$$

where $\Gamma$ and $\Gamma'$ are the spin matrices from the operator $\mathcal{O}^A$. The vertex function is related to our renormalisation matrix by the renormalisation condition,

$$Z_q^{-3/2} Z_{\mathrm{ND}}^{BC} \Lambda^C_{abc,\alpha\beta\gamma\delta} P^A_{abc,\beta\alpha\delta\gamma} = \delta^{BA}, \tag{6.28}$$

where $Z_q$ is the quark wave function renormalisation, and $P^A$ is a projection matrix. This projection is chosen so that the renormalisation condition holds true in the free field case, where $Z_q = 1$ and $Z_{\mathrm{ND}}^{AB} = \delta^{AB}$. Giving:

$$P^{SS} = \frac{1}{96}\epsilon^{abc}(C^{-1})^{\beta\alpha}\delta^{\delta\gamma}, \tag{6.29}$$

$$P^{PP} = \frac{1}{96}\epsilon^{abc}(\gamma_5 C^{-1})^{\beta\alpha}\gamma_5^{\delta\gamma} \tag{6.30}$$

$$P^{AA} = \frac{1}{384}\epsilon^{abc}(\gamma_5\gamma_\mu C^{-1})^{\beta\alpha}(\gamma_5\gamma_\mu)^{\delta\gamma}. \tag{6.31}$$

For convenience, we define the matrix $M^{AB}$,

$$M^{AB} = \Lambda^A_{abc,\alpha\beta\gamma\delta} P^B_{abc,\beta\alpha\delta\gamma}, \tag{6.32}$$

which from Eq. 6.28 is equal to $Z_q^{3/2} Z_{\mathrm{ND}}^{-1}$. To get $Z_{\mathrm{ND}}$, we therefore calculate $Z_q$ in Section 6.4.4 and $M$ in Section 6.4.5.

### 6.4.3 Scheme matching and RG running

We wish to present results for the matrix elements in the $\overline{\mathrm{MS}}$ scheme at some scale $\mu$. Our results from Section 6.4.5 will be calculated in the MOM scheme at a scale $p$, so we must first match to the $\overline{\mathrm{MS}}$ scheme, and then evolve to the new scale $\mu$. This leads to the equation for the evolution $U^{\overline{\mathrm{MS}}\leftarrow latt}(\mu)$,

$$U^{\overline{\mathrm{MS}}\leftarrow latt}(\mu) = U^{\overline{\mathrm{MS}}}(\mu;p)\frac{Z^{\overline{\mathrm{MS}}}(p)}{Z^{MOM}(p)} Z_{\mathrm{ND}}(p), \tag{6.33}$$

where $U^{\overline{\rm MS}}(\mu;p)$ is the renormalisation group evolution factor from the scale $p$ to scale $\mu$. $\frac{Z^{\overline{\rm MS}}(p)}{Z^{MOM}(p)}$ matches the continuum MOM scheme to the $\overline{\rm MS}$ scheme at scale $p$ and $Z_{\rm ND}(p)$ is the renormalisation matrix in the MOM scheme that we just calculated.

The matching factor is,

$$\frac{Z^{\overline{\rm MS}}(p)}{Z^{MOM}(p)} = 1 + \frac{\alpha_s}{4\pi}\left[\frac{433}{180} - \frac{1123}{90}\ln 2 + \xi\left(\frac{587}{180} - \frac{317}{90}\ln 2\right)\right], \tag{6.34}$$

as calculated by [80] to one loop in continuum perturbation theory. $\xi$ is the gauge parameter. In our lattice calculation, we gauge fix to Landau gauge where $\xi = 0$.

The $\overline{\rm MS}$ evolution factor is,

$$U^{\overline{\rm MS}}(\mu;p) = \left[\frac{\alpha_s(\mu)}{\alpha_s(p)}\right]^{\gamma_0/2\beta_0}\left[1 + \left(\frac{\gamma_1}{2\beta_0} - \frac{\beta_1\gamma_0}{2\beta_0^2}\right)\frac{\alpha_s(\mu)-\alpha_s(p)}{4\pi}\right], \tag{6.35}$$

$$\beta_0 = 11 - \frac{2}{3}N_f,\ \beta_1 = 102 - \frac{38}{3}N_f, \tag{6.36}$$

$$\tag{6.37}$$

where the anomalous dimension, $\gamma$,

$$\gamma = \gamma_0\frac{\alpha_s}{4\pi} + \gamma_1\left(\frac{\alpha_s}{4\pi}\right)^2, \tag{6.38}$$

$$\gamma_0 = -4,\ \gamma_1 = -\left(\frac{14}{3} + \frac{4}{9}N_f - 4\Delta\right), \tag{6.39}$$

of the nucleon decay operator has been calculated up to two loops in $\overline{\rm MS}$ scheme in Ref [83] and $\Delta = 0, -10/3$ for $LL, RL$ operators respectively.

For the running coupling $\alpha_s(p)$, we integrate numerically the four–loop $\beta$ function of Ref. [84], starting from $\alpha_s(M_Z) = 0.1176(2)$ [17], and match across the $b$, and $c$ thresholds.

### 6.4.4 Vector and axial vector bilinear current results

In order to calculate the NPR for the proton decay matrix elements, we shall also need a value of $Z_q$, the quark wavefunction renormalisation. However, we shall avoid calculating $Z_q$ directly, and instead exploit the accurate determination of $Z_A = 0.7162(2)$ in the chiral limit. This was computed from ratios of hadronic matrix elements in Ref. [85].

We define the Fourier transformed amputated vector and axial vector bilinear vertex func-

tions,

$$\begin{aligned}\Lambda^V(p^2) &= \left|\sum_x \mathrm{e}^{ip.x} G^V(x_0,x_1,x_2)\right|_{\mathrm{Amp}}, \\ \Lambda^A(p^2) &= \left|\sum_x \mathrm{e}^{ip.x} G^A(x_0,x_1,x_2)\right|_{\mathrm{Amp}},\end{aligned} \tag{6.40}$$

where $G^V(x_0,x_1,x_2)$ and $G^A(x_0,x_1,x_2)$ are the Green's functions of the vector and axial vector operators with external quark states,

$$\begin{aligned}G^V(x_0,x_1,x_2) &= \langle (u(x_0)\gamma_\mu d(x_0))\,\bar{u}(x_1)\bar{d}(x_2)\rangle, \\ G^A(x_0,x_1,x_2) &= \langle (u(x_0)\gamma_\mu\gamma_5 d(x_0))\,\bar{u}(x_1)\bar{d}(x_2)\rangle,\end{aligned} \tag{6.41}$$

We then calculate the amputated vector and axial vector bilinear vertex functions for several values of $ap$,

$$ap = \left(\frac{2\pi}{L_x}n_x, \frac{2\pi}{L_y}n_y, \frac{2\pi}{L_z}n_z, \frac{2\pi}{L_t}n_t\right), \tag{6.42}$$

where $L_x = L_y = L_z$ is the spatial size of the lattice and $L_t$ is the time extent. Combinations of $(n_x, n_y, n_z, n_t)$ such that $-2 \le n_x, n_y, n_z \le 2$ and $-4 \le n_t \le 4$ are chosen and then averaged into equal $p^2$ values. Then we run the result for each value of $(ap)^2$ to a scale $\mu = a^{-1}$. Figure 6.11 shows the average and difference of the amputated local axial vector and vector bilinear currents at scale $\mu = a^{-1}$, plotted as a function of the $(ap)^2$ at which they were calculated. The points with $(ap)^2 \ge 1.7$ are used to extrapolate $(ap)^2 \to 0$, in order to remove discretisation errors of order $(ap)^2$.

We can now use the average of the amputated vector and axial vector bilinear currents to evaluate the quark wavefunction renormalisation $Z_q = \frac{1}{2}Z_A(\Lambda^A + \Lambda^V)$. The non-zero difference of the amputated vector and axial vector bilinear currents may be taken as a measure of the systematic error of the renormalisation constant arising from the closing of the window where the RI–MOM NPR can be safely applied. It may be observed that for $(ap)^2 \ge 1.7$ there is $< 1\%$ effect, which is enhanced to 2% by extrapolation of $(ap)^2 \to 0$.

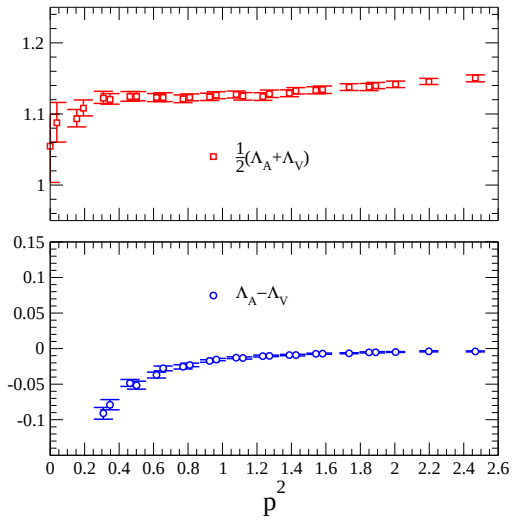


Figure 6.11: the average and difference of the amputated local axial vector and vector bilinear currents, with $am_u = 0.01$ and for the $16^3 \times 32$ dataset.

### 6.4.5 NPR results

Figure 6.12 shows the mixing matrix, $M^{AB}$, in the chirality basis as a function of external leg momentum for the three different light valence quark masses. The set of momenta used to calculate the mixing matrix is the same as used for the calculation of $Z_q$ in Section 6.4.4.

Operator mixing is induced by chiral symmetry breaking. The extent to which chiral symmetry is broken in the domain wall action is parametrised by the residual mass, $am_{\text{res}}$, and the induced mixing is expected to be suppressed by a factor $(am_{\text{res}})^2$ [86]. It may be seen from Figure 6.12 that, in the window of momenta for which contributions from both hadronic effects (low momenta) and contributions from discretisation effects (high momenta) are small, the chiral symmetry afforded by the domain wall fermions suppresses the mixing between different chirality operators and results in a mixing matrix which is essentially diagonal. This greatly simplifies the calculation of the proton decay matrix elements compared to, for example, Wilson fermions [37].

We then multiply by the appropriate factor of $Z_q$ from Section 6.4.4, rotate to the chirality basis and perform a linear chiral extrapolation. The latter may be done very precisely, as the mass dependence is extremely mild.

The $\overline{\text{MS}}$ renormalisation factors for the operators $O^{LL}$ and $O^{RL}$ are plotted at a fixed scale $\mu = 1/a$ in Figure 6.13 as a function of the square of the scale at which the lattice, MOM-scheme, renormalisation calculation was performed. The remaining momentum dependence, due to $O(a^2p^2)$ discretisation errors, is removed by performing a linear extrapolation in $(ap)^2$ to $(ap)^2 = 0$, which is also shown in Figure 6.13. This extrapolation is performed over the range

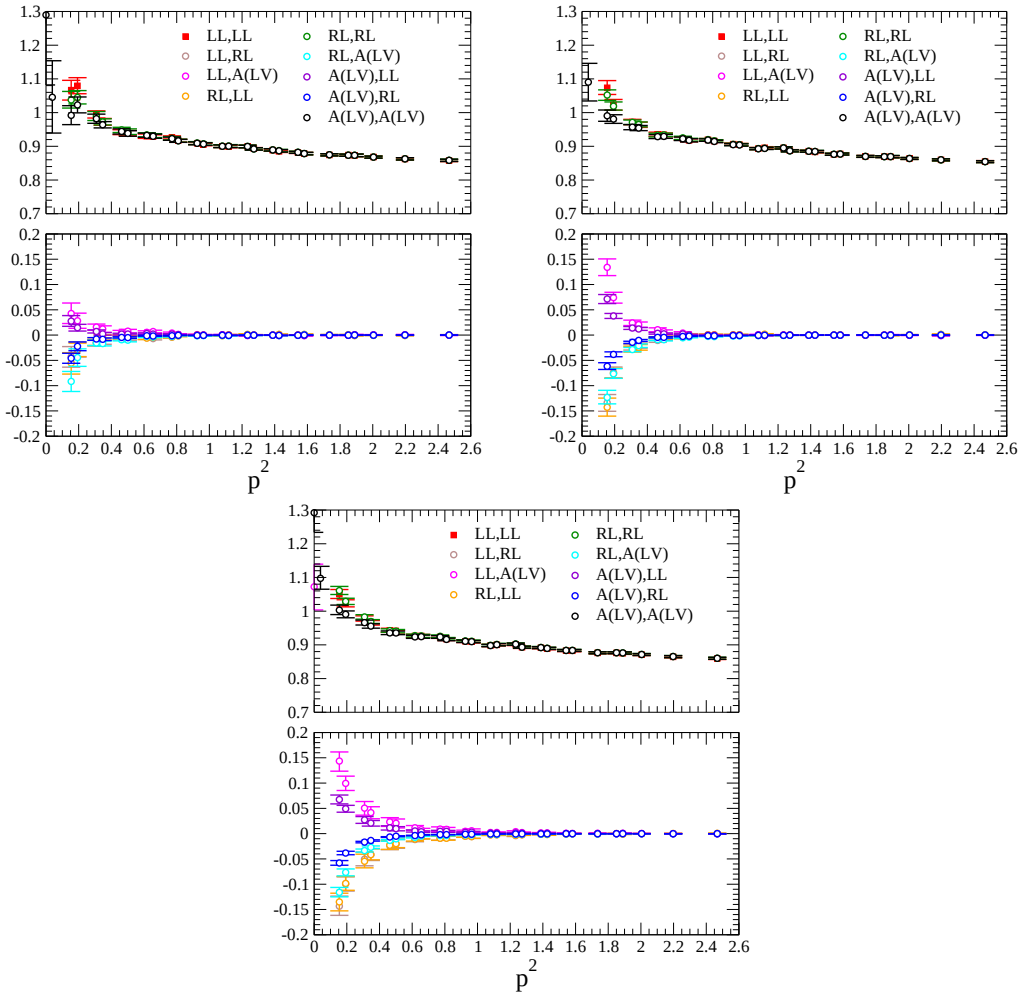


Figure 6.12: The mixing matrix, $M^{AB}$, in the chirality basis as a function of external leg momentum, as calculated on the $am_u = 0.01$, 0.02 and 0.03, $16^3 \times 32$ dataset.

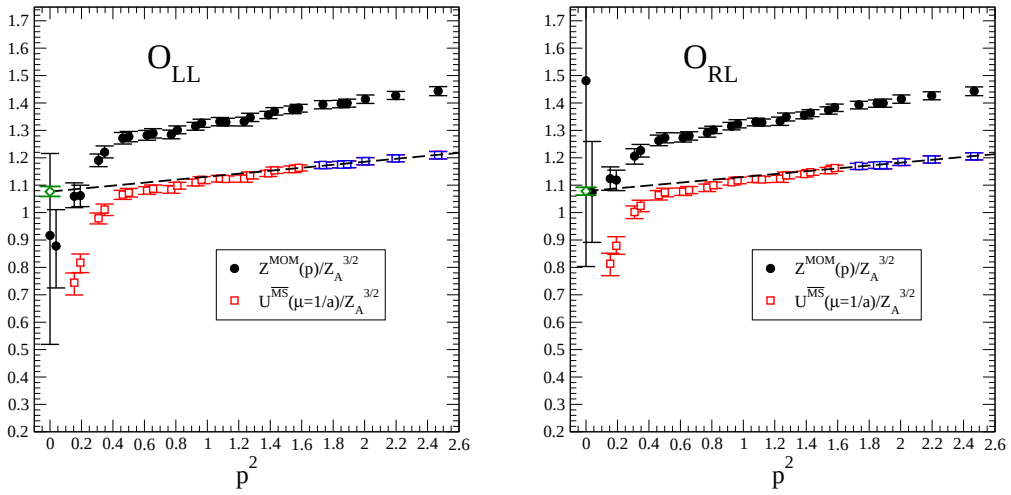


Figure 6.13: The $\overline{\rm MS}$ renormalisation factors, Eq. 6.33, for the $LL$ and $RL$ operators at a fixed scale $\mu = 1/a$, plotted as a function of the square of the scale at which the lattice, MOM-scheme, renormalisation calculation was performed. The blue points were those included in the extrapolation to $(ap)^2 = 0$, while the red points were not.

$1.7 < (ap)^2 < 2.5$ where the non-perturbative effect, estimated at 2%, is expected to be small.

Using Eq. 6.35 to run from $\mu = 1/a$ to $\mu = 2$ GeV we obtain:

$$\begin{aligned} U^{\overline{\rm MS}\leftarrow latt}(\mu = 2\ {\rm GeV})_{\rm LL} &= 0.662 \pm 0.010, \\ U^{\overline{\rm MS}\leftarrow latt}(\mu = 2\ {\rm GeV})_{\rm RL} &= 0.665 \pm 0.008. \end{aligned}$$

The systematic error on the NPR consists of the 2% error in $\Lambda^A$ due to the extrapolation to $(ap)^2 = 0$ and the error from truncating the perturbative factor in the matching factor at order $\alpha_s^2$ in Eq. 6.34. We estimate this latter systematic error to be 8%. Adding these errors in quadrature gives a total systematic error for the NPR of 8%.

# Chapter 7

# Conclusions

## 7.1 The *indirect* method

We now wish to calculate the values for the low energy constants, in physical units, renormalised at 2 GeV. First, we multiply the lattice values of $\alpha$ and $\beta$ by the NPR constants calculated in Section 6.4, and convert the lattice units to $\text{GeV}^3$ by multiplying by $a^{-3}$; using the inverse lattice spacing $a^{-1} = 1.73(3)$ GeV. We then combine the statistical errors on $\alpha$ and $\beta$, with the systematic errors discussed in Section 6.2.2 and with the systematic errors from the NPR given in Section 6.4, this gives our final results for $\alpha$ and $\beta$ renormalised at 2 GeV,

$$\alpha = -0.0112 \pm 0.0012_{(\text{stat})} \pm 0.0022_{(\text{syst})} \text{ GeV}^3, \quad (7.1)$$

$$\beta = 0.0120 \pm 0.0013_{(\text{stat})} \pm 0.0023_{(\text{syst})} \text{ GeV}^3. \quad (7.2)$$

The results for various determinations of $\alpha$ are summarised in Figure 7.1 and in Table 7.1. The agreement between recent lattice computations suggests that lattice QCD is being successful at determining the low-energy constants describing nucleon decay with increasingly smaller systematic uncertainty.

To reconstruct the proton decay matrix elements themselves we use the $\chi$PT results from from Table 2.1. The $\chi$PT requires the use of several QCD–scale constants. We use $F = 0.47(1)$ and $D = 0.80(1)$, as explained in Section 2.3. The remaining QCD–scale constants are taken from Ref [17], giving $m_N \approx 940$MeV and $f = 130$MeV. The average heavy baryon mass is taken to be $m_B \approx 1.15$GeV. As the error on all of these QCD scale quantities are so much smaller than the errors on $\alpha, \beta$, they are ignored. This gives:

| | | $\lvert\alpha\rvert$ [GeV$^3$] | |
|---|---|---|---|
| QCD model calculation | Donoghue and Goldwich [87] | 0.003 | Bag model |
| | Thomas and McKellar [88] | 0.02 | Bag model |
| | Meljanac et al. [89] | 0.004 | Bag model |
| | Ioffe [90] | 0.009 | Sum rule |
| | Krasnikov et al. [91] | 0.003 | Sum rule |
| | Ioffe and Smilga [92] | 0.006 | Sum rule |
| | Tomozawa [93] | 0.006 | Quark model |
| | Brodsky et al. [94] | 0.03 | |
| Lattice QCD $N_f = 0$ | Hara et al. [95] | 0.03 | WF, $a = 0.11$ fm |
| | Bowler et al. [96] | 0.013 | WF, $a = 0.22$ fm |
| | Gavela et al. [97] | 0.0056(8) | WF, $a = 0.09$ fm |
| | JLQCD [37] | 0.015(1) | WF, $a = 0.09$ fm |
| | CP-PACS & JLQCD [79] | $0.0090(9)(^{+5}_{-19})$ | WF, continuum limit |
| | Aoki et al. [80] | 0.0100(19) | DWF, $a = 0.15$ fm |
| Lattice QCD $N_f = 2$ | Aoki et al.[80] | 0.0118(21) | DWF, $a = 0.12$ fm |
| Lattice QCD $N_f = 2 + 1$ | This work (Aoki et al. [1]) | 0.0112(25) | DWF, $a = 0.12$ fm |

Table 7.1: Comparison of the low energy parameter of the nucleon decay chiral Lagrangian $\alpha$ among various QCD model calculation, lattice results in the literatures and the results from this work. In lattice QCD calculations, WF and DWF mean Wilson and domain-wall fermions. The results for $N_f = 2$, and our results for $N_f = 2 + 1$ are shown with the total error consisting of statistical and systematic errors on the bare matrix element and renormalization constant. The errors on the results from $N_f = 0$ are only statistical.

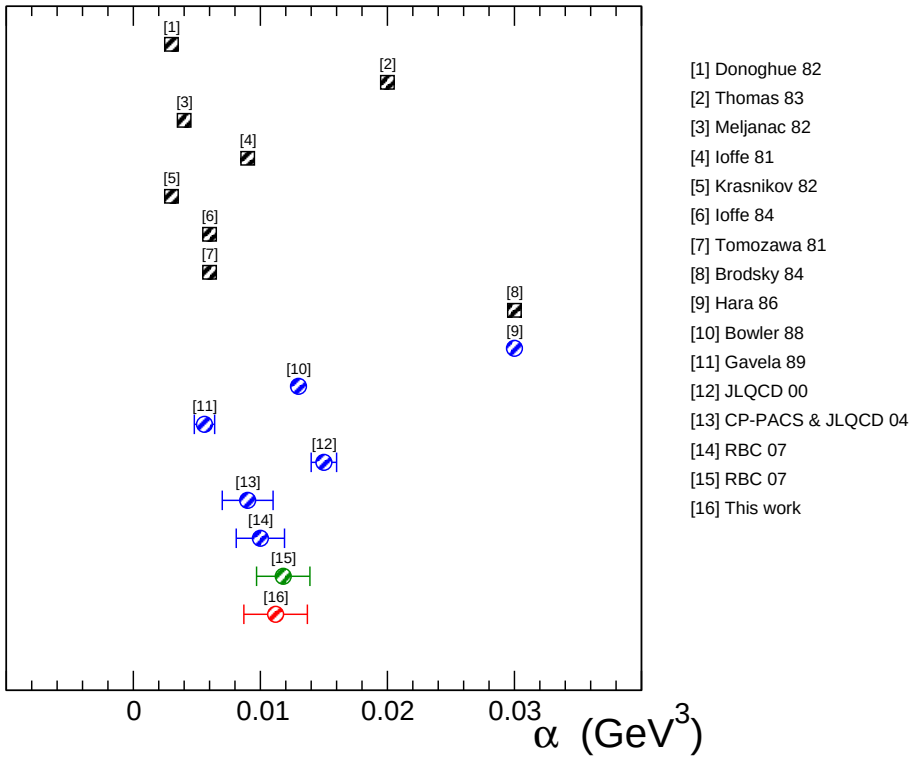


Figure 7.1: Summary of computations of the hadronic matrix element $\alpha$, as given in Table 7.1. Square points correspond to QCD model calculations, blue circles correspond to $N_f = 0$ lattice QCD calculations, the green circle is from $N_f = 2$ and the result from our $N_f = 2+1$ calculation is shown in red.

$$
\begin{aligned}
W^{LL}_{0;udu}(p \to \pi^0) &= 0.147(33)\,\mathrm{GeV}, \\
W^{RL}_{0;udu}(p \to \pi^0) &= -0.139(31)\,\mathrm{GeV}, \\
W^{LL}_{0;usu}(p \to K^0) &= 0.067(15)\,\mathrm{GeV}, \\
W^{RL}_{0;usu}(p \to K^0) &= 0.110(25)\,\mathrm{GeV}, \\
W^{LL}_{0;usd}(p \to K^+) &= 0.020(5)\,\mathrm{GeV}, \\
W^{RL}_{0;usd}(p \to K^+) &= -0.019(4)\,\mathrm{GeV}, \\
W^{LL}_{0;uds}(p \to K^+) &= 0.147(33)\,\mathrm{GeV}, \\
W^{LL}_{0;uds}(p \to K^+) &= -0.139(31)\,\mathrm{GeV}, \\
W^{LL}_{0;dsu}(p \to K^+) &= -0.107(24)\,\mathrm{GeV}, \\
W^{RL}_{0;dsu}(p \to K^+) &= -0.072(17)\,\mathrm{GeV}.
\end{aligned}
\tag{7.3}
$$

## 7.2 The *direct* method

As for the low energy constants from the *indirect* method, we wish to calculate the proton decay form factors from the *direct* method in physical units and renormalised at 2 GeV. We first multiply our form factors by the NPR constants calculated in Section 6.4, and convert the lattice units to $\mathrm{GeV}^3$ by multiplying by $a^{-3}$; using the inverse lattice spacing $a^{-1} = 1.73(3)$ GeV. We then combine the statistical errors on the form factors, with the systematic errors calculated in Section 6.3.2 with the NPR systematic errors in Section 6.4. This gives:

$$\begin{aligned}
W^{LL}_{0;udu}(p \to \pi^0) &= 0.079(55)\,\mathrm{GeV}, \\
W^{RL}_{0;udu}(p \to \pi^0) &= -0.125(57)\,\mathrm{GeV}, \\
W^{LL}_{0;usu}(p \to K^0) &= 0.065(22)\,\mathrm{GeV}, \\
W^{RL}_{0;usu}(p \to K^0) &= 0.110(37)\,\mathrm{GeV}, \\
W^{LL}_{0;usd}(p \to K^+) &= 0.045(20)\,\mathrm{GeV}, \\
W^{RL}_{0;usd}(p \to K^+) &= -0.037(21)\,\mathrm{GeV}, \\
W^{LL}_{0;uds}(p \to K^+) &= 0.141(49)\,\mathrm{GeV}, \\
W^{LL}_{0;uds}(p \to K^+) &= -0.057(38)\,\mathrm{GeV}, \\
W^{LL}_{0;dsu}(p \to K^+) &= -0.098(28)\,\mathrm{GeV}, \\
W^{RL}_{0;dsu}(p \to K^+) &= -0.040(15)\,\mathrm{GeV}.
\end{aligned} \tag{7.4}$$

## 7.3 Comparison of the *direct* and *indirect* results

In order to compare the *direct* and *indirect* results, the absolute value of each of the form factors calculated using both methods are plotted in Figure 7.2. Note that the *indirect* method tends to give a lower answer than the *direct* method, with the results varying by up to a factor of 2 between the two methods in the worst cases.

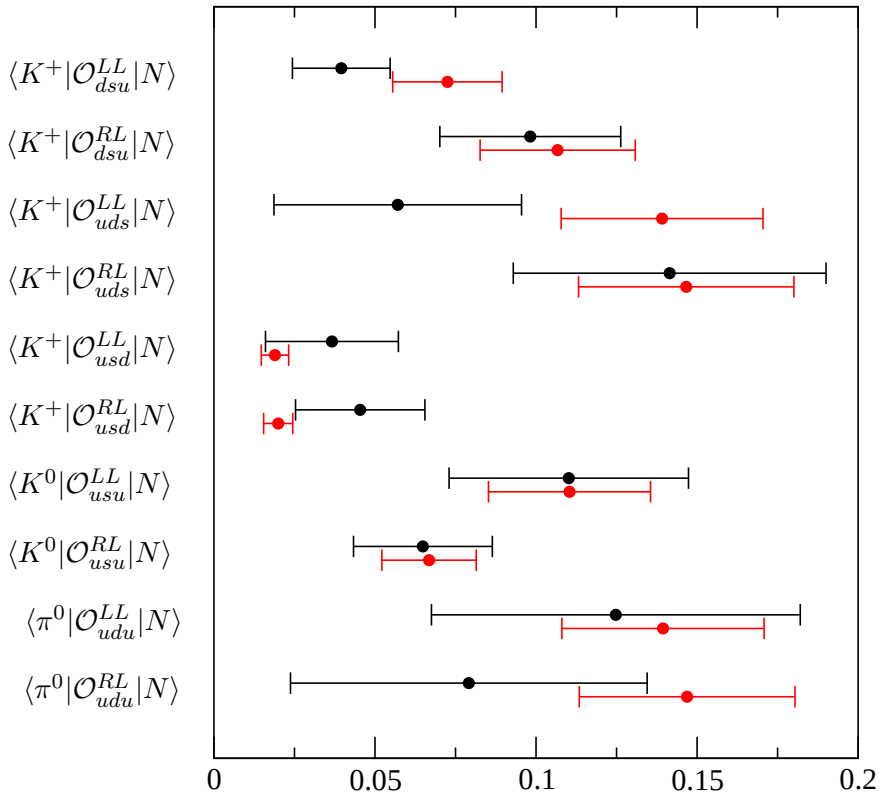


Figure 7.2: Summary of the absolute value of the renormalised matrix elements as calculated using the *direct* method (black points) and *indirect* method (red points).

## 7.4 Application to GUTs

Finally, let us discuss one way to use our result to discriminate between GUTs. As shown in Eq. 2.45, the proton partial decay width is:

$$\Gamma(N \to M + l) = \frac{m_N}{32\pi}\left(1 - \left(\frac{m_M}{m_N}\right)^2\right)^2 \left|\sum_i C^i W_0^i(N \to M + l)\right|^2 . \tag{7.5}$$

where the possible form factors $W_0^i$ have now been calculated and are given in Eqs. 7.3 and 7.4 for the *indirect* and *direct* methods respectively. Which form factors contribute to the sum, and their associated Wilson coefficients, $C^i$, will vary depending on which GUT is being considered.

### 7.4.1 The minimal $SU(5)$ GUT

In the minimal $SU(5)$ GUT, without super–symmetry, the possibly proton decay interactions are via X–boson exchange, as given in Figure 1.4(a).

For this case, the dominant decay mode is $p \to \pi^0$ [17], and there are two relevant form

factors,

$$\begin{aligned} W^{(1)} &\equiv W^{RL}_{0;udu}(p \to \pi^0), \\ W^{(2)} &\equiv W^{LR}_{0;udu}(p \to \pi^0). \end{aligned} \tag{7.6}$$

We note that these two form factors are equal (in fact when calculating $W^{RL}_{0;udu}$ we averaged together the form factors $W^{RL}_{0;udu}$ and $W^{LR}_{0;udu}$).

There are two corresponding Wilson coefficients which are non–zero [98],

$$\begin{aligned} C^{(1)} &= \mathrm{e}^{i\phi_u} \frac{g_5^4 A_R^2}{M_X^4}, \\ C^{(2)} &= \mathrm{e}^{i\phi_u} \frac{g_5^4 A_R^2}{M_X^4} \left(1 + |V_{ud}|^2\right), \end{aligned} \tag{7.7}$$

where $g_5$ is the unified coupling constant at the GUT scale $M_{\rm GUT} \approx 10^{15}$. $M_X \approx M_{\rm GUT}$ is the mass of the $X$ boson which mediates the decay and $A_R$ is the renormalisation factor. The phase factor $\mathrm{e}^{i\phi_u}$ factorises from the sum in the decay width (Eq. 2.45) and hence only appears in the lifetime as $|\mathrm{e}^{i\phi_u}|^2 = 1$. We also require the well known CKM matrix parameter $V_{ud} = 0.97418(27)$ from Ref. [17].

$g_5$ can be found by running the coupling constant to the GUT scale. Ref. [100] gives $\alpha_5 = g_5^2/4\pi = 0.0242$. Therefore $g_5 = 0.55$. The renormalisation factor was calculated in Ref. [100] to be 2.9.

The decay width is therefore,

$$\Gamma(p \to \pi^0\, e^+) = \frac{m_p}{32\pi} \left(1 - \left(\frac{m_\pi}{m_p}\right)^2\right)^2 \frac{g_5^4 A_R^2}{M_X^4} \left|1 + \left(1 + |V_{ud}|^2\right)^2\right| \left(W^{RL}_{0;udu}\right)^2. \tag{7.8}$$

For the form factor $W^{RL}_{0;udu}$, we have two estimates from the *direct* and *indirect* methods. The weakest constraint for GUTs comes from a prediction of a higher lifetime, and hence we choose the lowest value of the form factor, which in this case is the value from the *direct* method. Finally, as a conservative measure, we take the lower bound on the *direct* measurement of the form factor, rather than the average, again to give the weakest constraint.

We use the values of $g_5$, $A_R$ given earlier and choose $M_X = 1 \times 10^{15}$ GeV [17], which is the approximate scale for unification of the coupling constants. We also use the nucleon and pion masses: $m_p = 940$ MeV, $m_\pi = 140$ MeV. This gives:

$$\tau(p \to \pi^0\, e^+) = \left(\frac{W^{RL}_{0;udu}}{0.07)\,\mathrm{GeV}}\right)^{-2} \left(\frac{M_X}{10^{15}\,\mathrm{GeV}}\right)^4 \left(\frac{g_5}{0.55}\right)^{-4} \left(\frac{A_R}{2.9}\right)^{-2} \times 1.9 \times 10^{32}\,\mathrm{years}. \tag{7.9}$$

Using the proton partial lifetime for this decay channel from Ref. [32] $\tau > 8.2 \times 10^{33}$, we can see

that for this particular choice of $M_X$, the GUT is ruled out as it predicts a lifetime over an order of magnitude lower than the minimum experimental bound. This is in agreement with Ref. [34] which ruled out the $SU(5)$ GUT based upon then current, less stringent proton lifetime bounds in 1987.

Alternatively, we can use the limit on the partial lifetime, together with values for $W^{RL}_{0;udu}$, $g_5$ and $A_R$ to place a constraint on $M_X$,

$$M_X > 1.9 \times 10^{15}\,\text{GeV} \tag{7.10}$$

This is greater than the unification scale, $M_X \equiv M_{\text{GUT}} \approx 10^{15}\,\text{GeV}$.

### 7.4.2 The SUSY $SU(5)$ GUT

The minimal SUSY $SU(5)$ GUT also allows the decay $p \to \pi^0$ by X boson exchange; and the same form factors and Wilson coefficients appear in the decay width,

$$\Gamma(p \to \pi^0\, e^+) = \frac{m_p}{32\pi}\left(1 - \left(\frac{m_\pi}{m_p}\right)^2\right)^2 \frac{g_5^4 A_R^2}{M_X^4}\left|1 + \left(1 + |V_{ud}|^2\right)^2\right|\left(W^{RL}_{0;udu}\right)^2. \tag{7.11}$$

This time however, the GUT–scale (and hence the X boson mass $M_X$) is $\approx 2 \times 10^{16}$ GeV, the unified coupling coupling $\alpha_5 = 0.04$, giving $g_5 = 0.71$ and the renormalisation constant $A_R = 2.5$ [98].

Putting this together gives an expression for the lifetime of,

$$\tau(p \to \pi^0\, e^+) = \left(\frac{W^{RL}_{0;udu}}{0.07\,\text{GeV}}\right)^{-2}\left(\frac{M_X}{2 \times 10^{16}\,\text{GeV}}\right)^4\left(\frac{g_5}{0.71}\right)^{-4}\left(\frac{A_R}{2.5}\right)^{-2} \times 1.5 \times 10^{37}\,\text{years}. \tag{7.12}$$

Or equivalently using the bound on the proton partial lifetime for this decay channel from Ref. [32] $\tau > 8.2 \times 10^{33}$, we can set a bound on $M_X$,

$$M_X > 2.3 \times 10^{15}\,\text{GeV}. \tag{7.13}$$

In this decay channel, the proton lifetime bound is not enough to rule out the SUSY $SU(5)$ GUT with these parameters.

However, unlike in the $SU(5)$ GUT, in the minimal SUSY $SU(5)$ GUT, the dominant decay mode is expected to be the $p \to K^+\,\bar{\nu}_i$, via colour triplet Higgs exchange (see Figure 1.4(b)), with $i$ a generation label for the neutrino [17].

For this decay there are two important form factors:

$$W^{(1)} = W^{LL}_{0;usd},$$
$$W^{(2)} = W^{LL}_{0;uds}, \tag{7.14}$$

and there are therefore two possible Wilson coefficients. In this case however they are both equal [99], and given by:

$$C^{(1)} = C^{(2)} = \frac{2\alpha_2^2}{M_H} \frac{\bar{m}_c \bar{m}_{d_i} \mathrm{e}^{i\phi_c} V^*_{ud_i} V_{cd} V_{cs} A_L A_S}{m_W^2 \sin 2\beta_H} \left(1 + y^{tK}\right) \left(f(u,d) + f(u,e)\right). \tag{7.15}$$

These Wilson coefficients are functions of the CKM matrix elements $V^*_{ud_i}$, $V_{cd}$ and $V_{cs}$, the mass of the W boson $M_W$, the quark masses $\bar{m}_c$ and $\bar{m}_{d_i}$ and the $SU(2)$ coupling $\alpha_2 = g_2/4\pi$ at the SUSY breaking scale.

$A_S$ is the short distance renormalisation constant, representing the short range renormalisation effects between the GUT scale and the SUSY breaking scale. $A_L$ is the long distance renormalisation constant, representing the long range renormalisation effects between the SUSY breaking scale and the hadronic scale $\approx 1GeV$. $\beta_H$, $y^{tK}$, $f(u,d)$ and $f(u,e)$ are GUT parameters, for a discussion of these parameters, see Ref. [99].

We therefore have several GUT–scale constants; and the parameter space is considerably more complicated than for the minimal $SU(5)$ GUT. However, we notice that as the Wilson coefficients are equal, we can factor them out of the sum in the formula for the decay width (Eq. 2.45), to give,

$$\Gamma(p \to K^+ \bar{\nu}) = \frac{m_p}{32\pi} \left(1 - \left(\frac{m_K}{m_p}\right)^2\right)^2 \left|C^{(1)}\right|^2 \left(W^{LL}_{0;usd} + W^{LL}_{0;uds}\right)^2. \tag{7.16}$$

and given an experimental bound on the proton lifetime, we can now rearrange this equation to give a bound for the Wilson coefficient $C^{(1)}$. We can use the limit on the proton partial lifetime $\tau(p \to \bar{\nu} K^+) > 2.3 \times 10^{33}$ from [33], with the kaon and proton masses, $m_p = 940$ MeV, $m_K = 495$ MeV. The form factors $W^{LL}_{0;usd}$ and $W^{LL}_{0;uds}$ are chosen from the *direct* method results for the weakest constraint on the Wilson coefficients, and further we choose the lower bound of the error on these matrix elements, rather than the matrix element itself.

This gives a constraint on the Wilson coefficient of,

$$C^{(1)} < 3.7 \times 10^{-31}. \tag{7.17}$$

This constraint is valid for all GUTs where the dominant decay mode is $p \to K^+ \bar{\nu}_i$, and where the Wilson coefficients for the two relevant form factors are equal.

The analysis in Ref. [35] uses a conservative choice of the low energy constant $\beta = 0.003\mathrm{GeV}^3$

renormalised at a scale of 1 GeV, to constrain the mass of the colour triplet Higgs sufficiently to rule out the minimal SUSY SU(5) GUT. The higher value calculated in this work (running our value of $\beta$ to a scale of 1 GeV gives $\beta = 0.0109 \pm 23$ GeV$^3$ if we use Eq. 6.35) gives an even stronger constaint on the mass of the colour triplet Higgs and so confirms the fact that the minimal SUSY SU(5) GUT has been ruled out.

## 7.5 Summary

We have calculated the set of form factors which contribute to proton decay in grand unified theories using two different methods. The *direct* calculates the form factors directly from three–point correlation functions, while the *indirect* method relies on chiral perturbation theory and the calculation of two low energy constants from two–point correlation functions. Both of these methods give results which are generally consistant within errors, but with a factor of up to 2 difference in the worst cases between the two methods. This discrepancy is due to the use of leading order chiral perturbation theory.

The values of these form factors, together with fundamental QCD–scale constants can be used to set bounds on the Wilson coefficients in GUTs, or even to set bounds on GUT parameters. In the case of the $SU(5)$ and SUSY $SU(5)$ GUTs, these constraints are enough to rule out the GUTs entirely.

# Appendix A

# Two–point nucleon contractions

The proton correlation function, in the notation of Eq. 5.1, is given by,

$$f^{PS,PS}_{udu,udu} = \sum_{\vec{x}} \frac{1}{2}\left(1+\gamma_4\right) \langle \mathcal{O}^{PS}_{udu}(x) \bar{\mathcal{O}}^{PS}_{udu}(0) \rangle. \tag{A.1}$$

The operator $\mathcal{O}^{PS}_{udu}(x)$ is that defined by Eq. 5.1,

$$\mathcal{O}^{PS}_{udu}(x) = \epsilon^{abc} u^a_\alpha(x) (C\gamma_5)_{\alpha\beta} d^b_\beta(x) u^c_\gamma(x), \tag{A.2}$$

and the operator $\bar{\mathcal{O}}^{PS}_{udu}(0)$ is given by,

$$\bar{\mathcal{O}}^{PS}_{udu}(0) = \epsilon^{def} \bar{u}^d_\delta(0) \bar{d}^e_\epsilon(0) (C\gamma_5)_{\epsilon\zeta} \bar{u}^f_\zeta(0), \tag{A.3}$$

where we have used the fact that

$$\overline{C\gamma_5} = C\gamma_5. \tag{A.4}$$

We can therefore insert Eqs. A.2 and A.3 into Eq. A.1 to get,

$$f^{PS,PS}_{udu,udu} = \sum_{\vec{x}} \frac{1}{2}\left(1+\gamma_4\right) \langle \epsilon^{abc} u^a_\alpha(x) (C\gamma_5)_{\alpha\beta} d^b_\beta(x) u^c_\gamma(x) \epsilon^{def} \bar{u}^d_\delta(0) \bar{d}^e_\epsilon(0) (C\gamma_5)_{\epsilon\zeta} \bar{u}^f_\zeta(0) \rangle. \tag{A.5}$$

We now sum over all possible contractions of the quark and antiquark fields, where each contraction yields a quark propagator,

$$\overbrace{u^a_\alpha(x) \bar{u}^b_\beta(0)} = S^{ab}_{\alpha\beta}(x). \tag{A.6}$$

For the proton correlation function, there are two possible Wick contractions,

$$\left\langle u^a_\alpha(x) d^b_\beta(x) u^c_\gamma(x) \bar{u}^d_\delta(0) \bar{d}^e_\epsilon(0) \bar{u}^f_\zeta(0) \right\rangle = u^a_\alpha(x) d^b_\beta(x) u^c_\gamma(x) \bar{u}^d_\delta(0) \bar{d}^e_\epsilon(0) \bar{u}^f_\zeta(0)$$

$$+ \quad u^a_\alpha(x) d^b_\beta(x) u^c_\gamma(x) \bar{u}^d_\delta(0) \bar{d}^e_\epsilon(0) \bar{u}^f_\zeta(0). \qquad \text{(A.7)}$$

Giving,

$$f^{PS,PS}_{udu,udu} = \sum_{\vec{x}} \frac{1}{2}(1+\gamma_4)_{\delta\gamma} \epsilon^{abc} \epsilon^{def} (C\gamma_5)_{\alpha\beta} (C\gamma_5)_{\epsilon\zeta}$$
$$\left[ S^{af}_{\alpha\zeta}(x) S^{be}_{\beta\epsilon}(x) S^{cd}_{\gamma\delta}(x) - S^{ad}_{\alpha\delta}(x) S^{bf}_{\beta\zeta}(x) S^{ce}_{\gamma\epsilon}(x) \right]. \qquad \text{(A.8)}$$

# Appendix B

# Three–point function contractions

For the case of our three point proton decay matrix elements, we need to calculate

$$\langle \mathcal{O}^P_{q_i q_j}(y) \mathcal{O}^A(x) \bar{\mathcal{O}}^{PS}_{udu}(0) \rangle. \tag{B.1}$$

Writing all indices out fully, gives the following,

$$\begin{aligned}
\langle \mathcal{O}^P_{q_i q_j}(y) \mathcal{O}^A(x) \bar{\mathcal{O}}^{PS}_{udu}(0) \rangle_{\theta\zeta} \rangle &= \left[\bar{q}^a_{i\alpha}(y)(\gamma_5)_{\alpha\beta} q^a_{j\beta}(y)\right] \\
&\quad \left[\epsilon^{bcd}\epsilon_{kl}(q^b_{k\gamma}(x)(CP^{R/L})_{\gamma\delta} q^c_{l\delta})(x) P^L_{\theta\epsilon} q^d_{m\epsilon}(x)\right] \\
&\quad \left[\epsilon^{efg}\bar{u}^g_\zeta(0)(\bar{d}^f_\eta(0)(C\gamma_5)_{\eta\iota}\bar{u}^e_\iota(0))\right] \\
&= \epsilon^{bcd}\epsilon^{efg}\epsilon_{kl}(\gamma_5)_{\alpha\beta}(CP^{R/L})_{\gamma\delta} P^L_{\theta\epsilon}(C\gamma_5)_{\eta\iota} \\
&\quad \left[\bar{q}^a_{i\alpha}(y) q^a_{j\beta}(y) q^b_{k\gamma}(x) q^c_{l\delta}(x) q^d_{m\epsilon}(x) \bar{u}^g_\zeta(0) \bar{d}^f_\eta(0) \bar{u}^e_\iota(0)\right]. \qquad \text{(B.2)}
\end{aligned}$$

If we allow the flavours of the quark fields $i, j, k, l, m$ to be arbitrary, then there are 24 possible contractions:

- 

- 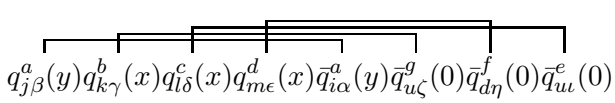

- 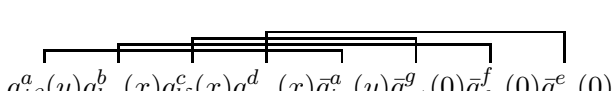

- 
$q^a_{j\beta}(y)q^b_{k\gamma}(x)q^c_{l\delta}(x)q^d_{m\epsilon}(x)\bar{q}^a_{i\alpha}(y)\bar{q}^g_{u\zeta}(0)\bar{q}^f_{d\eta}(0)\bar{q}^e_{u\iota}(0)$
- 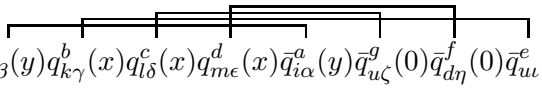
$q^a_{j\beta}(y)q^b_{k\gamma}(x)q^c_{l\delta}(x)q^d_{m\epsilon}(x)\bar{q}^a_{i\alpha}(y)\bar{q}^g_{u\zeta}(0)\bar{q}^f_{d\eta}(0)\bar{q}^e_{u\iota}(0)$
- 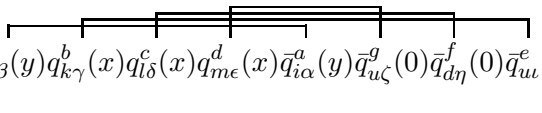
$q^a_{j\beta}(y)q^b_{k\gamma}(x)q^c_{l\delta}(x)q^d_{m\epsilon}(x)\bar{q}^a_{i\alpha}(y)\bar{q}^g_{u\zeta}(0)\bar{q}^f_{d\eta}(0)\bar{q}^e_{u\iota}(0)$
- 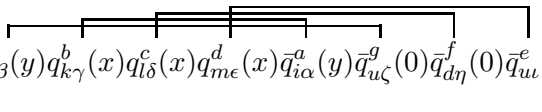
$q^a_{j\beta}(y)q^b_{k\gamma}(x)q^c_{l\delta}(x)q^d_{m\epsilon}(x)\bar{q}^a_{i\alpha}(y)\bar{q}^g_{u\zeta}(0)\bar{q}^f_{d\eta}(0)\bar{q}^e_{u\iota}(0)$
- 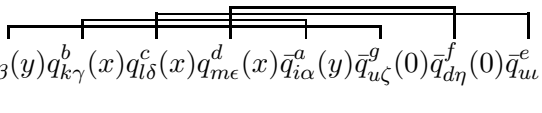
$q^a_{j\beta}(y)q^b_{k\gamma}(x)q^c_{l\delta}(x)q^d_{m\epsilon}(x)\bar{q}^a_{i\alpha}(y)\bar{q}^g_{u\zeta}(0)\bar{q}^f_{d\eta}(0)\bar{q}^e_{u\iota}(0)$
- 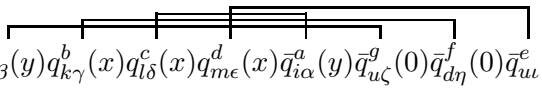
$q^a_{j\beta}(y)q^b_{k\gamma}(x)q^c_{l\delta}(x)q^d_{m\epsilon}(x)\bar{q}^a_{i\alpha}(y)\bar{q}^g_{u\zeta}(0)\bar{q}^f_{d\eta}(0)\bar{q}^e_{u\iota}(0)$
- 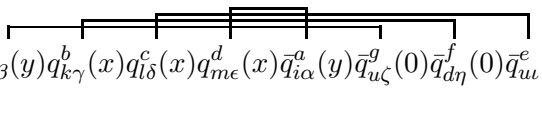
$q^a_{j\beta}(y)q^b_{k\gamma}(x)q^c_{l\delta}(x)q^d_{m\epsilon}(x)\bar{q}^a_{i\alpha}(y)\bar{q}^g_{u\zeta}(0)\bar{q}^f_{d\eta}(0)\bar{q}^e_{u\iota}(0)$
- 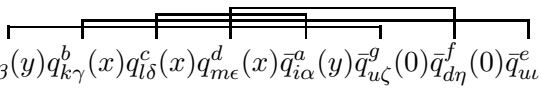
$q^a_{j\beta}(y)q^b_{k\gamma}(x)q^c_{l\delta}(x)q^d_{m\epsilon}(x)\bar{q}^a_{i\alpha}(y)\bar{q}^g_{u\zeta}(0)\bar{q}^f_{d\eta}(0)\bar{q}^e_{u\iota}(0)$
- 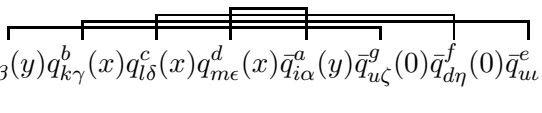
$q^a_{j\beta}(y)q^b_{k\gamma}(x)q^c_{l\delta}(x)q^d_{m\epsilon}(x)\bar{q}^a_{i\alpha}(y)\bar{q}^g_{u\zeta}(0)\bar{q}^f_{d\eta}(0)\bar{q}^e_{u\iota}(0)$
- 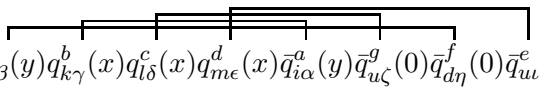
$q^a_{j\beta}(y)q^b_{k\gamma}(x)q^c_{l\delta}(x)q^d_{m\epsilon}(x)\bar{q}^a_{i\alpha}(y)\bar{q}^g_{u\zeta}(0)\bar{q}^f_{d\eta}(0)\bar{q}^e_{u\iota}(0)$
- 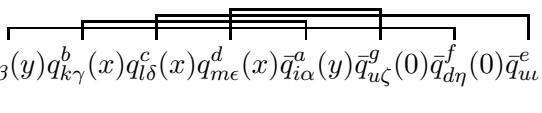
$q^a_{j\beta}(y)q^b_{k\gamma}(x)q^c_{l\delta}(x)q^d_{m\epsilon}(x)\bar{q}^a_{i\alpha}(y)\bar{q}^g_{u\zeta}(0)\bar{q}^f_{d\eta}(0)\bar{q}^e_{u\iota}(0)$
- 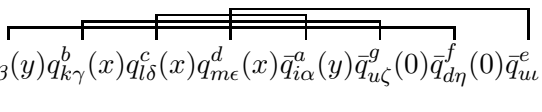
$q^a_{j\beta}(y)q^b_{k\gamma}(x)q^c_{l\delta}(x)q^d_{m\epsilon}(x)\bar{q}^a_{i\alpha}(y)\bar{q}^g_{u\zeta}(0)\bar{q}^f_{d\eta}(0)\bar{q}^e_{u\iota}(0)$

- 
$$q^a_{j\beta}(y)q^b_{k\gamma}(x)q^c_{l\delta}(x)q^d_{m\epsilon}(x)\bar{q}^a_{i\alpha}(y)\bar{q}^g_{u\zeta}(0)\bar{q}^f_{d\eta}(0)\bar{q}^e_{u\iota}(0)$$

- 
$$q^a_{j\beta}(y)q^b_{k\gamma}(x)q^c_{l\delta}(x)q^d_{m\epsilon}(x)\bar{q}^a_{i\alpha}(y)\bar{q}^g_{u\zeta}(0)\bar{q}^f_{d\eta}(0)\bar{q}^e_{u\iota}(0)$$

- 
$$q^a_{j\beta}(y)q^b_{k\gamma}(x)q^c_{l\delta}(x)q^d_{m\epsilon}(x)\bar{q}^a_{i\alpha}(y)\bar{q}^g_{u\zeta}(0)\bar{q}^f_{d\eta}(0)\bar{q}^e_{u\iota}(0)$$

- 
$$q^a_{j\beta}(y)q^b_{k\gamma}(x)q^c_{l\delta}(x)q^d_{m\epsilon}(x)\bar{q}^a_{i\alpha}(y)\bar{q}^g_{u\zeta}(0)\bar{q}^f_{d\eta}(0)\bar{q}^e_{u\iota}(0)$$

- 
$$q^a_{j\beta}(y)q^b_{k\gamma}(x)q^c_{l\delta}(x)q^d_{m\epsilon}(x)\bar{q}^a_{i\alpha}(y)\bar{q}^g_{u\zeta}(0)\bar{q}^f_{d\eta}(0)\bar{q}^e_{u\iota}(0)$$

- 
$$q^a_{j\beta}(y)q^b_{k\gamma}(x)q^c_{l\delta}(x)q^d_{m\epsilon}(x)\bar{q}^a_{i\alpha}(y)\bar{q}^g_{u\zeta}(0)\bar{q}^f_{d\eta}(0)\bar{q}^e_{u\iota}(0)$$

- 
$$q^a_{j\beta}(y)q^b_{k\gamma}(x)q^c_{l\delta}(x)q^d_{m\epsilon}(x)\bar{q}^a_{i\alpha}(y)\bar{q}^g_{u\zeta}(0)\bar{q}^f_{d\eta}(0)\bar{q}^e_{u\iota}(0)$$

- 
$$q^a_{j\beta}(y)q^b_{k\gamma}(x)q^c_{l\delta}(x)q^d_{m\epsilon}(x)\bar{q}^a_{i\alpha}(y)\bar{q}^g_{u\zeta}(0)\bar{q}^f_{d\eta}(0)\bar{q}^e_{u\iota}(0)$$

- 
$$q^a_{j\beta}(y)q^b_{k\gamma}(x)q^c_{l\delta}(x)q^d_{m\epsilon}(x)\bar{q}^a_{i\alpha}(y)\bar{q}^g_{u\zeta}(0)\bar{q}^f_{d\eta}(0)\bar{q}^e_{u\iota}(0)$$

These contractions correspond to the propagators,

$$
\begin{aligned}
&S^{aa}_{j,\beta\alpha}(0)\delta_{ji}S^{bg}_{k,\gamma\zeta}(x)\delta_{ku}S^{cf}_{l,\delta\eta}(x)\delta_{ld}S^{de}_{m,\epsilon\iota}(x)\delta_{mu}\\
&-S^{aa}_{j,\beta\alpha}(0)\delta_{ji}S^{bg}_{k,\gamma\zeta}(x)\delta_{ku}S^{ce}_{l,\delta\iota}(x)\delta_{lu}S^{df}_{m,\epsilon\eta}(x)\delta_{md}\\
&-S^{aa}_{j,\beta\alpha}(0)\delta_{ji}S^{bf}_{k,\gamma\eta}(x)\delta_{kd}S^{cg}_{l,\delta\zeta}(x)\delta_{lu}S^{de}_{m,\epsilon\iota}(x)\delta_{mu}\\
&+S^{aa}_{j,\beta\alpha}(0)\delta_{ji}S^{bf}_{k,\gamma\eta}(x)\delta_{kd}S^{ce}_{l,\delta\iota}(x)\delta_{lu}S^{dg}_{m,\epsilon\zeta}(x)\delta_{mu}\\
&+S^{aa}_{j,\beta\alpha}(0)\delta_{ji}S^{be}_{k,\gamma\iota}(x)\delta_{ku}S^{cg}_{l,\delta\zeta}(x)\delta_{lu}S^{df}_{m,\epsilon\eta}(x)\delta_{md}\\
&-S^{aa}_{j,\beta\alpha}(0)\delta_{ji}S^{be}_{k,\gamma\iota}(x)\delta_{ku}S^{cf}_{l,\delta\eta}(x)\delta_{ld}S^{dg}_{m,\epsilon\zeta}(x)\delta_{mu}\\
&-S^{ag}_{j,\beta\zeta}(y)\delta_{ju}S^{ba}_{k,\gamma\alpha}(x-y)\delta_{ki}S^{cf}_{l,\delta\eta}(x)\delta_{ld}S^{de}_{m,\epsilon\iota}(x)\delta_{mu}\\
&+S^{ag}_{j,\beta\zeta}(y)\delta_{ju}S^{ba}_{k,\gamma\alpha}(x-y)\delta_{ki}S^{ce}_{l,\delta\iota}(x)\delta_{lu}S^{df}_{m,\epsilon\eta}(x)\delta_{md}\\
&+S^{ag}_{j,\beta\zeta}(y)\delta_{ju}S^{bf}_{k,\gamma\eta}(x)\delta_{kd}S^{ca}_{l,\delta\alpha}(x-y)\delta_{li}S^{de}_{m,\epsilon\iota}(x)\delta_{mu}\\
&-S^{ag}_{j,\beta\zeta}(y)\delta_{ju}S^{bf}_{k,\gamma\eta}(x)\delta_{kd}S^{ce}_{l,\delta\iota}(x)\delta_{lu}S^{da}_{m,\epsilon\alpha}(x-y)\delta_{mi}\\
&-S^{ag}_{j,\beta\zeta}(y)\delta_{ju}S^{be}_{k,\gamma\iota}(x)\delta_{ku}S^{ca}_{l,\delta\alpha}(x-y)\delta_{li}S^{df}_{m,\epsilon\eta}(x)\delta_{md}\\
&+S^{ag}_{j,\beta\zeta}(y)\delta_{ju}S^{be}_{k,\gamma\iota}(x)\delta_{ku}S^{cf}_{l,\delta\eta}(x)\delta_{ld}S^{da}_{m,\epsilon\alpha}(x-y)\delta_{mi}\\
&+S^{af}_{j,\beta\eta}(y)\delta_{jd}S^{ba}_{k,\gamma\alpha}(x-y)\delta_{ki}S^{cg}_{l,\delta\zeta}(x)\delta_{lu}S^{de}_{m,\epsilon\iota}(x)\delta_{mu}\\
&-S^{af}_{j,\beta\eta}(y)\delta_{jd}S^{ba}_{k,\gamma\alpha}(x-y)\delta_{ki}S^{ce}_{l,\delta\iota}(x)\delta_{lu}S^{dg}_{m,\epsilon\zeta}(x)\delta_{mu}\\
&-S^{af}_{j,\beta\eta}(y)\delta_{jd}S^{bg}_{k,\gamma\zeta}(x)\delta_{ku}S^{ca}_{l,\delta\alpha}(x-y)\delta_{li}S^{de}_{m,\epsilon\iota}(x)\delta_{mu}\\
&+S^{af}_{j,\beta\eta}(y)\delta_{jd}S^{bg}_{k,\gamma\zeta}(x)\delta_{ku}S^{ce}_{l,\delta\iota}(x)\delta_{lu}S^{da}_{m,\epsilon\alpha}(x-y)\delta_{mi}\\
&+S^{af}_{j,\beta\eta}(y)\delta_{jd}S^{be}_{k,\gamma\iota}(x)\delta_{ku}S^{ca}_{l,\delta\alpha}(x-y)\delta_{li}S^{dg}_{m,\epsilon\zeta}(x)\delta_{mu}\\
&-S^{af}_{j,\beta\eta}(y)\delta_{jd}S^{be}_{k,\gamma\iota}(x)\delta_{ku}S^{cg}_{l,\delta\zeta}(x)\delta_{lu}S^{da}_{m,\epsilon\alpha}(x-y)\delta_{mi}\\
&-S^{ae}_{j,\beta\iota}(y)\delta_{ju}S^{ba}_{k,\gamma\alpha}(x-y)\delta_{ki}S^{cg}_{l,\delta\zeta}(x)\delta_{lu}S^{df}_{m,\epsilon\eta}(x)\delta_{md}\\
&+S^{ae}_{j,\beta\iota}(y)\delta_{ju}S^{ba}_{k,\gamma\alpha}(x-y)\delta_{ki}S^{cf}_{l,\delta\eta}(x)\delta_{ld}S^{dg}_{m,\epsilon\zeta}(x)\delta_{mu}\\
&+S^{ae}_{j,\beta\iota}(y)\delta_{ju}S^{bg}_{k,\gamma\zeta}(x)\delta_{ku}S^{ca}_{l,\delta\alpha}(x-y)\delta_{li}S^{df}_{m,\epsilon\eta}(x)\delta_{md}\\
&-S^{ae}_{j,\beta\iota}(y)\delta_{ju}S^{bg}_{k,\gamma\zeta}(x)\delta_{ku}S^{cf}_{l,\delta\eta}(x)\delta_{ld}S^{da}_{m,\epsilon\alpha}(x-y)\delta_{mi}\\
&-S^{ae}_{j,\beta\iota}(y)\delta_{ju}S^{bf}_{k,\gamma\eta}(x)\delta_{kd}S^{ca}_{l,\delta\alpha}(x-y)\delta_{li}S^{dg}_{m,\epsilon\zeta}(x)\delta_{mu}\\
&+S^{ae}_{j,\beta\iota}(y)\delta_{ju}S^{bf}_{k,\gamma\eta}(x)\delta_{kd}S^{cg}_{l,\delta\zeta}(x)\delta_{lu}S^{da}_{m,\epsilon\alpha}(x-y)\delta_{mi}. \qquad \text{(B.3)}
\end{aligned}
$$

We now need to specify the quark content of the meson and baryon number violating operators. Many of the contractions will vanish for a particular flavour combination due to the delta–functions in Eq. B.3. Further, for a specific flavour combination and with appropriate relabelling of dummy spin and colour indices, some of the contractions may result in identical expressions which may therefore be combined. We shall also write the final results in terms of

the sequential propagators,

$$\begin{aligned} S^{ab}_{u;\alpha\beta}(x-y)(\gamma_5)_{\beta\gamma}S^{bc}_{u;\gamma\delta}(y) &= S^{ac}_{\mathrm{seq};u;\alpha\delta}(x), \\ S^{ab}_{s;\alpha\beta}(x-y)(\gamma_5)_{\beta\gamma}S^{bc}_{u;\gamma\delta}(y) &= S^{ac}_{\mathrm{seq},s;\alpha\delta}(x), \end{aligned} \tag{B.4}$$

and then drop the position label from all propagators, as they will all be the same ($x$). This gives expressions for the primary matrix elements,

$$\begin{aligned} \langle \pi^+(\vec{p})|\mathcal{O}^{R/L\,L}_{udu}|N(\vec{k},s)\rangle &= \epsilon^{bcd}\epsilon^{efg}(CP^{R/L})_{\gamma\delta}P^L_{\theta\epsilon}(C\gamma_5)_{\eta\iota}\delta_{md}( \\ &\quad -2S^{bg}_{\mathrm{seq};u;\gamma\zeta}S^{ce}_{u;\delta\iota}S^{df}_{u;\epsilon\eta} + 2S^{dg}_{\mathrm{seq};u;\epsilon\zeta}S^{bf}_{u;\gamma\eta}S^{ce}_{u;\delta\iota} \\ &\quad +2S^{be}_{\mathrm{seq};u;\gamma\iota}S^{cg}_{u;\delta\zeta}S^{df}_{u;\epsilon\eta} - 2S^{de}_{\mathrm{seq};u;\epsilon\iota}S^{bg}_{u;\gamma\zeta}S^{cf}_{u;\delta\eta} \\ &\quad ) \end{aligned} \tag{B.5}$$

$$\begin{aligned} \langle K^0(\vec{p})|\mathcal{O}^{\Gamma\Gamma'}|N(\vec{k},s)\rangle &= \epsilon^{bcd}\epsilon^{efg}(CP^{R/L})_{\gamma\delta}P^L_{\theta\epsilon}(C\gamma_5)_{\eta\iota}( \\ &\quad +2S^{bf}_{\mathrm{seq};s;\gamma\eta}S^{cg}_{u;\delta\zeta}S^{de}_{u;\epsilon\iota} - 2S^{bf}_{\mathrm{seq};s;\gamma\eta}S^{ce}_{u;\delta\iota}S^{dg}_{u;\epsilon\zeta} \\ &\quad ) \end{aligned} \tag{B.6}$$

$$\begin{aligned} \langle K^+(\vec{p})|\mathcal{O}^{\Gamma\Gamma'}_{uds}|N(\vec{k},s)\rangle &= \epsilon^{bcd}\epsilon^{efg}(CP^{R/L})_{\gamma\delta}P^L_{\theta\epsilon}(C\gamma_5)_{\eta\iota}( \\ &\quad 2S^{dg}_{\mathrm{seq};s;\epsilon\zeta}S^{bf}_{u;\gamma\eta}S^{ce}_{u;\delta\iota} - 2S^{de}_{\mathrm{seq};s;\epsilon\iota}S^{bg}_{u;\gamma\zeta}S^{cf}_{u;\delta\eta} \\ &\quad ) \end{aligned} \tag{B.7}$$

$$\begin{aligned} \langle K^+(\vec{p})|\mathcal{O}^{\Gamma\Gamma'}_{dsu}|N(\vec{k},s)\rangle &= \epsilon^{bcd}\epsilon^{efg}(CP^{R/L})_{\gamma\delta}P^L_{\theta\epsilon}(C\gamma_5)_{\eta\iota}( \\ &\quad +2S^{bg}_{\mathrm{seq};s;\gamma\zeta}S^{cf}_{u,\delta\eta}S^{de}_{u,\epsilon\iota} - 2S^{be}_{\mathrm{seq};s;\gamma\iota}S^{cf}_{u,\delta\eta}S^{dg}_{u,\epsilon\zeta} \\ &\quad ) \end{aligned} \tag{B.8}$$

$$\begin{aligned} \langle K^+(\vec{p})|\mathcal{O}^{\Gamma\Gamma'}_{usd}|N(\vec{k},s)\rangle &= \epsilon^{bcd}\epsilon^{efg}(CP^{R/L})_{\gamma\delta}P^L_{\theta\epsilon}(C\gamma_5)_{\eta\iota}( \\ &\quad +2S^{bg}_{\mathrm{seq};s;\gamma\zeta}S^{ce}_{u;\delta\iota}S^{df}_{u;\epsilon\eta} - 2S^{be}_{\mathrm{seq};s;\gamma\iota}S^{cg}_{u;\delta\zeta}S^{df}_{u;\epsilon\eta} \\ &\quad ) \end{aligned} \tag{B.9}$$

# Bibliography


[1] Y. Aoki *et al.* [RBC-UKQCD Collaboration], Phys. Rev. D **78** (2008) 054505 [arXiv:0806.1031 [hep-lat]].

[2] P. Cooney, "Proton lifetime bounds from chirally symmetric lattice QCD," PoS (Lattice 2008) 283.

[3] S. Weinberg, Phys. Rev. Lett. **19** (1967) 1264.

[4] P. W. Higgs, Phys. Lett. **12** (1964) 132.

[5] M. E. Peskin and D. V. Schroeder, Reading, USA: Addison-Wesley (1995)

[6] W. M. Yao *et al.* [Particle Data Group], J. Phys. G **33**, 1, (2006).

[7] S. Willenbrock, "Symmetries of the Standard Model," (2004), arXiv:hep-ph/0410370.

[8] A. Signer, "The Standard Model," "Lectures presented at the school for young high energy physicists," (2002)

[9] P. Langacker, "Structure of the Standard Model," (1995), arXiv:hep-ph/0304186.

[10] J. Goldstone, A. Salam and S. Weinberg, Phys. Rev. **127** (1962) 965.

[11] N. Cabibbo, Phys. Rev. Lett. **10** (1963) 531.

[12] M. Kobayashi and T. Maskawa, Prog. Theor. Phys. **49** (1973) 652.

[13] J. H. Christenson, J. W. Cronin, V. L. Fitch and R. Turlay, Phys. Rev. Lett. **13** (1964) 138.

[14] B. Aubert *et al.* [BABAR Collaboration], Phys. Rev. Lett. **87** (2001) 091801 [arXiv:hep-ex/0107013].

[15] K. Abe *et al.* [Belle Collaboration], Phys. Rev. Lett. **87** (2001) 091802 [arXiv:hep-ex/0107061].

[16] G. W. Bennett *et al.* [Muon G-2 Collaboration], Phys. Rev. D **73** (2006) 072003 [arXiv:hep-ex/0602035].

[17] C. Amsler *et al.* [Particle Data Group], Phys. Lett. B **667** (2008) 1.

[18] P. Fayet, Phys. Lett. B **64** (1976) 159.

[19] P. Fayet, Phys. Lett. B **69** (1977) 489.

[20] G. R. Farrar and P. Fayet, Phys. Lett. B **76** (1978) 575.

[21] P. Fayet, Phys. Lett. B **84** (1979) 421.

[22] M. Claudson, M. B. Wise and L. J. Hall, Nucl. Phys. B **195** (1982) 297.

[23] S. Weinberg, Phys. Rev. Lett. **43** (1979) 1566.

[24] F. Wilczek and A. Zee, Phys. Rev. Lett. **43** (1979) 1571.

[25] L. F. Abbott and M. B. Wise, Phys. Rev. D **22** (1980) 2208.

[26] H. Georgi and S. L. Glashow, Phys. Rev. Lett. **32** (1974) 438.

[27] J. C. Pati and A. Salam, Phys. Rev. D **10** (1974) 275 [Erratum-ibid. D **11** (1975) 703].

[28] S. Dimopoulos, S. Raby and F. Wilczek, Phys. Rev. D **24** (1981) 1681.

[29] H. Georgi, AIP Conf. Proc. **23** (1975) 575.

[30] H. Fritzsch and P. Minkowski, Annals Phys. **93** (1975) 193.

[31] S. M. Barr, Phys. Lett. B **112** (1982) 219.

[32] T. Nishino and S. Clark [Kamiokande Collaboration], arXiv:0903.0676 [hep-ex].

[33] K. Kobayashi *et al.* [Super-Kamiokande Collaboration], Phys. Rev. D **72** (2005) 052007 [arXiv:hep-ex/0502026].

[34] W. J. Marciano, *IN *SYRACUSE 1987, PROCEEDINGS, GRAND UNIFICATION* 185-199.*

[35] H. Murayama and A. Pierce, Phys. Rev. D **65** (2002) 055009 [arXiv:hep-ph/0108104].

[36] S. Y. Hsueh *et al.*, Phys. Rev. D **38** (1988) 2056.

[37] S. Aoki *et al.* [JLQCD Collaboration], Phys. Rev. D **62** (2000) 014506 [arXiv:hep-lat/9911026].

[38] D. J. Gross and F. Wilczek, Phys. Rev. Lett. **30** (1973) 1343.

[39] H. D. Politzer, Phys. Rev. Lett. **30** (1973) 1346.

[40] K. G. Wilson, Phys. Rev. D **10** (1974) 2445.

[41] G. Curci, P. Menotti and G. Paffuti, Phys. Lett. B **130** (1983) 205 [Erratum-ibid. B **135** (1984) 516].

[42] Y. Iwasaki and T. Yoshie, Phys. Lett. B **143** (1984) 449.

[43] M. Lüscher and P. Weisz, Commun. Math. Phys. **97** (1985) 59 [Erratum-ibid. **98** (1985) 433].

[44] Y. Iwasaki, UTHEP-118 (1983) 40

[45] Y. Iwasaki, UTHEP-118 (1983) 33

[46] M. Bochicchio, L. Maiani, G. Martinelli, G. C. Rossi and M. Testa, Nucl. Phys. B **262** (1985) 331.

[47] H. B. Nielsen and M. Ninomiya, Nucl. Phys. B **185** (1981) 20 [Erratum-ibid. B **195** (1982) 541].

[48] P. H. Ginsparg and K. G. Wilson, Phys. Rev. D **25** (1982) 2649.

[49] M. Lüscher, Nucl. Phys. B **568** (2000) 162 [arXiv:hep-lat/9904009].

[50] H. Neuberger, Phys. Lett. B **427** (1998) 353 [arXiv:hep-lat/9801031].

[51] D. B. Kaplan, Phys. Lett. B **288** (1992) 342 [arXiv:hep-lat/9206013].

[52] V. Furman and Y. Shamir, Nucl. Phys. B **439** (1995) 54 [arXiv:hep-lat/9405004].

[53] Y. Shamir, Nucl. Phys. B **406**, 90 (1993) [arXiv:hep-lat/9303005].

[54] R. Narayanan and H. Neuberger, Phys. Lett. B **302** (1993) 62 [arXiv:hep-lat/9212019].

[55] D. J. Antonio *et al.* [RBC and UKQCD Collaborations], Phys. Rev. D **77** (2008) 014509 [arXiv:0705.2340 [hep-lat]].

[56] G. Martinelli, C. Pittori, C. T. Sachrajda, M. Testa and A. Vladikas, Nucl. Phys. B **445**, 81 (1995) [arXiv:hep-lat/9411010].

[57] H. J. Rothe, World Sci. Lect. Notes Phys. **74** (2005) 1.

[58] S. Duane, A. D. Kennedy, B. J. Pendleton and D. Roweth, Phys. Lett. B **195** (1987) 216.

[59] D. J. E. Callaway and A. Rahman, Phys. Rev. Lett. **49** (1982) 613.

[60] D. J. E. Callaway and A. Rahman, Phys. Rev. D **28** (1983) 1506.

[61] N. Metropolis, A. W. Rosenbluth, M. N. Rosenbluth, A. H. Teller and E. Teller, J. Chem. Phys. **21** (1953) 1087.

[62] S. A. Gottlieb, W. Liu, D. Toussaint, R. L. Renken and R. L. Sugar, Phys. Rev. D **35** (1987) 2531.

[63] M. A. Clark and A. D. Kennedy, Nucl. Phys. Proc. Suppl. **129** (2004) 850 [arXiv:hep-lat/0309084].

[64] M. A. Clark, A. D. Kennedy and Z. Sroczynski, Nucl. Phys. Proc. Suppl. **140** (2005) 835 [arXiv:hep-lat/0409133].

[65] M. A. Clark and A. D. Kennedy, Phys. Rev. Lett. **98**, 051601 (2007) [arXiv:hep-lat/0608015].

[66] C. Allton *et al.* [RBC and UKQCD Collaborations], Phys. Rev. D **76** (2007) 014504 [arXiv:hep-lat/0701013].

[67] J. R. Shewchuk, "An Introduction to the Conjugate Gradient Method Without the Agonizing Pain," (1994)

[68] C. R. Allton *et al.* [UKQCD Collaboration], Phys. Rev. D **47** (1993) 5128 [arXiv:hep-lat/9303009].

[69] P. Boyle [UKQCD Collaboration], J. Comput. Phys. **179** (2002) 349 [arXiv:hep-lat/9903033].

[70] P. Bacilieri *et al.* [APE Collaboration], Nucl. Phys. B **317** (1989) 509.

[71] M. Albanese *et al.* [APE Collaboration], Phys. Lett. B **192** (1987) 163.

[72] T. A. DeGrand and S. Schaefer, Phys. Rev. D **71** (2005) 034507 [arXiv:hep-lat/0412005].

[73] Y. Aoki *et al.*, Phys. Rev. D **72** (2005) 114505 [arXiv:hep-lat/0411006].

[74] B. Efron, Ann. Stat. 7, 1-26 (1979).

[75] D. Toussaint and W. Freeman, arXiv:0808.2211 [hep-lat].

[76] C. Michael, Phys. Rev. D **49** (1994) 2616 [arXiv:hep-lat/9310026].

[77] C. Allton *et al.* [RBC and UKQCD Collaborations], Phys. Rev. D **78** (2008) 114509 [arXiv:0804.0473 [hep-lat]].

[78] D. J. Antonio *et al.* [RBC and UKQCD Collaborations], Phys. Rev. D **75** (2007) 114501 [arXiv:hep-lat/0612005].

[79] N. Tsutsui *et al.* [CP-PACS and JLQCD Collaborations], Phys. Rev. D **70** (2004) 111501 [arXiv:hep-lat/0402026].

[80] Y. Aoki, C. Dawson, J. Noaki and A. Soni, Phys. Rev. D **75** (2007) 014507 [arXiv:hep-lat/0607002].

[81] W. H. Press, S. A. Teukolsky, W. T. Vetterling and B. P. Flannery, "Numerical Recipes in C++: The Art of Scientific Computing," Third Edition (2007), Cambridge University Press.

[82] Y. Aoki *et al.*, Phys. Rev. D **78** (2008) 054510 [arXiv:0712.1061 [hep-lat]].

[83] T. Nihei and J. Arafune, Prog. Theor. Phys. **93** (1995) 665 [arXiv:hep-ph/9412325].

[84] T. van Ritbergen, J. A. M. Vermaseren and S. A. Larin, Phys. Lett. B **400** (1997) 379 [arXiv:hep-ph/9701390].

[85] D. J. Antonio *et al.*, arXiv:hep-lat/0702026.

[86] T. Blum *et al.*, Phys. Rev. D **66**, 014504 (2002) [arXiv:hep-lat/0102005].

[87] J. F. Donoghue and E. Golowich, Phys. Rev. D **26** (1982) 3092.

[88] A. W. Thomas and B. H. J. Mckellar, Nucl. Phys. B **227** (1983) 206.

[89] S. Meljanac, D. Palle, I. Picek and D. Tadic, Nucl. Phys. B **206** (1982) 298.

[90] B. L. Ioffe, Nucl. Phys. B **188** (1981) 317 [Erratum-ibid. B **191** (1981) 591].

[91] N. V. Krasnikov, A. A. Pivovarov and N. N. Tavkhelidze, JETP Lett. **36** (1982) 333 [Pisma Zh. Eksp. Teor. Fiz. **36** (1982) 272].

[92] B. L. Ioffe and A. V. Smilga, Nucl. Phys. B **232** (1984) 109.

[93] Y. Tomozawa, Phys. Rev. Lett. **46** (1981) 463 [Erratum-ibid. **49** (1982) 507].

[94] S. J. Brodsky, J. R. Ellis, J. S. Hagelin and C. T. Sachrajda, Nucl. Phys. B **238** (1984) 561.

[95] Y. Hara, S. Itoh, Y. Iwasaki and T. Yoshie, Phys. Rev. D **34** (1986) 3399.

[96] K. C. Bowler, D. Daniel, T. D. Kieu, D. G. Richards and C. J. Scott, Nucl. Phys. B **296** (1988) 431.

[97] M. B. Gavela, S. F. King, C. T. Sachrajda, G. Martinelli, M. L. Paciello and B. Taglienti, Nucl. Phys. B **312** (1989) 269.

[98] J. Hisano, arXiv:hep-ph/0004266.

[99] J. Hisano, H. Murayama and T. Yanagida, Nucl. Phys. B **402** (1993) 46 [arXiv:hep-ph/9207279].

[100] W. J. Marciano, "Proton Decay Theory," (1983)

[101] P. Boyle *et al.* IBM Journal of Research and Development 49, 2/3, 351 (2005).

[102] P. Boyle *et al.* ECONF C0303241, THIT003 (2003), [hep-lat/0306023].

[103] P. Boyle *et al.* J. Phys. Conf. Ser. 16, 129 (2005).

# Acknowledgements

I first wish to thank my supervisor Luigi Del Debbio and STFC for funding me through my PhD. I also thank all the members of the University of Edinburgh Particle Physics Theory group, in particular Peter Boyle, Chris Maynard, James Zanotti, Jan Wennekers, Rob Tweedie, Brian Pendleton, Roger Horsley and Tony Kennedy.

I also wish to thank all my fellow PhD students, in particular my office mates George Burton, Thomas Reiter and Rudy Arthur.

Finally I thank the members of the RBC–UKQCD collaboration, especially Yasumichi Aoki and Amarjit Soni.

The calculations reported here were done on the QCDOC computers [101, 102, 103] at Columbia University, Edinburgh University, and at Brookhaven National Laboratory (BNL). At BNL, the QCDOC computers of the RIKEN-BNL Research Center and the USQCD Collaboration were used. Computations for this work were carried out in part on facilities of the USQCD Collaboration, which are funded by the Office of Science of the U.S. Department of Energy. I thank RIKEN, BNL and the U.S. DOE for providing the facilities essential for the completion of this work.